# **NOTE TO USERS**

Page(s) missing in number only; text follows. Page(s) were scanned as received.

Pgs. viii, 22, 64, 80, 84, 108

This reproduction is the best copy available.



# Contention Resolution and Label Switching in Optical Multiprotocol Label Switching Networks

Reuven Eli Gordon



Photonic Systems Group

Department of Electrical and Computer Engineering

McGill University

Montréal, Québec, Canada

October 2005

A thesis submitted to the Faculty of Graduate Studies and Research in partial fulfillment of the requirements for the degree of Master of Engineering

© Reuven Eli Gordon, 2005



Library and Archives Canada

Branch

Published Heritage

395 Wellington Street Ottawa ON K1A 0N4 Canada Bibliothèque et Archives Canada

Direction du Patrimoine de l'édition

395, rue Wellington Ottawa ON K1A 0N4 Canada

> Your file Votre référence ISBN: 978-0-494-24959-8 Our file Notre référence ISBN: 978-0-494-24959-8

#### NOTICE:

The author has granted a non-exclusive license allowing Library and Archives Canada to reproduce, publish, archive, preserve, conserve, communicate to the public by telecommunication or on the Internet, loan, distribute and sell theses worldwide, for commercial or non-commercial purposes, in microform, paper, electronic and/or any other formats.

#### AVIS:

L'auteur a accordé une licence non exclusive permettant à la Bibliothèque et Archives Canada de reproduire, publier, archiver, sauvegarder, conserver, transmettre au public par télécommunication ou par l'Internet, prêter, distribuer et vendre des thèses partout dans le monde, à des fins commerciales ou autres, sur support microforme, papier, électronique et/ou autres formats.

The author retains copyright ownership and moral rights in this thesis. Neither the thesis nor substantial extracts from it may be printed or otherwise reproduced without the author's permission.

L'auteur conserve la propriété du droit d'auteur et des droits moraux qui protège cette thèse. Ni la thèse ni des extraits substantiels de celle-ci ne doivent être imprimés ou autrement reproduits sans son autorisation.

In compliance with the Canadian Privacy Act some supporting forms may have been removed from this thesis.

While these forms may be included in the document page count, their removal does not represent any loss of content from the thesis.

Conformément à la loi canadienne sur la protection de la vie privée, quelques formulaires secondaires ont été enlevés de cette thèse.

Bien que ces formulaires aient inclus dans la pagination, il n'y aura aucun contenu manquant.



#### **ABSTRACT**

The last decade has witnessed an explosive growth in internet protocol, packet based traffic. Although long-haul fiber backbone networks provide capacities on the order of Tb/s, a bottleneck at the access network has arisen due to electronic domain signal processing. Recent developments in optical multiprotocol label switching (MPLS) access networks promise to remove this bottleneck and allow Gb/s capacities per user and satisfy foreseeable future bandwidth requirements.

This thesis introduces an optical MPLS network where packet payloads are wavelength multiplexed and labels correspond to spectral optical code division multiple access codes. Using this network, we examine payload and label processing issues in nodes as packets transit through the core network. We develop a software package to model data traffic flow in a node, where reduced sets of realistic wavelength converters are used to mitigate payload wavelength contentions. Furthermore, we successfully demonstrate an all-photonic label switching system to convert (7,4) spectral m-sequence labels using commercially available optical components.

#### SOMMAIRE

Au cours de la dernière décennie, il y a eu une explosion du trafique sur les réseaux de télécommunication par paquet. Bien que les réseaux optiques aillent des capacités de l'ordre des Tb/s sur de longues distances, des limitations sur la performance sont apparues au niveau des réseaux d'accès en raison du traitement électronique des signaux. Des développements récents dans les réseaux d'accès basés sur les étiquettes optiques multi-protocoles (multiprotocol label switching) permettrons d'enlever ces limitations et de fournir une vitesse de transmission dans les Gb/s pour chaque utilisateur, ce qui devrait suffire à satisfaire les besoins en bande passante pour les années à venir.

Cette thèse présente un réseau optique à étiquettes multi-protocoles où l'information contenue par les paquets est transmise sur des longueurs d'onde dédiées et où les étiquettes correspondent à des codes spectraux développés pour les réseaux OCDMA (optical code division multiple access). Ce réseau fut utilisé pour mener une étude des problématiques entourant la transmission des charges et des étiquettes à l'intérieur des nœuds. Un logiciel pour modéliser le trafique à l'intérieur des nœuds est développé. Il est basé sur l'utilisation d'un nombre réduit de convertisseur de longueur d'onde afin d'éviter les conflits lors de la transmission des charges. Finalement, l'implémentation d'un système de commutation d'étiquettes tout photonique constitué de composantes disponibles commercialement est présentée. Ce système convertit des étiquettes spectrales faites de «(7,4) m-sequence».

### **ACKNOWLEDGEMENTS**

The past two years have been incredibly rewarding, and I am indebted to the many people I have met, the friends I have made, and colleagues I have worked with along the way.

Firstly, to my supervisor Professor Lawrence Chen, I thank you. At every stage of my Masters, your support went far beyond the call of a regular supervisor. You encouraged me to seek out challenges, and your door was always open for discussion. I have thoroughly enjoyed working with you, and I am proud of what we have achieved.

Secondly, my thanks to Professor Mark Coates. Your ideas and input on the probabilistic traffic analysis in this thesis were invaluable. I learnt a great deal from our meetings during Fall 2004, and I could not have built the software package without your assistance.

To the people of PSG, I am honoured to have worked by your side. To Rhys Adams, your help with my lab work (amongst other things) was fantastic. Without your aid, I would still be stuck splicing fiber at ITF. I would also like to thank Dominik Pudo for his help in both theoretical and practical photonics problems, Julien Faucher for his help with the BERT and CSA, Michaël Ménard for translating my abstract, Alan Li, Cristina Marinescu and Luay Thomas. Thanks must also go to the lab manager Nicolas Belanger for his great help at ITF and all things lab related, and the guru Chris Rolston; PSG runs so smoothly thanks in large part to your work. Finally, to the Professors of this group, David Plant, Andrew Kirk and Lawrence Chen, I have enjoyed learning from you and working with you, and I have nothing but the greatest respect for you all.

I would like to thank the ITF technical staff for allowing use of their resources in performing length measurements on my AWG multiplexer and couplers.

Merci Isabelle. Avec toi, cette année fut la plus agréable et récompensante de ma vie.

And finally, my parents Avi and Ron Gordon have been my steady ship throughout not only this degree, but my whole life. We sit half a world apart, but mum and dad, you have supported me through the highs and lows, the good and the bad, the challenges and successes. Words cannot convey the honour and gratitude I feel for your enduring love, confidence and support.

This work was supported by the Canadian Institute for Photonic Innovations (CIPI) and the Gar Lam Yip Memorial Fellowship.

This thesis is dedicated to my Grandpa Hyman Gordon. Hymie, you believed in and encouraged me from the day I was born. Never have I met a man who has shown so much love and support to not only his own family, but countless others. You left us this year, but your memory remains, and I aspire to live a life as rich and rewarding as yours.

# **TABLE OF CONTENTS**

1	INTR	ODUCTION	1
	1.1 1.2 1.3	MOTIVATION THESIS OBJECTIVES AND CONTRIBUTIONS THESIS OUTLINE	3
2	Орт	ICAL ACCESS NETWORKS	5
	2.1	PROTOCOL STACKS AND MPLS IN OPTICAL ACCESS NETWORKS	5
	2.2	CIPI PROPOSAL: OPTICAL MPLS NETWORK	6
		2.2.1 Inside a Network Node	7
	2.3	PACKET PAYLOAD AND LABEL CODING	8
		2.3.1 Time Domain Optical MPLS [14, 24]	8
		2.3.2 Subcarrier Multiplexing Optical MPLS [18, 27]	9
		2.3.3 Wavelength Division Optical MPLS	9
		2.3.4 Code Division Optical MPLS	
	2.4	SPECTRAL OCDMA LABEL CODING	
		2.4.1 m-sequences for spectral OCDMA label codes	13
	2.5	PAYLOAD CONTENTIONS IN A NETWORK NODE	
		2.5.1 Wavelength Conversion to Resolve Payload Contentions	
	2.6	SPACE SWITCH AND WC ARCHITECTURES IN A NETWORK NODE	
		2.6.1 Space Switch Architecture	
		2.6.2 Buffered versus Bufferless	
		2.6.3 Single Per Channel (SPC)	18
		2.6.4 Shared Per Node (SPN)	
	2.7	2.6.5 Shared Per Output Fiber (SPOF)	
3		ELENGTH CONVERSION: TECHNIQUES AND LIMITATIONS	
J			
	3.1	XGM IN AN SOA	
	3.2	XPM in an SOA	
	3.3	FWM IN AN SOA	
	3.4	DISCUSSION	26
4		A THROUGHPUT ANALYSIS IN AN OPTICAL MPLS NETWORK NODE WITH	
	Wav	ELENGTH CONVERTERS	27
	4.1	SINGLE SLOT (UNIFORM) ANALYSIS OF TRAFFIC FLOW IN A BUFFERLESS SPACE	
		SWITCH WITH REDUCED SETS OF FRWC'S	
		4.1.1 Introduction and Assumptions	
		4.1.2 Equivalent Model	
		4.1.3 Theoretical Formulation	
		4.1.4 Computing the conditional probability matrix C <sub>N,n</sub>	
		4.1.5 Monte-Carlo Simulation and Model Verification	
		4.1.6 Results	
	4.0	4.1.7 Observations and Discussion	
	4.2	MULTIPLE SLOT (BURSTY) ANALYSIS OF TRAFFIC FLOW IN A BUFFERLESS SPACE	
		SWITCH WITH REDUCED SETS OF FRWC'S	
		4.2.1 Bursty Traffic Arrival Process	
		4.2.2 I IIIUIIIY UIC FLF	77

		4.2.3 Monte-Carlo Simulation and Model Verification	
		4.2.4 Results	
		4.2.5 Observations	49
	4.3	GENERAL ANALYSIS OF TRAFFIC FLOW IN A BUFFERLESS SPACE SWITCH WITH	
		REDUCED SETS OF LRWC'S	
		4.3.1 Random Matching Algorithm	
		4.3.2 Optimum Matching Algorithm	
		4.3.3 Brute-Force Matching Algorithm	
		4.3.4 Limited-Range Wavelength Conversion Scenarios	00
		4.3.6 Observations	
	4.4	SOFTWARE PACKAGE	
i	4.5	DISCUSSION AND COST CONSIDERATIONS	
5			
<b>O</b>		ONSTRATION OF AN ALL-PHOTONIC, SPECTRAL, LABEL SWITCHING PHOTONIC E CONVERTER	65
	5.1	BUILDING THE PCC	
		5.1.1 Experimental Setup	
		5.1.2 Principle of Operation	
	5.2	SPECTRAL AND STATIC TRANSFER CHARACTERISTICS	
	5.2	5.2.1 Zero Wavelength Overlap	
		5.2.2 One Wavelength Overlap	
		5.2.3 Two Wavelength Overlap	
	5.3	STEP RESPONSE	
		5.3.1 Zero Wavelength Overlap	
		5.3.2 One Wavelength Overlap	
		5.3.3 Two Wavelength Overlap	77
	5.4	DISCUSSION	77
		5.4.1 Limitations	78
6	Con	CLUSIONS	81
	6.1	SUMMARY	81
	6.2	FUTURE DIRECTIONS	
7	Deci	ERENCES	QΕ
_			
8	APP	ENDIX A: MONTE-CARLO ALGORITHM FLOWCHARTS	
	8.1	BURSTY TRAFFIC IN A SWITCH WITH REDUCED SETS OF FR-PCC'S	93
9	APP	ENDIX B: ALL-PHOTONIC CLOCK RECOVERY	95
	9.1	INTRODUCTION	95
	9.2	LASER SETUP	95
	9.3	PRINCIPLE OF OPERATION	
	9.4	PRELIMINARY RESULTS	
		9.4.1 One Input Wavelength to One Output Wavelength	
		9.4.2 Four Input Wavelengths to Four Output Wavelengths	
	9.5	DISCUSSION	
10	APP	ENDIX C: PUBLICATIONS ACCEPTED FOR CONFERENCES	101
44	A DD	ENDLY D. LABORATORY PICTURES OF THE BCC SETUR	100

# **LIST OF FIGURES**

Figure 1.1: Multiple access techniques- TDMA, WDMA and 2-dimensional OCDMA [1]. 2
Figure 2.1: Moving from a traditional protocol stack to a merged IP and MPLS stack for
an optical access network5
Figure 2.2: IP packet encapsulated by multiple MPLS labels [15]5
Figure 2.3: Optical MPLS core network interfacing with IP LAN's [17]7
Figure 2.4: Label and payload processing in a NN of an optical MPLS network [17] 8
Figure 2.5: Time domain label enoding9
Figure 2.6: Subcarrier multiplexing encoding [14]9
Figure 2.7: Wavelength division label coding. (a) Wavelength-time packet representation
(b) Spectral packet representation
Figure 2.8: Coherent code division encoding
Figure 2.9: Non-coherent code division encoding [14]11
Figure 2.10: Subset of (7,4) m-sequences highlighting their cyclic property 14
Figure 2.11: Operation of a WC. (a) Packet requests to an output fiber. (b) Transmission
without WC's. (c) Transmission with WC's
Figure 2.12: Space switch architecture showing data flow. Control logic is not shown. 16
Figure 2.13: Space switch with optical buffers
Figure 2.14: Buffering vs WC's for solving payload wavelength contentions. (a) Using a
buffer. (b) Using WC's18
Figure 2.15: Single Per Channel architecture. The $1 \times N$ and $1 \times n$ splitters as well as
optical gates are not included in the space switch block for clarity 19
Figure 2.16: Shared Per Node architecture
Figure 2.17: Shared Per Output Fiber architecture21
Figure 3.1: XGM in an SOA (a) co-propagating (b) counter-propagating configuration 23
Figure 3.2: MZI configuration for XPM in an SOA [50]24
Figure 3.3: FWM in an SOA. Inputs are pump wave $\omega_{\scriptscriptstyle \rho}$ and control wave $\omega_{\scriptscriptstyle c}$ [50] 25
Figure 4.1: General SPOF architecture showing physical space switch connections 28
Figure 4.2: Equivalent switch re-drawn for modelling. Only one output fiber is modelled
due to the symmetric traffic assumption

Figure 4.3: Flowchart to implement MC algorithm and numerically simulate traffic flow in
a SPOF switch. The WS Selection and Output Sources subroutines are illustrated in
Figure 4.4
Figure 4.4: (a) WS Selection subroutine. (b) Output Sources subroutine
Figure 4.5: PLP vs load for a 4×4 switch with 7 wavelengths per fiber with reduced sets
of FRWC's under uniform traffic. Inset: PLP vs WC's at a load of 0.4 and 0.739
Figure 4.6: PLP vs load for a 4×4 switch with 15 wavelengths per fiber with reduced sets
of FRWC's under uniform traffic. Inset: PLP vs WC's at a load of 0.4 and 0.739
Figure 4.7: PLP vs load for a 4×4 switch with 31 wavelengths per fiber with reduced sets
of FRWC's under uniform traffic. Inset: PLP vs WC's at a load of 0.4 and 0.7 40
Figure 4.8: PLP vs load for an 8×8 switch with 15 wavelengths per fiber with reduced
sets of FRWC's under uniform traffic. Inset: PLP vs WC's at a load of 0.4 and 0.7 40
Figure 4.9: PLP vs load for an 8×8 switch with 31 wavelengths per fiber with reduced
sets of FRWC's under uniform traffic. Inset: PLP vs WC's at a load of 0.4 and 0.7 41
Figure 4.10: ON-OFF model of the $nN$ identical bursty traffic sources to the switch. $\beta$ is
the mean burst length
Figure 4.11: PLP vs load for a 4×4 switch with 15 wavelengths per fiber with reduced
sets of FRWC's under bursty traffic with $\beta$ = 2. Inset: PLP vs WC's at a load of 0.7 47
Figure 4.12: PLP vs load for a 4×4 switch with 15 wavelengths per fiber with reduced
sets of FRWC's under bursty traffic with $\beta$ = 4. Inset: PLP vs WC's at a load of 0.7 48
Figure 4.13: PLP vs load for an 8×8 switch with 15 wavelengths per fiber with reduced
sets of FRWC's under bursty traffic with $\beta$ = 2. Inset: PLP vs WC's at a load of 0.7 48
Figure 4.14: Matching problem in a space switch. The WC's are assumed to have a
limited range conversion constraint described above. The matching shown in (a)
requires 0 conversions and transmits 4 packets, while that shown in (b) requires 2
conversions but transmits 5 packets
Figure 4.15: PLP vs CR for a $4\times4$ switch with 15 wavelengths per fiber with reduced sets
of LRWC's under uniform traffic with $ ho$ = 0.7. The RMA (solid lines) and OMA (dashed
lines) are used separately and down conversion is considered. The optimum PLP with a
complete set of FRWC's assuming all output wavelengths are available is $5.51 \times 10^{-3}54$
Figure 4.16: PLP vs CR for a $4\times4$ switch with 15 wavelengths per fiber with reduced sets
of LRWC's under uniform traffic with $\rho$ = 0.7. The RMA and OMA are used together and

down conversion is considered. The optimum PLP with a complete set of FRWC's
assuming all output wavelengths are available is $5.51 \times 10^{-3}$
Figure 4.17: PLP vs CR for a 4×4 switch with 31 wavelengths per fiber with reduced sets
of LRWC's under uniform traffic with $ ho$ = 0.7. The RMA and OMA are used together and
down conversion is considered. The optimum PLP with a complete set of FRWC's
assuming all output wavelengths are available is 8.37×10 <sup>-4</sup> 55
Figure 4.18: PLP vs CR for a 4×4 switch with 31 wavelengths per fiber with reduced sets
of LRWC's under uniform traffic with $ ho$ = 0.7. The RMA (solid lines) and OMA (dashed
lines) are used separately and <i>up and down conversion</i> is considered
Figure 4.19: PLP vs CR for a 4×4 switch with 31 wavelengths per fiber with reduced sets
of LRWC's under uniform traffic with $ ho$ = 0.7. The RMA and OMA are used together and
up and down conversion is considered
Figure 4.20: PLP vs CR for an 8×8 switch with 31 wavelengths per fiber with reduced
sets of LRWC's under uniform traffic with $ ho$ = 0.7. The RMA and OMA are used together
and <i>up and down conversion</i> is considered57
Figure 4.21: PLP vs CR for a 16×16 switch with 32 wavelengths per fiber with reduced
sets of LRWC's at $ ho$ = 0.7 assuming <i>up and down conversion</i> . A combined RMA-OMA
is used and compared to the overlaid FAA results from Figure 18 of [55]59
Figure 4.22: Software package GUI to analyse throughput in a NN of an optical MPLS
network60
Figure 5.1: Conversion from input to output code using a PCC
Figure 5.2: Experimental setup for the quad-wavelength, all-photonic PCC using XGM in
an SOA66
Figure 5.3: Input-output code spectra for zero wavelength overlap70
Figure 5.4: Static TF for zero wavelength overlap. A power meter measures the total
input power70
Figure 5.5: Input-output code spectra for one wavelength overlap71
Figure 5.6: Static TF for one wavelength overlap72
Figure 5.7: Input-output code spectra for two wavelength overlap72
Figure 5.8: Static TF for two wavelength overlap73
Figure 5.9: Step response for conversion from code $i_1$ to $j$ (zero wavelength overlap)75
Figure 5.10: Zoomed version of step response of Figure 5.9 to highlight transient
behaviour
Figure 5.11: Step response for conversion from code $i_2$ to $i$ (one wavelength overlap)76

Figure 5.12: Step response for conversion from code $i_3$ to $j$ (two wavelength overlap) 7	7
Figure 5.13: Negating label inversion by switching from label $i$ to $j$ using an intermedia	te
step with dedicated control wavelength $\lambda_c$ .	<b>7</b> 9
Figure 8.1: Flowchart to implement MC algorithm for bursty (multiple slot) traff	fic
presented in Section 4.2. The Mapping subroutine is illustrated in Figure 8.2	)3
Figure 8.2: Mapping subroutine from Figure 8.1	<b>)</b> 4
Figure 9.1: Input RZ PRBS operating on $\lambda_i$ and modulated at 2.22GHz = 638f <sub>0</sub>	}7
Figure 9.2: Recovered clock on $\lambda_{j1}$ . Sample mode acquisition used in the CSA	}7
Figure 9.3: CSA trace (16x sampling) for input RZ PRBS (blue) and recovered close	ck
output (red). The clock of the incoming data on four wavelengths defined by code $i_1$	is
multicast to four wavelengths defined by code j	99
Figure 11.1: Reuven Gordon characterising stages of initial PCC10	)9
Figure 11.2: Final PCC setup to make step response measurements10	)9
Figure 11.3: Panorama view of all-photonic clock recovery setup11	I C

## LIST OF ACRONYMS

AC ATM AWG BER BERT BFMA	Auto-Correlation Asynchronous Transfer Mode Arrayed Waveguide Grating Bit Error Rate Bit Error Rate Tester Brute-Force Matching Algorithm	NN NRZ OC OMA OSA OSNR	Network Node Non-Return to Zero Optical Circulator Optimal Matching Algorithm Optical Spectrum Analyser Optical Signal to Noise Ratio
CC CDMA CDR CIPI	Cross-Correlation Code Division Multiple Access Clock and Data Recovery Canadian Institute for Photonic Innovations	PC PCC PLP PR	Polarization Controller Photonic Code Converter Packet Loss Probability Photo-receiver
CR C/R CSA	Conversion Ratio Contrast Ratio Communication Signal	PRBS PSP RMA	Pseudorandom Bit Sequence Packet Success Probability Random Matching Algorithm
CW DBR EDFA EEN	Analyser Continuous Wave Distributed Bragg Reflector Erbium Doped Fiber Amplifier Egress Edge Node	RV RZ SFRL SI-FBG	Random Variable Return to Zero Semiconductor Fiber Ring Laser Superimposed Fiber Bragg Grating
ER FDL FRWC	Extinction Ratio Fiber Delay Line Full-Range Wavelength Converter	SOA SONET TDMA	Semiconductor Optical Amplifier Synchronous Optical Network Time Division Multiple Access
FWM IEN IP	Four Wave Mixing Ingress Edge Node Internet Protocol	TF TLS TO-BPF	Transfer Function Tuneable Laser Source Tuneable Optical Band Pass Filter
LAN LRWC	Local Area Network Limited-Range Wavelength Converter	TTL VOA	Time to Live Variable Optical Attenuator
LSP MAI	Label Switched Path Multiple Access Interference	WC WDM	Wavelength Converter Wavelength Division Multiplexing
MC	Monte-Carlo	WDMA	Wavelength Division Multiple Access
MOD MOEMS	Modulator Micro-Opto-Electro- Mechanical Switch	WS XGM	Wavelength Set Cross Gain Modulation
MPLS MZI	Multiprotocol Label Switching Mach-Zehnder Interferometer	XPM	Cross Phase Modulation

### 1 Introduction

#### 1.1 Motivation

Historically driven by military needs, the requirement for fast, reliable and secure telecommunication networks has ensured sustained research, and development in this field has advanced at a relentless pace. From such simple systems as the optical telegraphs of the 1600's, where two synchronised stations would communicate with a sequence of coded flag signals, systems have evolved into international networks carrying vast amounts of information.

Over the past several decades, backbone wire-line communication systems have increasingly been replaced with SONET based long-haul fiber-optic cables, resulting in Terabit per second (Tb/s) bandwidths between service providers. However, metropolitan and local access networks (LAN) are still limited to capacities of hundreds of Megabit per second (Mb/s) due to data conversion and processing in the electronic domain.

In recent times, there has been significant growth in new communication services and applications such as internet protocol (IP) telephony, high-definition video broadcasts and three-dimensional data visualization. These applications require end user bandwidths ranging from kilo to Gigabit per second (Gb/s) as well as bit error rates (BER) anywhere from  $10^{-3}$  to  $10^{-12}$  [1]. Given that hundreds of users can be operating simultaneously in a LAN, capacities of hundreds of Gb/s could be required. With current electronics technology, a throughput bottleneck at the metropolitan and LAN arises and such capacity requirements cannot be met.

By replacing the electronic processing in these networks with an all-photonic configuration, the bottleneck between long haul and access networks can be eliminated. Three multiple access techniques commonly used to share the available bandwidth of a fiber are time division multiple access (TDMA), wavelength division multiple access (WDMA), and optical code division multiple access (OCDMA). These techniques are shown in Figure 1.1.

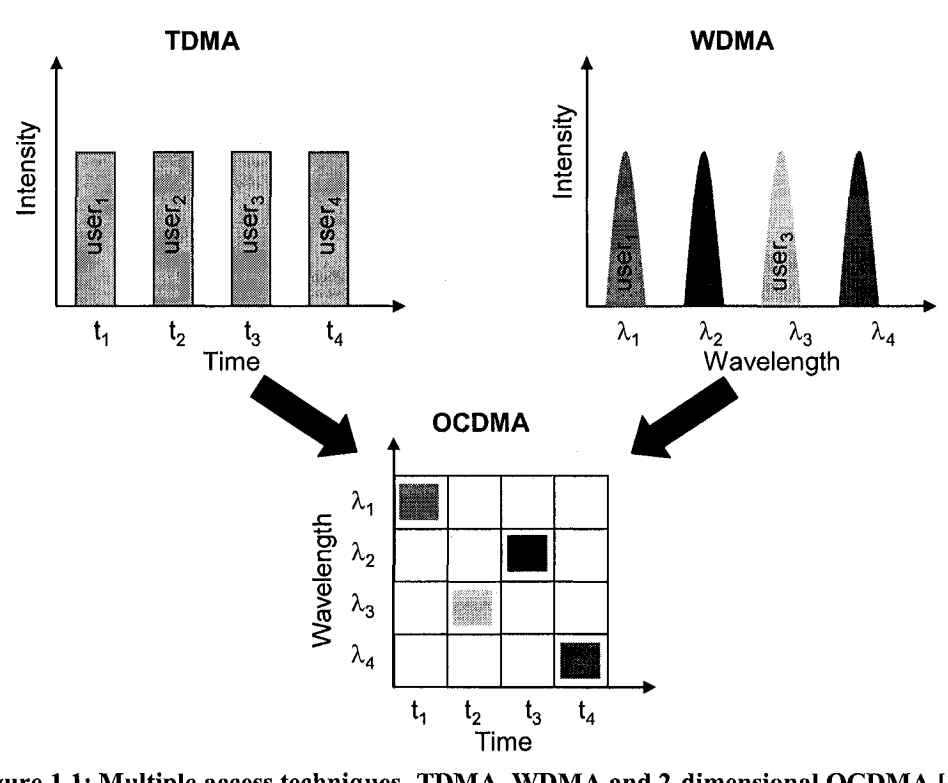


Figure 1.1: Multiple access techniques- TDMA, WDMA and 2-dimensional OCDMA [1].

In TDMA, users occupy the allowed wavelength band at different time slots. Each user is assigned a set of slots for communication, with transmission possible only during an allocated slot. After this, a user must wait until the next available slot before continuing Synchronisation plays an essential role in TDMA, and a central unit transmission. controlling the timing and allocation of time slots is required. For bursty traffic, TDMA cannot take the full advantage of statistical multiplexing gain due to its allocation of dedicated time slots [1].

WDMA utilizes the immense bandwidth of single-mode fiber by supporting many high speed channels and dramatically increases transmission capacity. Wavelength division multiplexing (WDM) networks offer many advantages including protocol transparency, dynamic reconfigurability and improved survivability at the expense of requiring a significant amount of dynamic co-ordination between nodes [2-5].

As opposed to the previous techniques, OCDMA requires neither time nor wavelength management at network nodes as users operate over all wavelengths at the same time. Each user is assigned a unique code with ideally optimum auto- and cross-correlation (AC and CC respectively) properties to minimise multiple access interference (MAI). As a result, OCDMA networks are soft-limited in that BER depends on the number of active users. This is a significant advantage over TDMA and WDMA systems where the maximum capacity is determined by the total number of slots or wavelengths (hard-limited). However, system implementation complexity, component technology requirements and code performance issues are major drawbacks of OCDMA.

### 1.2 Thesis Objectives and Contributions

This thesis studies traffic flow and enabling technologies in a multiprotocol label switching (MPLS) optical access network where the data payload is wavelength multiplexed and the packet labels are spectrally OCDMA coded. Firstly, we build a software package to study traffic throughput in a bufferless network node (NN), where reduced sets of limited-range wavelength converters (WC's) are used to resolve payload wavelength contentions. After verifying the data throughput improvement attainable using these realistic sets of WC's, we build an all-photonic label switching system to demonstrate switching of length seven, weight four packet label codes.

In building the software package, we extend previous research in WDM networks where throughput with reduced sets of WC's were modelled [6-8]. By studying bursty traffic patterns, as well as accounting for limited-range wavelength conversion and using new optimal matching algorithms, our model presents a more realistic picture of the benefits of WC's in optical MPLS networks. Our practical work extends single WC demonstrators in WDM networks [9-11] by moving to concurrent multiple wavelength conversion for label switching. In this work, we exploit cross gain modulation (XGM) in a semiconductor fiber ring laser (SFRL) with a semiconductor optical amplifier (SOA) gain medium. The operation of the label switcher in converting coded packet labels is successfully demonstrated.

The original research contributions of this thesis have been reported in the following conferences and can be found in Appendix C:

- The demonstration of all-photonic packet label code conversion in OCDMA NN's using a semiconductor fiber ring laser was presented at the *OSA Information Photonics Conference 2005* under the title, "Demonstration of All-Photonic Code Conversion in a Semiconductor Fiber Ring Laser for OCDMA Networks" [12].
- The throughput study in a bufferless WDM switch under bursty traffic using limited range WC's with optimal wavelength matching algorithms was presented at the *OSA Information Photonics Conference 2005* under the title, "Analysis of a WDM Packet Switch with a Reduced Set of Limited-Range Wavelength Converters" [13].

#### 1.3 Thesis Outline

This thesis is organised as follows. Chapter 2 presents an optical MPLS access network and discusses the motivations for incorporating WC's and label switchers into NN's. Reviews of NN architectures comprising a space switch and sets of WC's are included in this chapter. Chapter 3 compares and contrasts common wavelength conversion technologies to determine their realistic limitations and assess their viability in a label switcher design. In Chapter 4, a model studying data throughput in NN's with reduced sets of limited-range WC's to solve data wavelength contentions is presented. A rigorous probabilistic traffic analysis is combined with Monte-Carlo simulation. Various space switch wavelength matching algorithms are analysed, and conclusions are drawn concerning the effects on throughput of the number of WC's, their conversion range, number of wavelengths, number of fibers, and traffic pattern in the NN's. In Chapter 5, we demonstrate an all-photonic label switcher to perform concurrent quad-wavelength conversion. Static transfer characteristics are presented, as well as step response plots for the three cases of zero, one and two wavelength overlap between input and output codes. Based on these results, 2R-regeneration (re-amplifying and re-shaping) is expected for slowly modulated labels. Finally, Chapter 6 summarises the main results of this thesis and discusses future research directions to improve packet processing technologies in optical MPLS networks. A simple modification of our label switcher is discussed to provide other important processing functions such as all-photonic clock recovery from the data payload.

### 2 Optical Access Networks

### 2.1 Protocol Stacks and MPLS in Optical Access Networks

The viability of optical access networks depends strongly on its ability to support the explosion of IP packet based traffic. To this end, routing and switching technologies in the optical domain are required. Moving away from a traditional IP over asynchronous transfer mode (ATM) over SONET over optical approach, a merged protocol combining IP and MPLS over optical [14] could be used as shown in Figure 2.1.

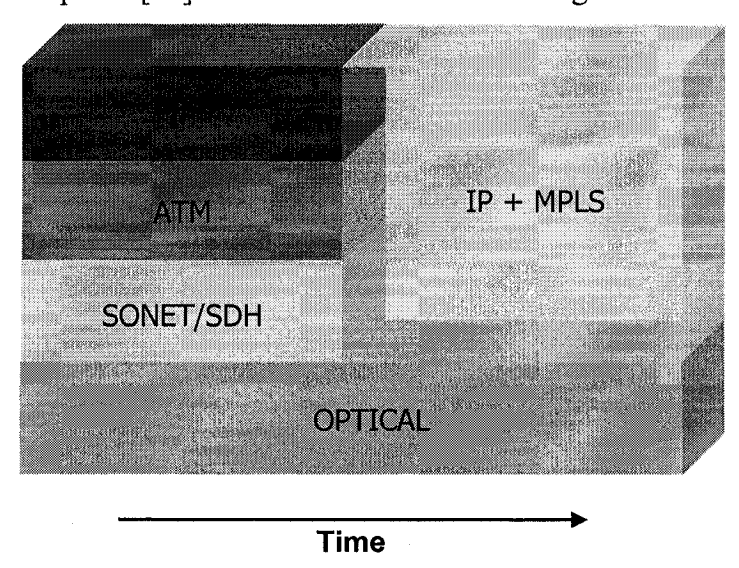


Figure 2.1: Moving from a traditional protocol stack to a merged IP and MPLS stack for an optical access network.

MPLS does not use the cell-switching and signalling protocol of ATM, as the small 48 byte ATM cells are not practical in optical access networks where bandwidths in the order of hundreds of gigabits are expected and much longer packets would be used. MPLS encapsulates an arbitrarily long packet with a header containing one or more labels to make up a label stack. In current MPLS networks, each label stack entry contains a 20-bit label value with an additional 12-bits containing experimental information (Exp), a bottom of stack flag *S* and time to live (TTL) data as shown in Figure 2.2 [15, 16].

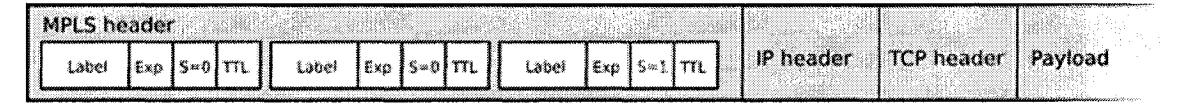


Figure 2.2: IP packet encapsulated by multiple MPLS labels [15].

To forward a packet through the network, an MPLS tunnel, or label switched path (LSP) is established between source (ingress) and destination (egress) edge nodes (IEN and EEN respectively). The NN's (often referred to as label switch routers) mentioned in Chapter 1, make up all transit nodes between the IEN and EEN. When a packet arrives at a NN, the uppermost label is studied and the next node on the LSP is determined based on its contents. Before transmission on the next hop, one of three operations will be performed on the current label:

- **Switch**: The current packet label is switched to a new label indicating the next NN on the LSP.
- **Push:** A new label is pushed on top of the current label increasing stack depth.
- **Pop:** The current label is removed revealing the label below. The bottom label of the stack will be popped at the EEN leaving the original packet at its destination.

The combination of IP and MPLS over an optical transport technology such as WDM or OCDMA would provide interoperability and end-to-end quality of service (QoS) with high capacity and reliable transport [14]. Furthermore, packet processing time in each NN would be minimised as the MPLS protocol examines only the uppermost label in the stack, rather than performing time consuming IP longest prefix matching.

### 2.2 CIPI Proposal: Optical MPLS Network

The optical MPLS network architecture studied in this thesis is based on a Canadian Institute for Photonic Innovations (CIPI) project with collaboration between McGill University, Université Laval and the University of Toronto and is shown in Figure 2.3 [17]. This network will potentially allow a large number of users (>100) to operate simultaneously while supporting high bandwidths per user (>1Gb/s) over relatively large distances (>10km).

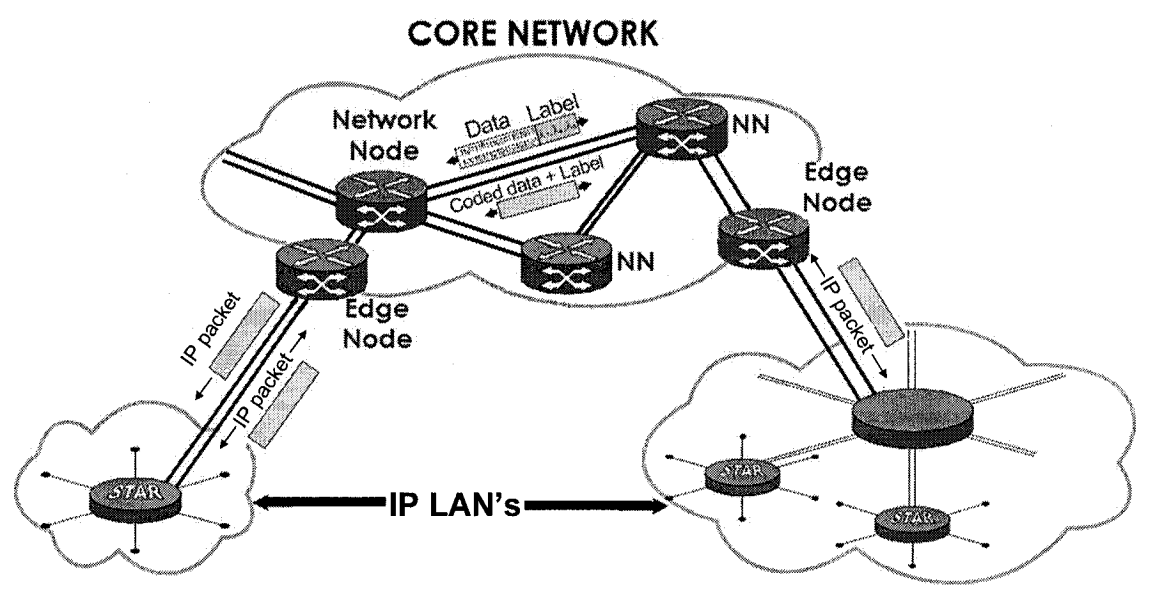


Figure 2.3: Optical MPLS core network interfacing with IP LAN's [17].

In the network of Figure 2.3, end users are interconnected in LAN's using IP over an optical transport technology. For communication between LAN's, IP packets are sent to an IEN for multi-hop transmission through the MPLS core network. Based on the contents of the IP packet, the IEN encodes the packet payload and encapsulates it with an optical MPLS header. The header contains a fixed length label indicating the IEN source address and EEN destination address, along with extra fields containing priority, packet duration and TTL information [18]. The labelled packet is then multiplexed onto a shared fiber and passed to the first NN on the LSP [19, 20].

#### 2.2.1 Inside a Network Node

As a packet enters a NN, two essential functions are performed. Firstly, a decision on the routing of the next hop (towards the EEN) is made. Following this, the NN physically forwards the packet. A systems level NN architecture is illustrated in Figure 2.4, where N fibers enter and exit the node.

For each packet entering the NN, the clock is recovered from the payload [21, 22] and the data undergoes 2R-regeneration. The packet label is extracted using optical correlation header recognition techniques [18, 23, 24]. Based on the current label, the next hop on the LSP is determined from an optical lookup table (generated by mapping IP addresses onto labels and distributing them across the network with a label distribution protocol

[14]). A switch operation is then performed where the current label is switched to a new label associated with the next NN. Having completed label processing, the electronic control system (in red) uses the forwarding information to determine whether payload wavelength contentions will occur in the space switch. Along with the next hop routing information, this contention information is used in the switch control to ensure contending packets are sent to WC's before being multiplexed onto an output fiber.

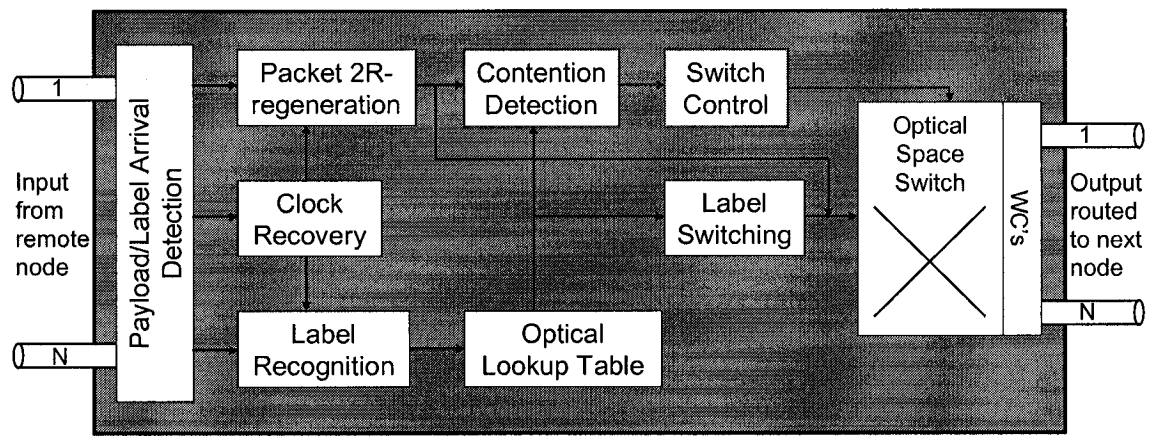


Figure 2.4: Label and payload processing in a NN of an optical MPLS network [17].

### 2.3 Packet Payload and Label Coding

The strategy used to encode the packet payload and corresponding label as it hops between NN's is fundamental to successful optical MPLS network operation. Ideally, a coding strategy should satisfy the following criteria as discussed in [14]:

- Optical labels should not interfere with the data payload.
- Label switching should be easily implemented in the optical domain.
- Labels should be immune to dispersion, timing jitter and interference from other co-propagating labels.
- In the time domain, the label rate should be less than or equal to the data rate, ensuring large overhead for label processing in the NN is not required.

Based on these criteria, optical MPLS coding strategies have data and labels encoded in time, subcarrier, wavelength or code.

### 2.3.1 Time Domain Optical MPLS [14, 24]

A promising technique for label recognition, labels are implemented before the payload in the time domain as shown in Figure 2.5. The bit rate of the label is usually the same as

or lower than the data rate [25]. At the same data rate, time domain buffering is avoided although the label processor must operate in the order of Gb/s. At a lower data rate, label processing can be performed by electronics although buffering is required. Label switching is realized by optical XOR processing with another label [26].

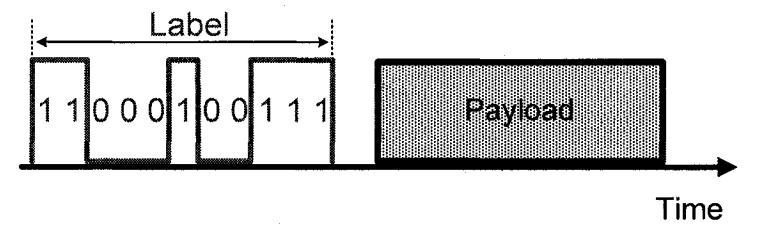


Figure 2.5: Time domain label enoding.

### 2.3.2 Subcarrier Multiplexing Optical MPLS [18, 27]

This strategy treats the payload as a baseband signal while including the label as the subcarrier as shown in Figure 2.6. Compared to time-domain labelling, this strategy facilitates label switching in that frequency-dependent separation of the label and data payload is feasible. Packet transparency can be achieved by setting a fixed label bit rate independent of the packet bit rate. Unfortunately, a payload bit-rate limitation arises due to a required spectral guard band between payload and label to avoid interference. The costs of RF components are also significant drawbacks to this strategy.

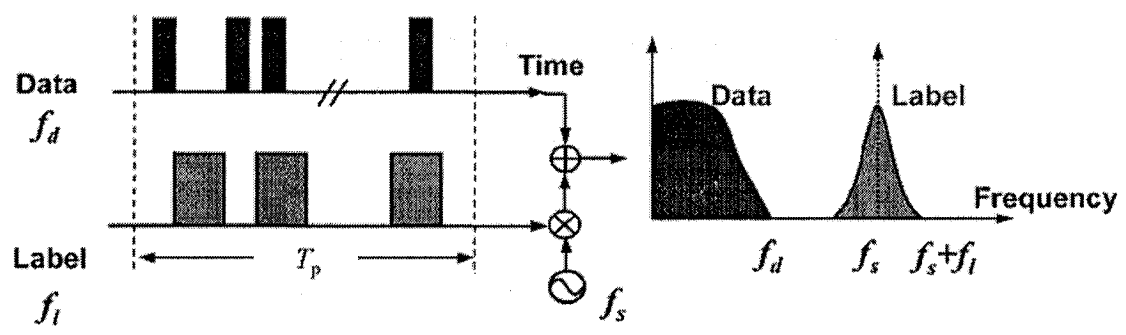


Figure 2.6: Subcarrier multiplexing encoding [14].

### 2.3.3 Wavelength Division Optical MPLS

As illustrated in Figure 2.7, each label is encoded with multiple wavelengths from a designated "label wavelength band". A spectral label is transmitted for the duration of the packet with its payload (which operates on a separate, single wavelength selected from a payload band in a WDM scheme). By splitting the label band into several subbands, hierarchical addressing can be achieved. The advantages of this method include:

- A K chip-long (weight K) label selected from a label wavelength band comprising W wavelengths will result in W!/(W-K)! labels; A large set for few reserved wavelengths [28].
- Compatibility with hierarchical addressing.
- High-speed label recognition and switching capability [17].
- Efficient implementation and reasonable cost.

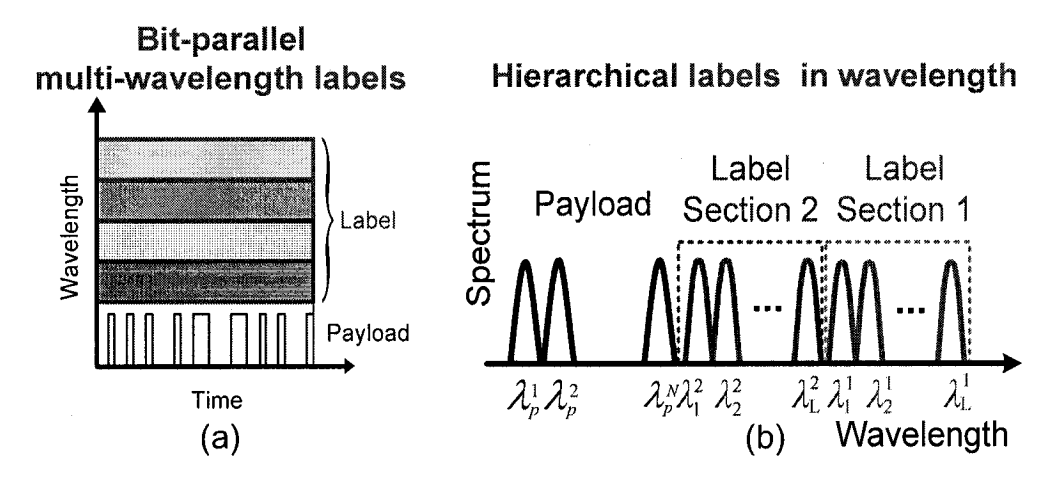


Figure 2.7: Wavelength division label coding. (a) Wavelength-time packet representation (b) Spectral packet representation.

### 2.3.4 Code Division Optical MPLS

Several code division packet encoding strategies have been proposed for optical MPLS networks. In one dimension (1-D), these include coherent or non-coherent encoding in the time or wavelength domain. Higher dimensional coding schemes could also be used; For example, a 2-D coding scheme in time and wavelength [29, 30]. A 2-D scheme would provide many more labels than a 1-D scheme for the same label length at the expense of system complexity.

#### 2.3.4.1 Coherent time domain code division MPLS

As shown in Figure 2.8, each packet label is time spread using coherent binary phase shift keying. The phase shifts of each time chip within the bit period define a unique code. Matched filtering followed by time gating and threshold detection is used to detect the labels. Using this method, logic operations are eliminated in the forwarding table (previously a difficult challenge for optical processing).

According to [31], a network operating with this scheme can achieve throughputs of hundreds of Tb/s with NN processing speeds of 10Gpackets/s. The drawbacks of this method are the complexity involved in coherent signalling, high splitting losses and large number of components required.

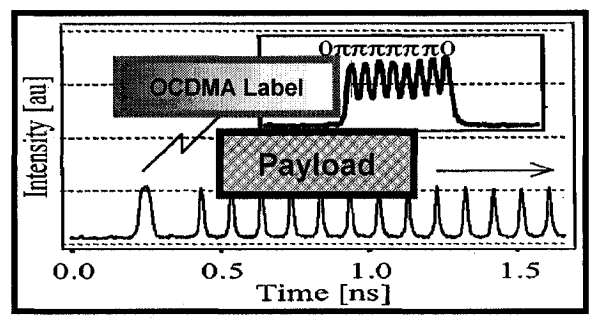


Figure 2.8: Coherent code division encoding.

### 2.3.4.2 Non-coherent time domain code division MPLS [14]

In this scheme, a data bit is modulated by an OCDMA code in the time domain. For example, a "1" data bit sends the code, while no code is sent for the "0" bit, as illustrated in Figure 2.9. By further using the code as the optical label, logic operations are eliminated in the NN lookup process with only optical correlation required. A good choice of code family will minimise MAI allowing many labels to operate simultaneously.

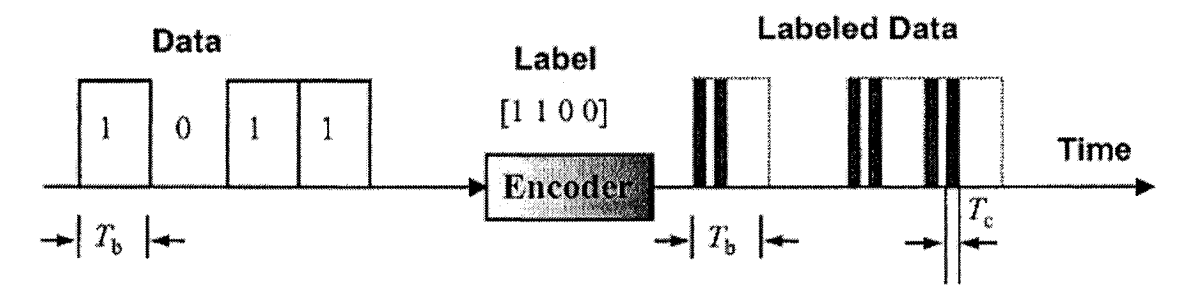


Figure 2.9: Non-coherent code division encoding [14].

### 2.3.4.3 Wavelength domain (spectral) code division MPLS

This technique enhances wavelength division encoding with OCDMA techniques. As in Section 2.3.3, the payload is encoded on a single wavelength in a WDM scheme while the label is comprised of hierarchical sets of wavelengths. However in this case, each label corresponds to a unique set of wavelengths forming a spectral code. In addition to the advantages discussed in Section 2.3.3, pseudo-orthogonal spectral codes minimise label interference and allow many labels to operate simultaneously. A network using this

strategy would be scalable in that many more label codes could be available with minimal increase in hardware [17]. The simplicity and advantages of this scheme would make it ideal for optical MPLS networks and this encoding is assumed for the remainder of the thesis.

### 2.4 Spectral OCDMA Label Coding

A fundamental difference between wireless and OCDMA is that wireless CDMA codes consist of {-1,1} values encoded in the phase of the electromagnetic field, and are known as bipolar sequences. In OCDMA systems, where photonic detectors more readily measure signal energy, codes are unipolar and consist of {0,1} values. It has been shown in [32] that substitution of the -1 values in established bipolar codes for 0 values to create analogous OCDMA unipolar codes results in codes with much poorer AC and CC properties. As a result, novel, spectral, unipolar codes must be created for OCDMA applications and satisfy the desired label characteristics discussed in Section 2.3. Examples of these codes and their impacts on system performance are discussed in [1, 32, 33].

To characterise a code family, the following metrics are used [1]:

- **Hamming weight:** Equal to the number of ones in a code. Also called the nonshifted AC, this value should be as large as possible. As a result, the received decoded signal will be much larger than the background noise in the system.
- Shifted AC: This should be much less than the Hamming weight, and will ensure the output of the correlating receiver is small when the transmitter is not synchronised with the receiver. The AC is defined as

$$R_{AC}(\tau) = \sum_{n=0}^{L-1} x(n)x(n+\tau) \quad ; \quad 0 \le \tau \le L-1$$
 (2.1)

where  $x(\cdot)$  is a unique code, L is the length of the code and  $\tau$  is a shift for asynchronous transmission. Depending on the coding domain,  $\tau$  could correspond to a shift in time, wavelength or space.

• CC: The CC between any pair of codes must be minimised. This ensures that each codeword can be easily distinguished from every other address sequence. A

small CC will minimise MAI compared to the energy contained in a received information bit. CC is defined as

$$R_{CC}(\tau) = \sum_{n=0}^{L-1} x(n)y(n+\tau) \quad ; \quad 0 \le \tau \le L-1$$
 (2.2)

• Cardinality: The number of codes in the family. This should be large to enable many users to operate on an individual code with a minimal chance of code contention.

### 2.4.1 m-sequences for spectral OCDMA label codes

We seek a code family that yields an optimal compromise between the metrics discussed in Section 2.4. One such family is spectrally coded unipolar m-sequences. An (N,k) m-sequence has length N and weight k, and consists of a pattern of zeros and ones with good randomness properties. m-sequences are easily generated using an N-stage linear feedback shift register with feedback taps configured using finite (Galois) field mathematics [34]. The main properties of m-sequences are [35]:

- The length is  $N = 2^n 1$  for integer n.
- The cardinality is *N*.
- There are  $\frac{N+1}{2}$  ones (Hamming weight) and  $\frac{N+1}{2}-1$  zeros in the sequence.
- Any circular shift of the code sequence added (mod-2) to itself is another m-sequence.
- Due to their cyclic nature, the shifted AC and CC are the same and are given by

$$R_{AC}(\tau) = R_{CC}(\tau) = \frac{N+1}{4} \quad ; \quad \tau \neq lN$$
 (2.3)

where *l* is an integer.

The good AC and CC properties coupled with their high weight and simplicity make m-sequences ideal for spectral label coding in optical MPLS networks. As an example, a set of (7,4) optically encoded m-sequences are shown in Figure 2.10.

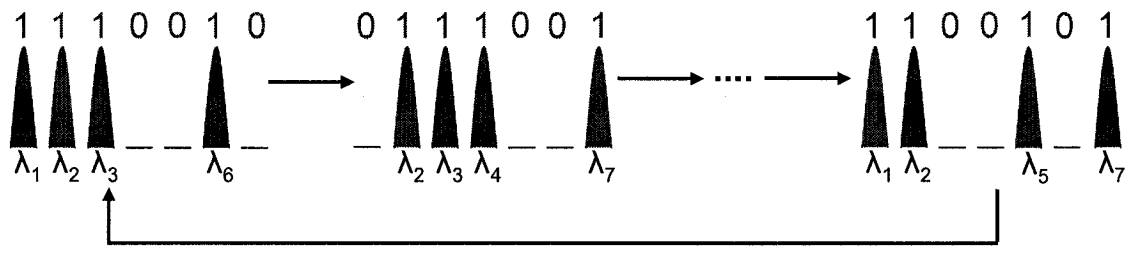


Figure 2.10: Subset of (7,4) m-sequences highlighting their cyclic property.

### 2.5 Payload Contentions in a Network Node

In Section 2.2.1, the possibility of payload wavelength contentions occurring in a NN space switch was introduced. Essentially, if two or more packets (with their payloads on the same wavelength) are to be routed to the same NN on their next hop, a contention will be detected on that wavelength in the current NN. Without a contention resolution scheme, several scenarios could arise. These are discussed below for the case of two contending packets.

- One packet is directed to a fiber delay line (FDL) where it is buffered until the other packet has finished transmission.
- One packet is dropped.
- Both contending packets are dropped. This is the worst case scenario.

Obviously all three scenarios are less than ideal. In the first case, many kilometres of fiber buffer would be required in each NN coupled with a complex scheduling algorithm to control the position of packets in the buffer. In the second and third cases, packet loss could lead to a dramatic reduction in throughput depending on the traffic load and the number of wavelengths used.

#### 2.5.1 Wavelength Conversion to Resolve Payload Contentions

An example of WC operation is shown in Figure 2.11. In this scenario, we consider a system operating on four payload wavelengths and a set of three WC's per output fiber in the space switch. Thus a maximum of four packets can be transmitted in a slot, with a maximum of three conversions taking place. In this time slot, three packets on  $\lambda_I$ , and two packets on  $\lambda_2$  request transmission to the same output fiber as shown in Figure 2.11(a). Without WC's as shown in Figure 2.11(b), only one packet on both  $\lambda_I$  and  $\lambda_2$  would be transmitted, resulting in the loss of three packets. However using the WC's in

Figure 2.11(c), two packets can be converted to the free wavelengths  $\lambda_3$  and  $\lambda_4$ . This results in the loss of just one packet.

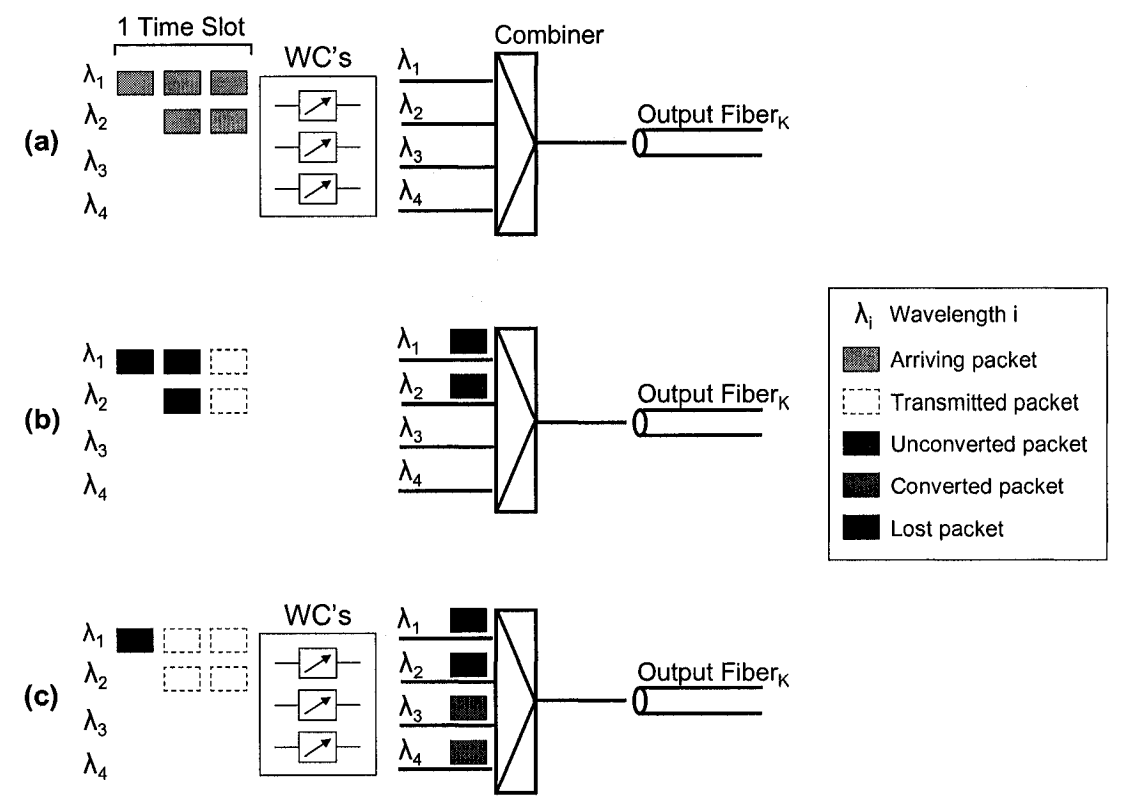


Figure 2.11: Operation of a WC. (a) Packet requests to an output fiber. (b) Transmission without WC's. (c) Transmission with WC's.

We expect many advantages by including WC's in a NN space switch. Firstly, a significant throughput improvement will be achieved as demonstrated in the previous example and in other WDM network studies [6, 8]. Moreover, by utilizing the wavelength dimension, FDL's are not required as buffering is intrinsically performed logically at the network level. Another advantage of including WC's in a space switch is the generalisation of a light-path in a network to a light-tree (one source node with several light-paths to multiple destination nodes) [36, 37]. This allows optical multicast capability whereby a packet entering a NN could be transmitted to many other nodes using different wavelengths. This capability would be useful in 1+1 optical layer protection (transmitting a source signal simultaneously on primary and backup paths), high-definition TV broadcasts and optical storage area networks.

### 2.6 Space Switch and WC Architectures in a Network Node

In this section, several space switch and WC architectures are examined for use in a NN. All architectures have various advantages and drawbacks. Based on these trade-offs, we select an architecture to use in the NN of the CIPI proposed label-switching network.

### 2.6.1 Space Switch Architecture

The space switch alone is common to all the following architectures and is illustrated in Figure 2.12. The switch is made up of power splitters, passive couplers and optical gates implemented with SOA's. N fibers enter the space switch, each carrying up to n payload wavelengths  $(\lambda_1, ..., \lambda_n)$ . A demultiplexer attached to each input fiber demultiplexes each wavelength onto a single, dedicated fiber, resulting in nN individual channels entering the switch. Upon entering, each channel is passively split N times to be directed to the N output fibers. Optical gates are placed after each split channel and comprise the switching matrix. Based on the label code and payload contention information, control logic is used to determine the switching matrix configuration to perform routing from an input to a desired output fiber.

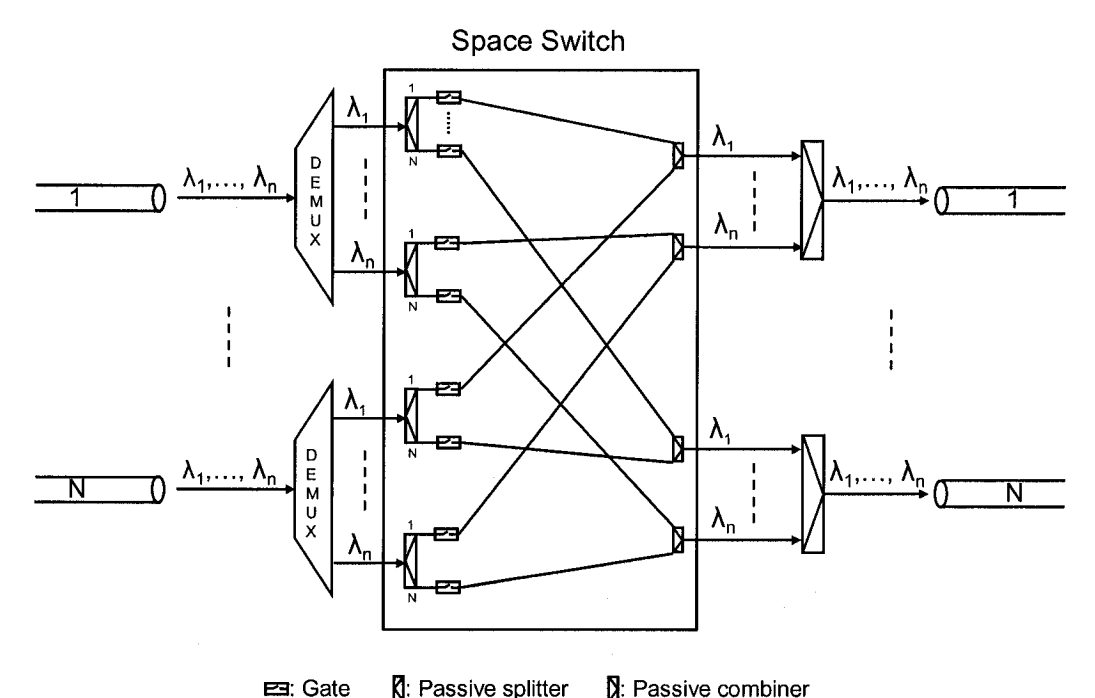


Figure 2.12: Space switch architecture showing data flow. Control logic is not shown.

A limitation of this space switch architecture is the number of times a signal is passively split as it moves through the switch. For many fibers (N large), amplifiers would be

required to boost signal power before transmission through the switch. This would increase system complexity, cost and reduce optical signal to noise ratio (OSNR).

#### 2.6.2 Buffered versus Bufferless

Due to the lack of storage capability in optical networks, buffering is currently achieved using FDL's with lengths equal to multiples of the packet duration. This technique makes the structure of an optical switch close to an electronic switch and has been extensively studied in WDM networks [38, 39]. An architecture combining buffers into a switch is illustrated in Figure 2.13. The switch output has a single direct line and B/n FDL's going to each combiner, where n is the number of available wavelengths, and B is the number of packet positions for the buffer [40].

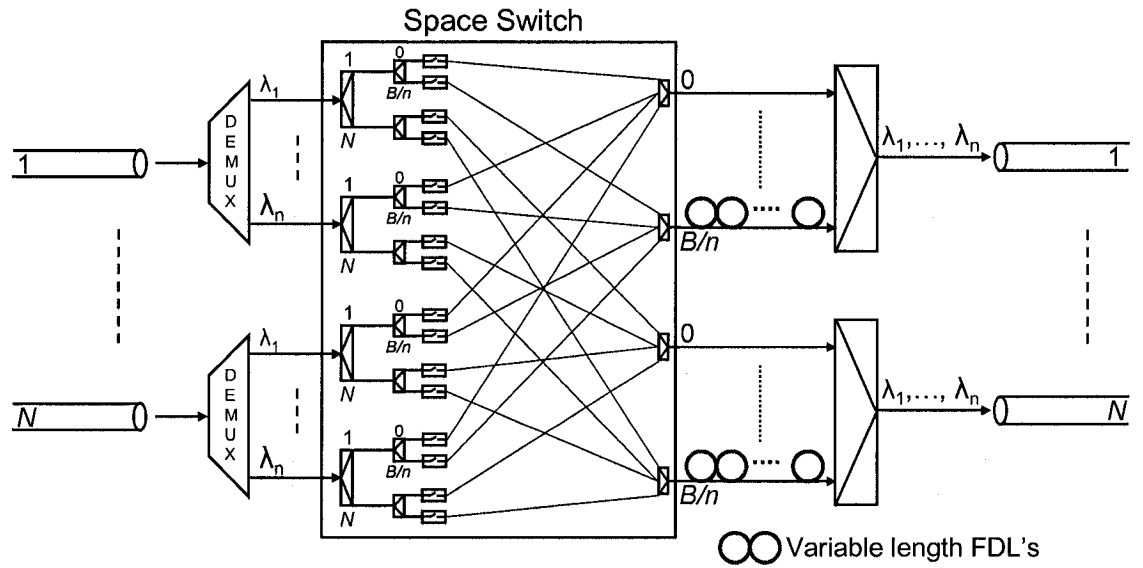


Figure 2.13: Space switch with optical buffers.

In this architecture, incoming wavelengths are demultiplexed and split N times to be directed to each output fiber. Each channel is then split a further B/n+1 times corresponding to the number of output fibers entering each combiner. These channels are sent to the space switch where the SOA gates control routing. If a contention arises in a time slot, contending packets can be directed to the FDL's where they are buffered until the contention has been resolved.

Although buffers reduce contentions and improve throughput, bundling accurate lengths of FDL's into a switch and developing an associated control algorithm makes buffered

switches undesirable in optical networks. However, as previously illustrated in Figure 2.11, the use of WC's negates the need for buffering. Figure 2.14 highlights this by juxtaposing the roles of buffers and WC's. In this case, two payloads (from different fibers) operating on the same wavelength request access to the same output fiber. In Figure 2.14(a), one packet is sent directly while the other is sent to a buffer before both are combined into the output fiber. In Figure 2.14(b) one packet is converted to a free wavelength before both are combined into the output fiber.

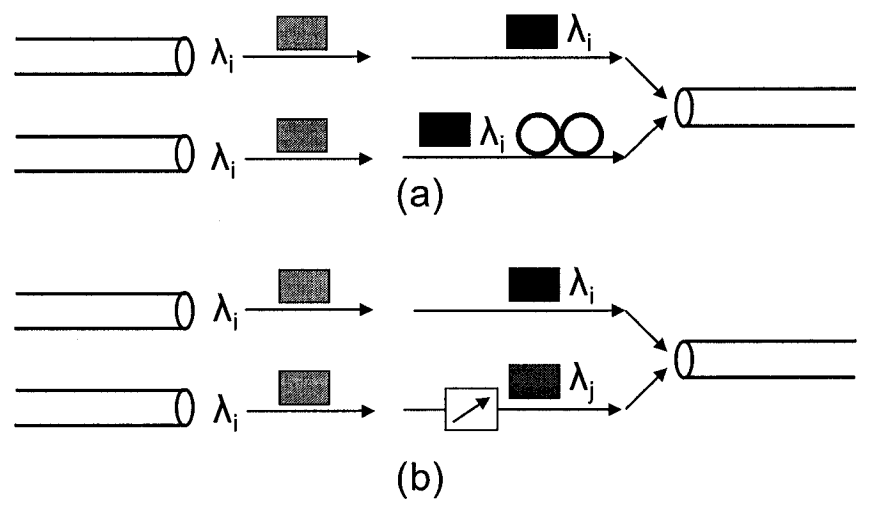


Figure 2.14: Buffering vs WC's for solving payload wavelength contentions. (a) Using a buffer. (b) Using WC's.

As space switches equipped with WC's do not require buffers, all following architectures are bufferless.

### 2.6.3 Single Per Channel (SPC)

This architecture has a dedicated WC for each wavelength channel output from the space switch [41] and is illustrated in Figure 2.15. The nN individual channels entering the switch are split N times to allow routing to each output fiber. Each resulting channel is split another n times and directed towards the n-1 WC's and the single direct line before being combined onto an output fiber. The direct line is not equipped with a WC as there is always at least one wavelength not requiring conversion.

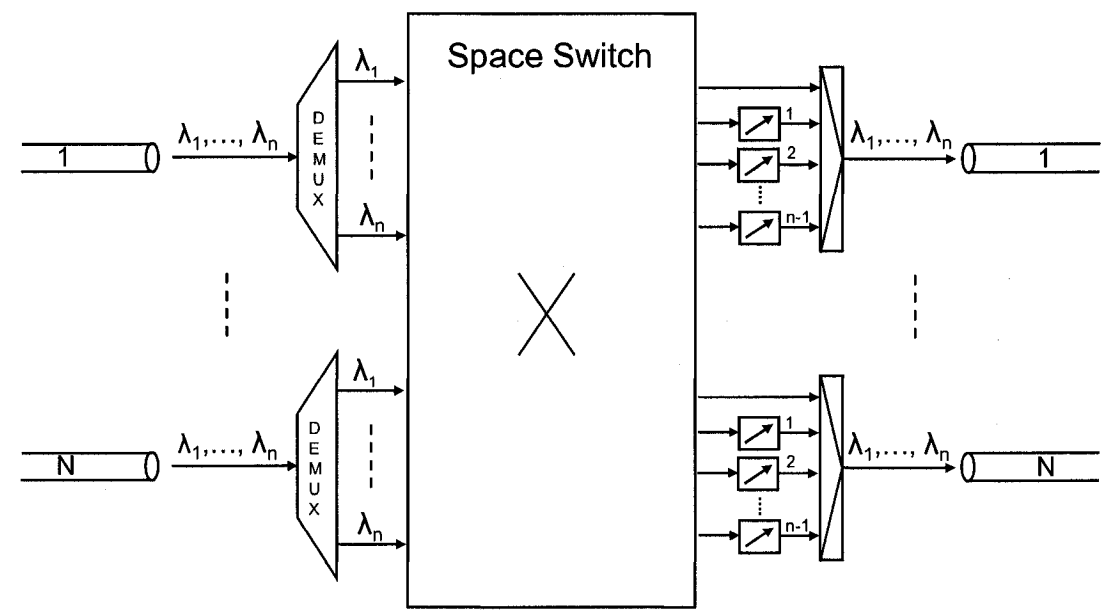


Figure 2.15: Single Per Channel architecture. The  $1 \times N$  and  $1 \times n$  splitters as well as optical gates are not included in the space switch block for clarity.

Assuming that each WC can convert from one wavelength to any other in the wavelength set, there are up to n output packet payloads on n wavelengths at the output fiber. If more than n packets are directed to an output fiber, n will be forwarded while the remaining will be dropped.

With a dedicated WC for each output wavelength channel, (n-1)N WC's are required in the space switch. This will always yield the optimal throughput by allowing the maximum number of conversions to take place. However the large numbers of WC's in this architecture make it highly cost-ineffective as often not all WC's are required at the same time.

### 2.6.4 Shared Per Node (SPN)

In the SPN architecture, a bank of L WC's are shared amongst all input wavelength channels. By appropriately configuring the switching matrix, any contending input channel can access this bank. The SPN architecture is shown in Figure 2.16.

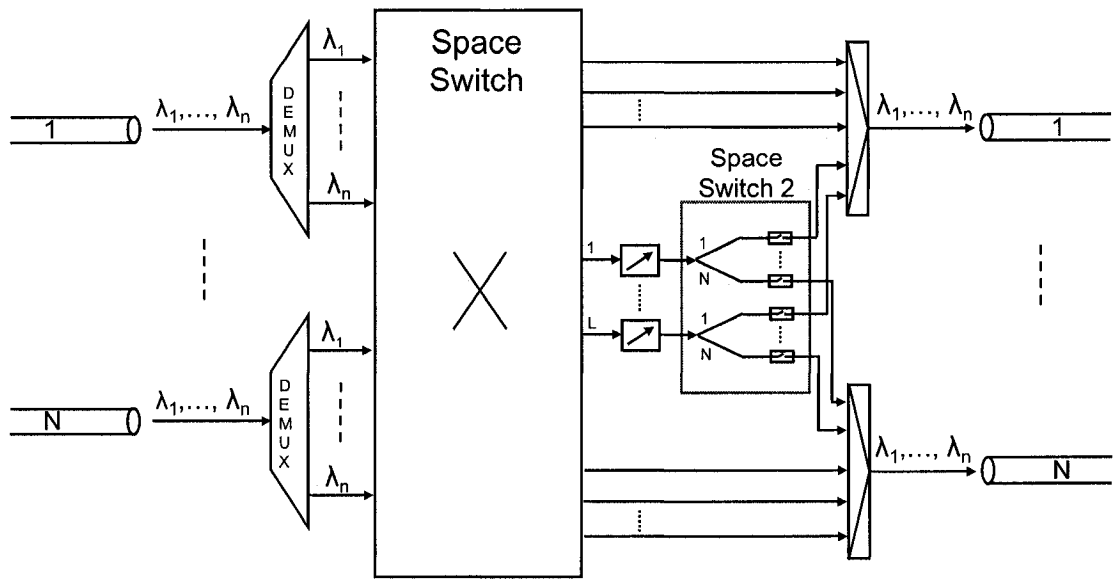


Figure 2.16: Shared Per Node architecture.

This architecture requires the least number of WC's to achieve a required throughput threshold [41]. However, by sharing a bank of WC's, an additional set of splitters and SOA gates are needed to allow the wavelengths requiring conversion to be directed to the WC bank and to allow access to the output combiners. These extra components are illustrated in space switch 2 of Figure 2.16 and cause a system complexity increase and OSNR degradation.

### 2.6.5 Shared Per Output Fiber (SPOF)

Similar to the SPC architecture, this architecture shares WC's per output fiber as shown in Figure 2.17. Each output fiber has a set of L WC's and n-L direct lines combined into the combiner. L can vary from 0 (no conversion capability) to n-1 (complete set-SPC).  $1 \times N$  followed by  $1 \times n$  splitters are required (as per the SPC architecture) after decoding the wavelength from the input fibers. Wavelengths requiring conversion are sent to the output lines with WC's.

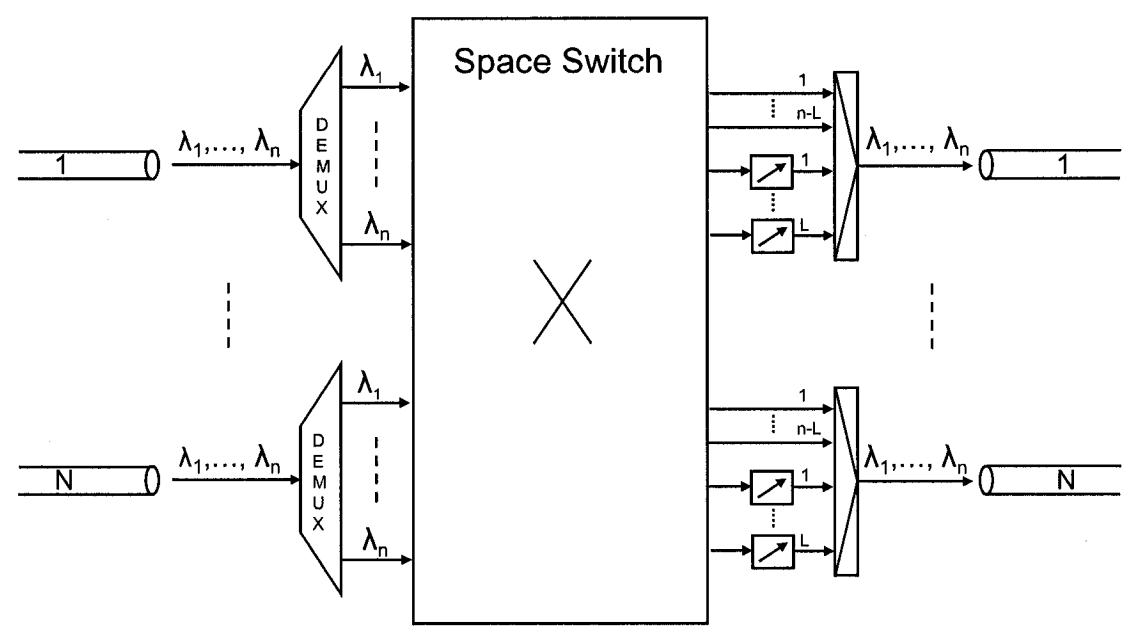


Figure 2.17: Shared Per Output Fiber architecture.

This architecture reduces the number of WC's required for a given throughput compared to the SPC architecture, but does not make as much savings as the SPN. However, the lower number of SOA gates required reduces the switch matrix complexity compared to SPN [42] and makes it attractive for the optical MPLS network. This architecture is assumed for the remainder of this thesis.

#### 2.7 Discussion

This chapter discussed several fundamental issues in implementing an optical MPLS network employing WDM encoded payloads and spectral OCDMA label codes. Payload wavelength contention resolution and label switching were shown to be essential packet processing stages in each NN of the core network. In the following chapters, we study the advantages of incorporating sets of realistic WC's in a NN space switch to improve data throughput, and demonstrate a spectral label switching system in the laboratory.

# 3 Wavelength Conversion: Techniques and Limitations

To analyse data throughput in the NN's of an optical MPLS network with WC's for payload wavelength contention resolution, it is important to understand the physical limitations of current wavelength conversion technologies. In addition, to perform label switching in the NN using spectral OCDMA labels, concurrent, multiple wavelength conversion is required. This is a significant extension to single wavelength conversion technology.

Many techniques have been shown to achieve all-optical wavelength conversion. Less common methods include injection locked Y-lasers, bistable lasers incorporating saturable absorbers and intensity modulated DBR lasers [43]. Cross-phase modulation (XPM) and four-wave mixing (FWM) in nonlinear fiber have also been demonstrated [44-46]. However, the most common techniques are XGM, XPM and FWM in an SOA [43, 47]. The advantages and physical limitations of these three common SOA based wavelength conversion techniques will be discussed in this chapter.

#### 3.1 XGM in an SOA

The simplest of all wavelength conversion methods, the XGM configuration requires one SOA and takes as inputs a data (control) signal  $\lambda_c$  and a continuous wave (CW) probe  $\lambda_p$ . The control and probe wavelengths can be launched in a co- or counter-propagating manner as shown in Figure 3.1(a) and (b). When the control signal goes ON, the SOA enters saturation, and the probe experiences little to no gain and is attenuated. When the control goes OFF, the probe experiences the full gain of the SOA and is amplified. This results in an inverted version of  $\lambda_c$  being impressed on  $\lambda_p$ . Besides its simplicity, XGM based converters are stable and polarization insensitive (with correct design) [43].

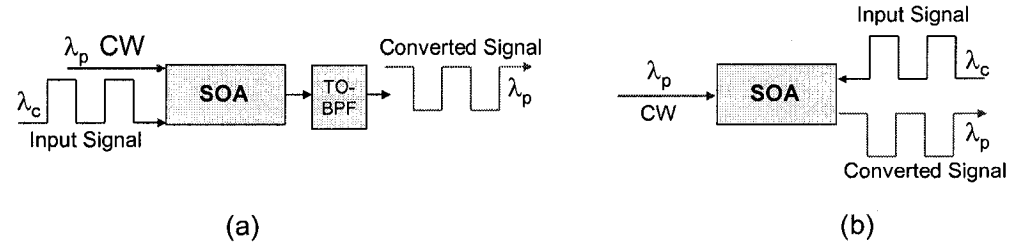


Figure 3.1: XGM in an SOA (a) co-propagating (b) counter-propagating configuration

A disadvantage of the co-propagating configuration is that it requires a tuneable optical band-pass filter (TO-BPF) at the SOA output to block the control signal. As a TO-BPF is tuned mechanically or thermally, it is difficult to build fast tuneable WC's using this scheme. Using the counter-propagating configuration, a TO-BPF is not required and conversion can be performed to the same wavelength. However, the maximum SOA modulation bandwidth of this configuration is often many times less than in a co-propagating scheme [48], strongly limiting maximum bit-rates.

Additional drawbacks to the XGM method include the inverted pulses having a red-shifted chirp on the leading edge and a blue-shifted chirp on the trailing edge. This chirp results in pulse broadening when used with anomalous dispersion fibers, limiting transmission distance [48]. Furthermore, when converting to longer wavelengths (up conversion), there is an extinction ratio (ER) degradation. This limits the cascadability of SOA's using XGM. Finally, pattern dependent effects at high bit-rates comparable with the SOA dynamic bandwidth result in eye closure and appearance of an error floor for the converted data [49].

#### 3.2 XPM in an SOA

The XPM method uses two SOA's in a Mach-Zender Interferometer (MZI) configuration shown in Figure 3.2. The control signal is injected into one arm and modulates the phase of that arm. The MZI configuration converts this phase modulation to amplitude modulation in the CW probe [27, 47].

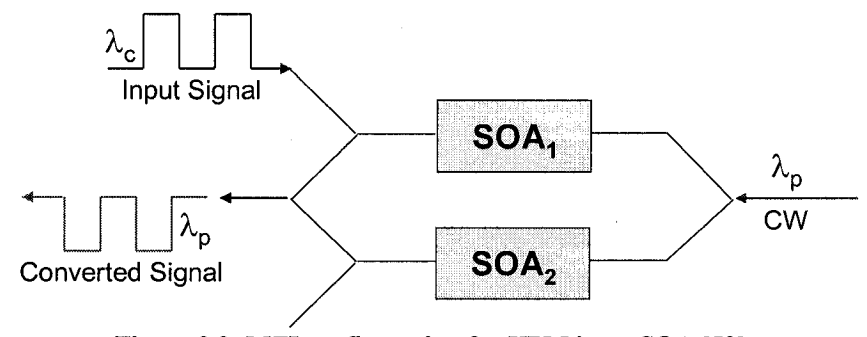


Figure 3.2: MZI configuration for XPM in an SOA [50].

The advantages of the XPM method include:

• Non-inverted data can be obtained on the probe signal.

- Conversion to the same wavelength can be performed.
- Wavelengths can be up converted without ER degradation.
- Converted pulses have a narrower spectrum than for XGM (although a small chirp is still observed), allowing transmission over longer distances [27].
- XPM conversion is more power efficient than XGM conversion [43].
- 2R regeneration is more readily observed.

The main drawbacks of this method are its complexity and stability. It is very difficult to assemble a stable MZI configuration with two SOA's without on-chip integration. Additionally, as for XGM, pattern dependent limitations arise at high bit-rates.

#### 3.3 FWM in an SOA

As shown in Figure 3.3, FWM takes a pump wave with angular frequency  $\omega_p$  and a control wave  $\omega_c$  as inputs. Using the 3<sup>rd</sup> order nonlinear susceptibility  $\chi^{(3)}$ , a new wave  $\omega_n$  is generated.  $\omega_n$  is a linear combination of the angular frequencies of the pump and control waves, such that  $\omega_n = 2\omega_p - \omega_c$ . Furthermore, the intensity of  $\omega_n$  is proportional to the products of the interacting waves [27, 50].

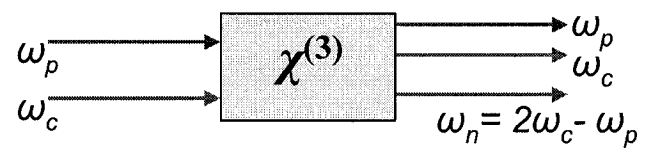


Figure 3.3: FWM in an SOA. Inputs are pump wave  $\omega_p$  and control wave  $\omega_c$  [50].

FWM is the only conversion mechanism to offer full range (strict and digital) transparency [51]. In this mechanism, phase and amplitude information is preserved, and digital signals of any bit rate up to a certain limit can be accommodated by the system. As the response speed of  $\chi^{(3)}$  is extremely fast (100THz demonstrated in [52]), high bitrate, wide-bandwidth conversion is possible, and operation in the order of Tb/s is expected. Another advantage of the FWM method is that chirp is almost non-existent [50].

Several disadvantages of this method include:

• The pump and control waves must have the same polarization.

- For negative detuning  $(\omega_p < \omega_c)$ , the conversion efficiency is lower than for positive detuning.
- The conversion efficiency of this method is much lower than XGM/XPM schemes.
- Phase matching must be considered, but is not as critical as for  $2^{nd}$  order nonlinear wave mixing, as  $\omega_p$ ,  $\omega_c$  and  $\omega_n$  are all in the same wavelength band [50].

#### 3.4 Discussion

All conversion techniques have limited capabilities. For example, a WC may have limited range, in that it can convert from one input wavelength to a limited subset of output wavelengths. In an XGM scheme, down conversion may only be possible due to the ER penalty associated with up conversion. This limitation must be taken into account when modelling data traffic flow in a NN equipped with realistic WC's.

Although XGM and XPM "optical gating" methods have limited transparency compared to FWM, their higher conversion efficiency makes them more attractive for implementation in current systems. Given that spectral labels are switched at a fraction of the payload switching rate, the simplicity of XGM makes it ideal for initial label switching system demonstrations. In particular, the counter-propagating configuration is particularly attractive as it allows for conversion between labels containing several common wavelengths. When much higher switching rates are required (>100Gb/s), FWM will most likely be the technology of choice.

# 4 Data Throughput Analysis in an Optical MPLS Network Node with Wavelength Converters

In this chapter, we model traffic flow through a NN in an optical MPLS network. The objective is to develop a software package that allows us to determine the advantages of incorporating WC's (for payload wavelength contention resolution) into the space switch of a NN.

To this point, extensive work has been performed by various research groups investigating wavelength contention resolution in WDM networks. Beginning in 1997, research from the Technical University of Denmark focussed on the throughput improvement in a WDM packet switch. Complete sets of full-range WC's¹ and FDL optical buffers were used to negate wavelength contentions under a bursty traffic assumption [8, 40, 53]. This work was followed by a multitude of papers from the University of Rome La Sapienza. In these papers, the authors removed the FDL buffers and rigorously modelled reduced sets of full-range WC's in the various bufferless switch configurations (discussed in Section 2.6) under uniform traffic [6, 41, 42, 54]. Further research focussed on reduced sets of limited-range WC's in a bufferless switch under the same traffic assumption. The authors presented a random scheduling algorithm and a first available algorithm (FAA) to solve the wavelength matching problems [7, 55]. The work of this thesis improves on the previous analyses by accounting for both bursty traffic and reduced sets of limited-range converters, as well as presenting new wavelength matching algorithms in the space switch.

The network we consider uses spectral OCDMA (m-sequence) labels with WDM coded payload as presented in Section 2.3.4.3. Inside each NN, the space switch and WC's are organised in a bufferless SPOF architecture. Each of the N input fibers carries n wavelengths. Each output fiber has a bank of L WC's and n-L direct fibers combined into the passive coupler. L can vary from 0 (no conversion capability) to n-1 (SPC complete set). The space switch requires  $n^2N^2$  gates. Packet arrivals to the NN are

<sup>&</sup>lt;sup>1</sup> Explanation of full- and limited-range WC's are presented on the following page.

assumed to be slot synchronised. This "fine synchronisation" assumption allows for asynchronous operation as complete packets do not have to be synchronised [34]. A detailed illustration of this architecture is shown in Figure 4.1 with the space switch connections included.

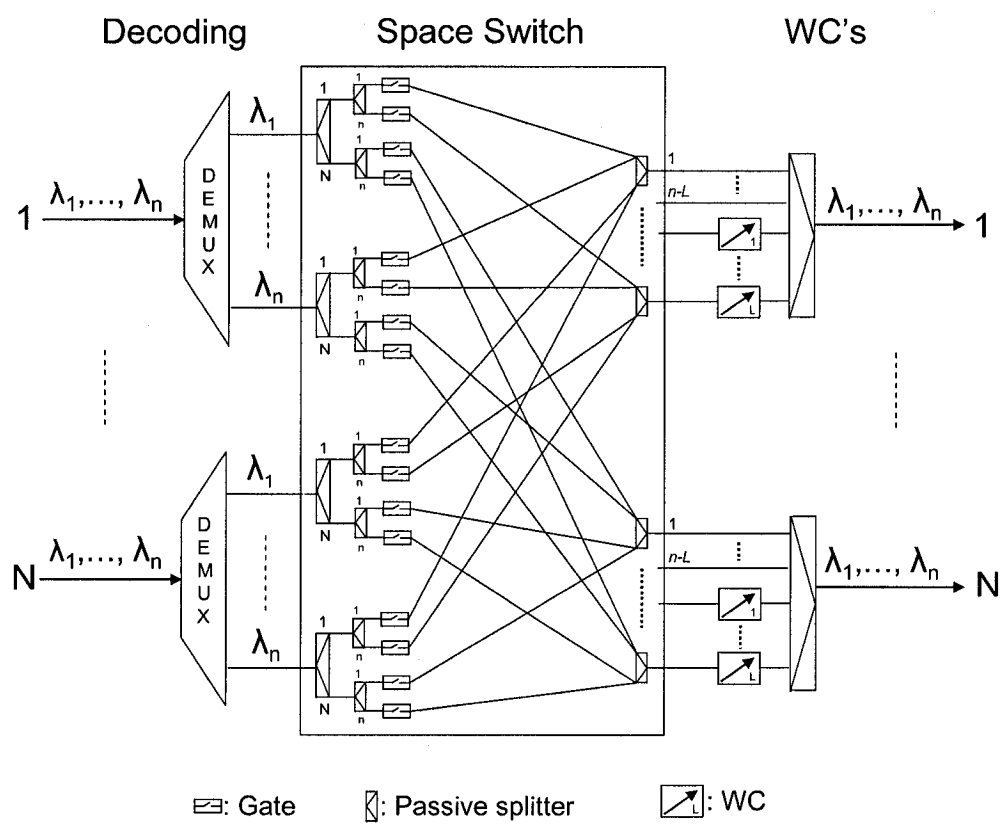


Figure 4.1: General SPOF architecture showing physical space switch connections.

Throughput this chapter, various nomenclatures are used to classify different switch and WC models. These are:

- Complete and Reduced sets of WC's: A complete set of WC's means there are *n*-1 WC's per output fiber, as in the SPC architecture. A reduced set implies the number of WC's per output fiber can range from 0 to *n*-1 (as per SPOF).
- Full-Range and Limited-Range WC's (FRWC, LRWC): As discussed in Chapter 3, a realistic WC may not be able to convert from an input wavelength to all others in the set. A LRWC takes this into account. The specific constraint on the range of a LRWC is given on a per case basis. A FRWC is the ideal case and is used in Sections 4.1 and 4.2 to develop closed form expressions for traffic throughput. A study with reduced sets of LRWC's is conducted in Section 4.3.

# 4.1 Single Slot (Uniform) Analysis of Traffic Flow in a Bufferless Space Switch with Reduced Sets of FRWC's

# 4.1.1 Introduction and Assumptions

In this section, the following assumptions are made:

- All WC's have full-range conversion capability. That is, we model FRWC's.
- Data traffic flow is uniformly distributed (non bursty). We consider each slot independently of the others in a packet payload. Consequently, a single slot analysis is performed.
- The number of payload wavelengths entering the NN (active sources) is modelled by a Bernoulli Random Variable (RV) with probability of being active ρ.
- Traffic is symmetric. Each active source has the same probability (1/N) to be directed to any output line.
- Correlation between traffic on various wavelengths is neglected. If traffic from the same source is split into several wavelength channels (multicasting) this assumption is not valid. In this analysis, traffic on different channels is assumed to originate from different sources.
- The bufferless switch configuration means that if greater than n packets are directed at a given output fiber, only n will be selected at random for transmission.

## 4.1.2 Equivalent Model

For the purposes of modelling, the general SPOF switch in Figure 4.1 is redrawn as an equivalent switch shown in Figure 4.2.  $\lambda_i^K$  refers to a payload on wavelength i from input fiber K, and wavelength set i ( $WS_i$ ) refers to all payloads on wavelength i.

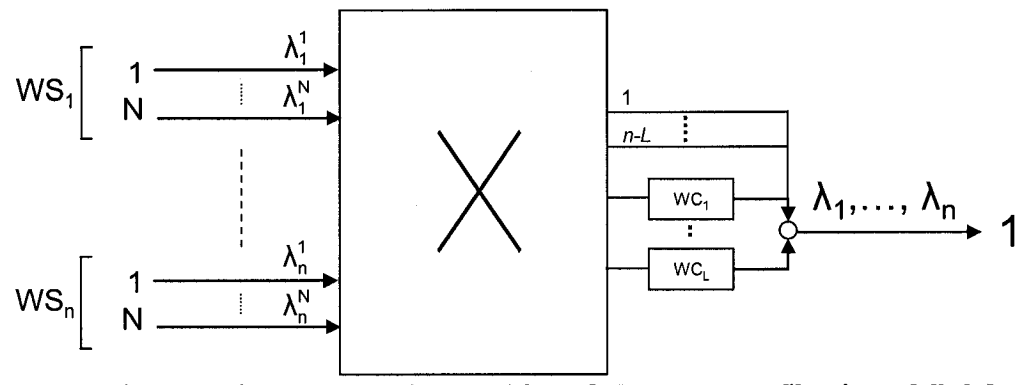


Figure 4.2: Equivalent switch re-drawn for modelling. Only one output fiber is modelled due to the symmetric traffic assumption.

In this Figure, there are nN equivalent input channels. These channels have been grouped by their wavelength into WS's rather than by their input fiber as in Figure 4.1. As each channel carries load  $\rho$ , the load directed at one output fiber must be  $\rho/N$  due to the symmetric traffic assumption.

Given nN Bernoulli sources, each having a probability of being active  $\rho/N$ , the probability of the number of active sources (channels) J in a given time slot can be determined. J is a Binomial RV, and  $J \sim B[nN, \rho/N]$ . If J > n, only n sources will be directed to the output fiber (no buffering).

If there are J active sources in a timeslot, there can be M wavelength contentions, where M is a RV defined by  $M \in [0, \min(J-1, n-1)]$ . A contention will occur when there is greater than one active source in any given WS. For example, if in  $WS_I$ , there are 4 active sources, there will be 3 contentions (as all sources in a given WS operate on the same wavelength). We seek to determine the probability of m contentions given m active sources, m (m).

There are L FRWC's on each output fiber, where  $L \in [0, n-1]$ . Based on the symmetric traffic assumption, only one output fiber is modelled as this is representative of the entire switch.

#### 4.1.3 Theoretical Formulation

To measure the performance of this system, the packet success probability (PSP) metric is used and defined as

$$PSP = \sum_{j=0}^{nN} \frac{\text{#successfully transmitted sources given } j \text{ active sources}}{j} P(J=j) \quad (4.1)$$

Using the uniform traffic assumption, the probability that j sources are active is given by the Binomial Distribution

$$P(J=j) = \binom{nN}{j} \left(\frac{\rho}{N}\right)^{j} \left(1 - \frac{\rho}{N}\right)^{nN-j} \tag{4.2}$$

The number of successful transmissions given j active sources is defined as

$$n - \overline{\lambda}_{j} \tag{4.3}$$

where  $\overline{\lambda}_j$  represents the mean number of free wavelengths at the output given j active sources, and thus n minus this value is the number of used wavelengths since each output fiber can carry n different wavelengths without buffering.  $\overline{\lambda}_j$  is determined by summing over the probabilities of the number of contentions occurring (m) given j active sources, and multiplying by the resulting number of free wavelengths. That is,

$$\overline{\lambda}_{j} = \sum_{m} P(M = m | J = j) \lambda_{j,m}$$
(4.4)

where  $\lambda_{j,m}$  is the number of free wavelengths at the output fiber given j active sources and m contentions. This value depends on j, m, and the number of contentions that can be resolved by the set of WC's, L. Thus  $\lambda_{j,m}$  is defined piecewise as

$$\lambda_{j,m} = \begin{cases} n-j & ; j \le n \cap m \le L \\ n-(j-m+L); j \le n \cap m > L \\ 0 & ; j > n \cap m \le L \\ m-L & ; j > n \cap m > L \end{cases}$$

$$(4.5)$$

To understand (4.5), recall that the number of free wavelengths is n minus the number of used wavelengths. For example, when  $j \le n$  and there are more WC's available than contentions ( $L \ge m$ ), all contending wavelengths will be converted to free wavelengths

and the number of used wavelengths will be j. Thus n-j wavelengths will be free. When there are more contentions than WC's (m > L), there will be j-m+L used wavelengths at the output. When j > n, the same equations as before apply, except j has been replaced by n as a maximum of n wavelengths are accepted by the output fiber.

By substituting (4.5) into (4.4), a single expression for  $\overline{\lambda}_i$  is given by

$$\overline{\lambda}_{j} = nI(j=0) + \sum_{m=0}^{\min(L,j-1)} P(M=m | J=j)(n-j).I(1 \le j \le n) 
+ \sum_{m=L+1}^{j-1} P(M=m | J=j)(n-(j-m+L)).I(1 \le L+1 < j \le n) 
+ \sum_{m=L+1}^{n-1} P(M=m | J=n)(m-L).I(j>n)$$
(4.6)

where  $I(\zeta)$  is the indicator function, and equals 1 for  $\zeta$  TRUE, 0 for  $\zeta$  FALSE.

At this stage, the only unknown in the expression for PSP is the conditional probability P(M = m | J = j) for all values of m and j. We determine these values by defining a conditional probability matrix for the number of fibers N and number of wavelengths n,  $C_{N,n}$ , where each element  $C_{N,n}(j,m) = P(M = m | J = j)$ .

# 4.1.4 Computing the conditional probability matrix $C_{N,n}$

Before computing the conditional probability matrix  $C_{N,n}$ , we determine a conditional combinations matrix,  $K_{N,n}$ .  $K_{N,n}(j,m)$  refers to the number of ways (combinations) m contentions can occur given j active sources. Recalling that  $m \le j-1$ , we can eliminate many unknown elements in this matrix by setting them to 0, resulting in the lower diagonal matrix shown in (4.7). The value of the element in row j, column m,  $K_{N,n}(j,m)$ , corresponds to the number of "legal" ways (combinations) m contentions can occur given j active sources.

$$K_{N,n} = \begin{bmatrix} m & 0 & 1 & \cdots & n-1 \\ 1 & K(1,0) & 0 & \cdots & 0 \\ 2 & K(2,0) & K(2,1) & \ddots & \vdots \\ \vdots & \vdots & \ddots & 0 \\ n-1 & K(n-1,0) & K(n-1,2) & \cdots & 0 \\ n & K(n,0) & K(n,2) & \cdots & K(n,n-1) \end{bmatrix}$$

$$(4.7)$$

Each element (j,m) in the probability matrix  $C_{N,n}$  is evaluated by taking the corresponding element from  $K_{N,n}$  and dividing it by the sum of all combinations in row j as shown in (4.8). This ensures all rows of  $C_{N,n}$  sum to one.

$$C_{N,n}(j,m) = \frac{K_{N,n}(j,m)}{\sum_{i=0}^{j-1} K_{N,n}(j,i)}$$
(4.8)

To determine the elements of  $K_{N,n}$ , we look first at the cases N=2 and N=3, which give strong insight into solving this problem.

#### 4.1.4.1 Case N = 2

When two fibers are input to the switch, each WS can have 0, 1 or 2 active sources at any time instant. Under this assumption, the numbers of ways that m contentions can occur given j active sources is given by:

$$K_{N=2,n}(j,m) = \left[ \binom{n}{m} \binom{n-m}{j-2m} I(j \ge 2m) \right] \left[ \prod_{i=1}^{m} \binom{j-2(i-1)}{2} \prod_{i=1}^{j-2m} \binom{j-1(i-1)}{1} \right]$$
(4.9)

The terms of (4.9) are explained as follows:

- $\binom{n}{m}$ : Given n WS's, select m of these to have 1 contention (2 active sources).
- $\binom{n-m}{j-2m}$ : There are (n-m) WS's available after selecting m previously. From these, select (j-2m) WS's to have 1 active source (0 contentions) and thus account for all the j active sources.

•  $I(j \ge 2m)$ : When j < 2m this function is zero. It ensures that only legal combinations will be accepted.

At this stage, the number of legal ways to have m contentions given j active sources has been found. However, the ordering of the active sources in each combination has not been accounted for. For example, consider N = 2, n = 3, j = 3, m = 1, with 2 active sources in WS<sub>1</sub> (say Source<sub>1</sub> and Source<sub>2</sub>), and 1 active source in WS<sub>2</sub> (say Source<sub>3</sub>). The terms in the first square brackets of (4.9) will give this as one combination. However, the combination where Sources<sub>2,3</sub> are active in WS<sub>1</sub> and Source<sub>1</sub> is active in WS<sub>2</sub> also causes one contention. This is accounted for in the final two terms of (4.9):

- $\prod_{i=1}^{m} {j-2(i-1) \choose 2}$ : This applies to the m WS's that have 1 contention (2 active sources). Initially there are j active sources. Select 2 of these for the 1<sup>st</sup> WS with 1 contention. For the 2<sup>nd</sup> WS, there are j-2 active sources left, and again select another 2. Continue this through all WS's having 2 active sources.
- $\prod_{i=1}^{j-2m} {j-1(i-1) \choose 1}$ : As before, except this applies to the j-2m WS's that have 1 active source (0 contentions).

# 4.1.4.2 Case N = 3

When N = 3, each WS can have 0, 1, 2 or 3 active sources at any time instant. Under this assumption, the number of ways m contentions can occur given j active sources is given by:

$$K_{N=3,n}(j,m) = \sum_{m_2=0}^{\lfloor m/(N-1)\rfloor} \left\{ \begin{bmatrix} n \\ m_2 \end{bmatrix} \binom{n-m_2}{m-2m_2} \binom{n-m+m_2}{j-2m+m_2} I(j \ge 2m-m_2) \end{bmatrix}.$$

$$\left[ \prod_{i=1}^{m_2} \binom{j-3(i-1)}{3} \prod_{i=1}^{m-2m_2} \binom{j-2(i-1)-3m_2}{2} \prod_{i=1}^{j-2m+m_2} \binom{j-1(i-1)-2(m-2m_2)-3m_2}{1} \right] \right\}$$

$$(4.10)$$

where  $\lfloor \cdot \rfloor = floor(\cdot)$ .

In (4.10), the same procedure has been performed for the case N=2, except there is a sum over a new variable  $m_2$ , which defines the number of WS's with 2 contentions. The value  $m-2m_2$  is the number of WS's with 1 contention and will be denoted  $m_1$  for simplicity (obviously for m contentions,  $m=2m_2+1m_1$ ). Note that regardless of N,  $m_1$  is always a dependent variable.

#### 4.1.4.3 General N

For the general case of N input fibers to the switch, the expression to determine  $K_{N,n}(j,m)$  is given in (4.11)

$$K_{N,n}(j,m) = \sum_{m_{N-1}=0}^{m_{N-1},u_p} \cdots \sum_{m_z=0}^{m_{z,u_p}} \cdots \sum_{m_2=0}^{m_{z,u_p}} \left\{ \binom{n}{m_{N-1}} \left[ \prod_{i=2}^{N-2} \binom{n-\sum_{k=i+1}^{N-1} m_k}{m_i} \right] \left[ \binom{n-\sum_{k=2}^{N-1} m_k}{m_i} \right] I(N > 2) \right\}$$

$$\left( \binom{n-m+\sum_{k=2}^{N-1} (k-1)m_k}{j-2m+\sum_{k=2}^{N-1} (k-1)m_k} I\left( j \ge 2m-\sum_{k=2}^{N-1} (k-1)m_k \right) \cdot \left[ \prod_{i=1}^{m_{N-1}} \binom{j-N(i-1)}{N} \right] \right)$$

$$\prod_{i=1}^{m_{N-2}} \left( j-(N-1)(i-1)-\sum_{z=N-1}^{N-1} (z+1)m_z \right) \cdots \prod_{i=1}^{m_1} \left( j-2(i-1)-\sum_{z=2}^{N-1} (z+1)m_z \right)$$

$$\prod_{i=1}^{m_0} \left( j-1(i-1)-\sum_{z=1}^{N-1} (z+1)m_z \right) \right\}$$

$$\left\{ (4.11) \right\}$$

For (4.11), the bounds in the sums and products are defined as:

Bounds in the Sums 
$$\begin{cases} m_{N-1,up} = \left\lfloor \frac{1}{N-1} m \right\rfloor \\ \vdots \\ m_{x,up} = \left\lfloor \frac{1}{x} \left( m - \sum_{y=x+1}^{N-1} y m_y \right) \right\rfloor \\ \vdots \\ m_{2,up} = \left\lfloor \frac{1}{2} \left( m - \sum_{y=3}^{N-1} y m_y \right) \right\rfloor \end{cases}$$

$$\begin{cases} m_1 = m - \left( \sum_{y=2}^{N-1} y m_y \right) I(N > 2) \\ m_0 = j - 2m + \sum_{y=1}^{N-1} (y - 1) m_y \end{cases}$$

$$(4.12)$$

Having found  $K_{N,n}$  for each value of j and m,  $C_{N,n}$  is determined from (4.8). This allows the calculation of  $\overline{\lambda}_j$  using (4.6). Finally packet loss probability (PLP) can be found from PSP using (4.1)-(4.3):

$$PLP = 1 - PSP = 1 - \sum_{j=0}^{nN} \frac{n - \overline{\lambda}_j}{j} P(J = j)$$
 (4.13)

At this stage, we have a complete theoretical description of uniform (single slot) data traffic flow in a switch employing reduced sets of FRWC's in an SPOF architecture. Given values of N and n, equations (4.1)-(4.13) can be implemented in a computer program. By varying the load  $\rho$ , PLP versus  $\rho$  curves can be obtained for various values of FRWC's.

#### 4.1.5 Monte-Carlo Simulation and Model Verification

To verify the model presented in this section, Monte-Carlo (MC) numerical simulations of uniform traffic flow through the SPOF switch are performed. The flowchart for the MC algorithm with S trials given N, n and  $\rho$  is shown in Figure 4.3. In this figure, two subroutines are used; The "WS Selection subroutine" determines what WS each source belongs to, and the "Output Sources subroutine" determines how many sources can reach

the output fiber given the number of FRWC's. The flowcharts for these subroutines are illustrated in Figure 4.4(a) and (b) respectively.

By running this algorithm for multiple load values, we determine the validity of the theoretical model.

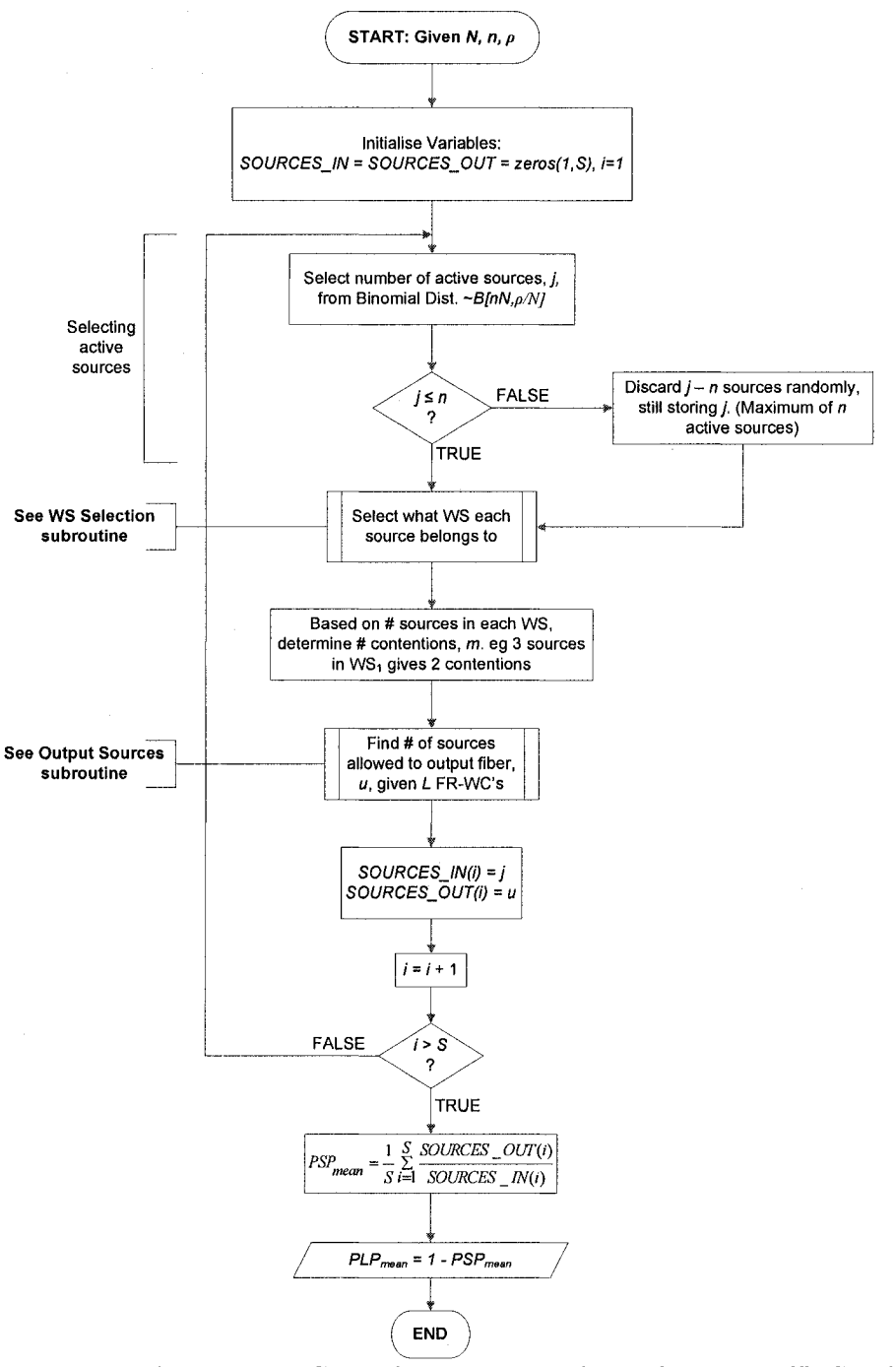


Figure 4.3: Flowchart to implement MC algorithm and numerically simulate traffic flow in a SPOF switch. The WS Selection and Output Sources subroutines are illustrated in Figure 4.4.

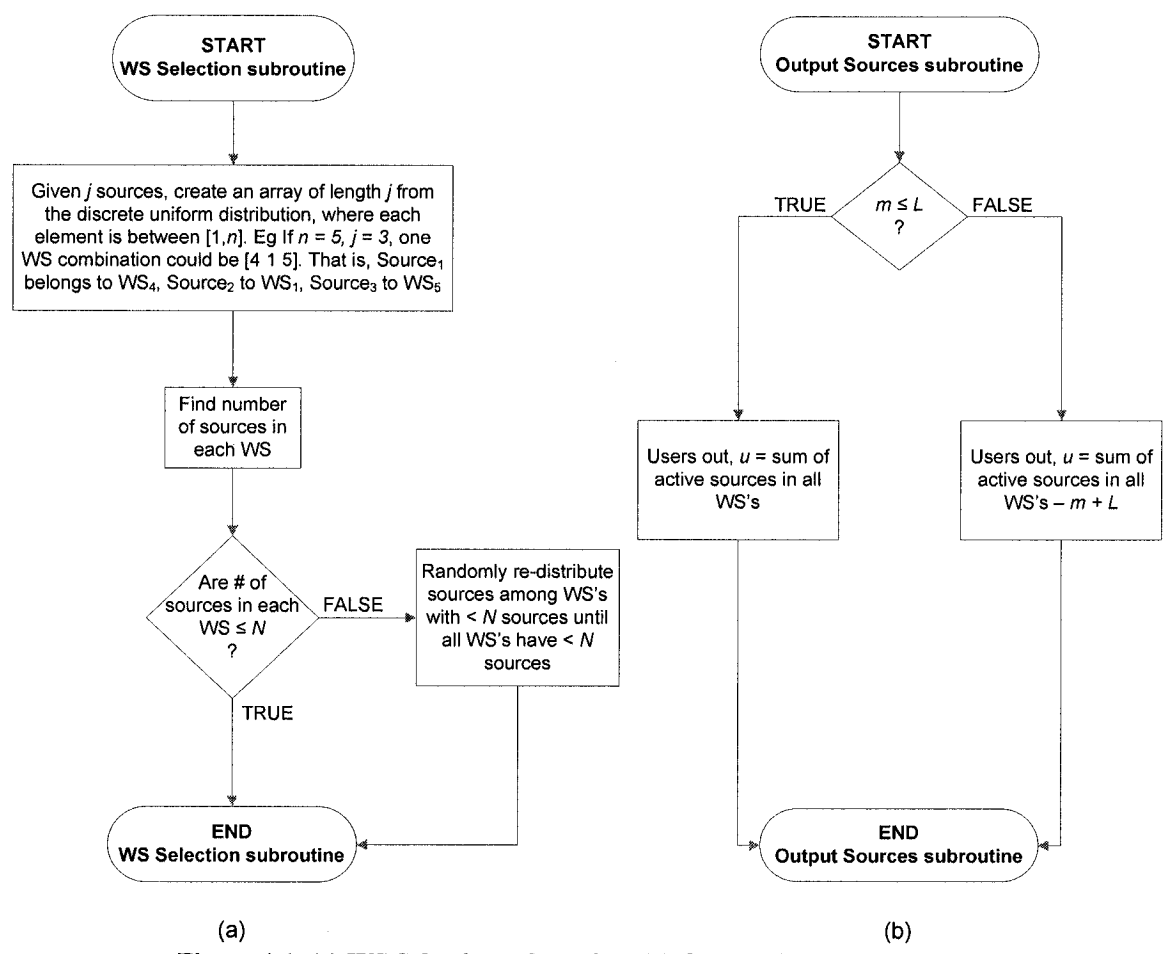


Figure 4.4: (a) WS Selection subroutine. (b) Output Sources subroutine.

#### 4.1.6 Results

By plotting PLP against load, the results of the theoretical analysis (solid lines) and MC simulations (crosses) in modelling uniform data traffic flow in a switch with reduced sets of FRWC's are found. The various scenarios considered and their corresponding plots are indicated in Table 4.1. The number of FRWC's is varied from 0 to n-1 and S=30,000 trials are used for all MC simulations.

Table 4.1: Uniform traffic switch scenarios modelled. For each scenario, the corresponding plots are given.

Number of fibers Wavelengths per fiber Figure			
4	7	Figure 4.5	
4	15	Figure 4.6	
4	31	Figure 4.7	
8	15	Figure 4.8	
8	31	Figure 4.9	

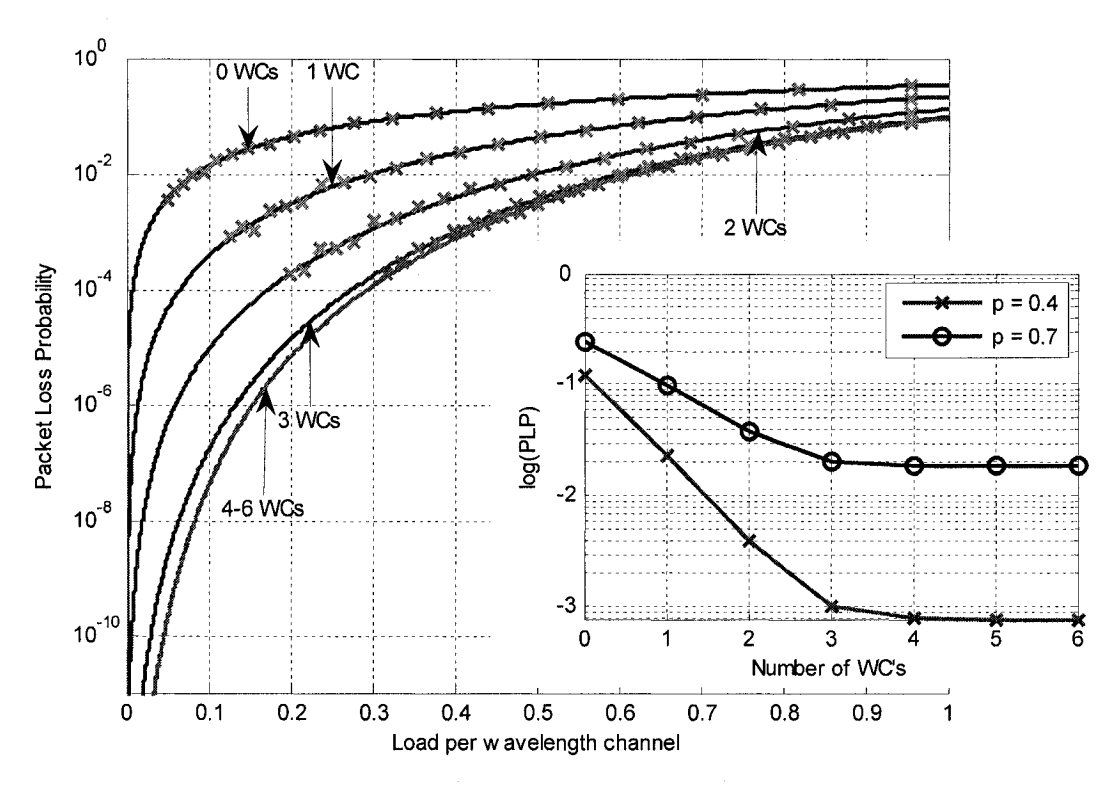


Figure 4.5: PLP vs load for a 4×4 switch with 7 wavelengths per fiber with reduced sets of FRWC's under uniform traffic. Inset: PLP vs WC's at a load of 0.4 and 0.7.

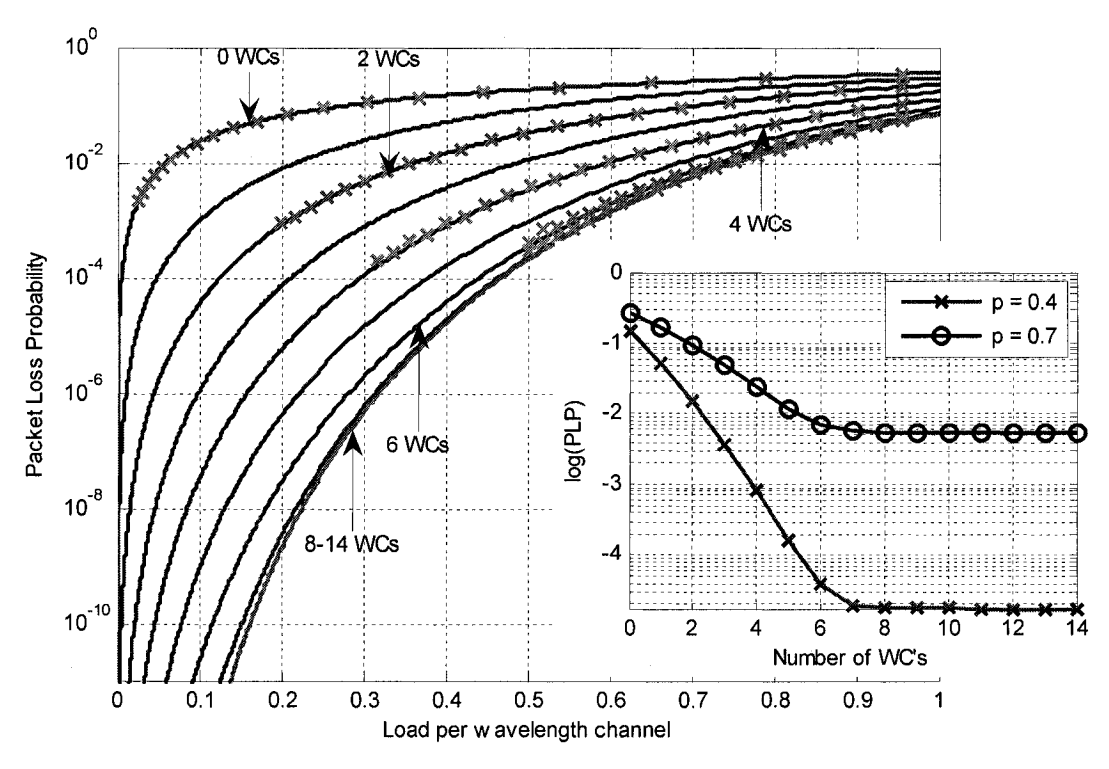


Figure 4.6: PLP vs load for a 4×4 switch with 15 wavelengths per fiber with reduced sets of FRWC's under uniform traffic. Inset: PLP vs WC's at a load of 0.4 and 0.7.

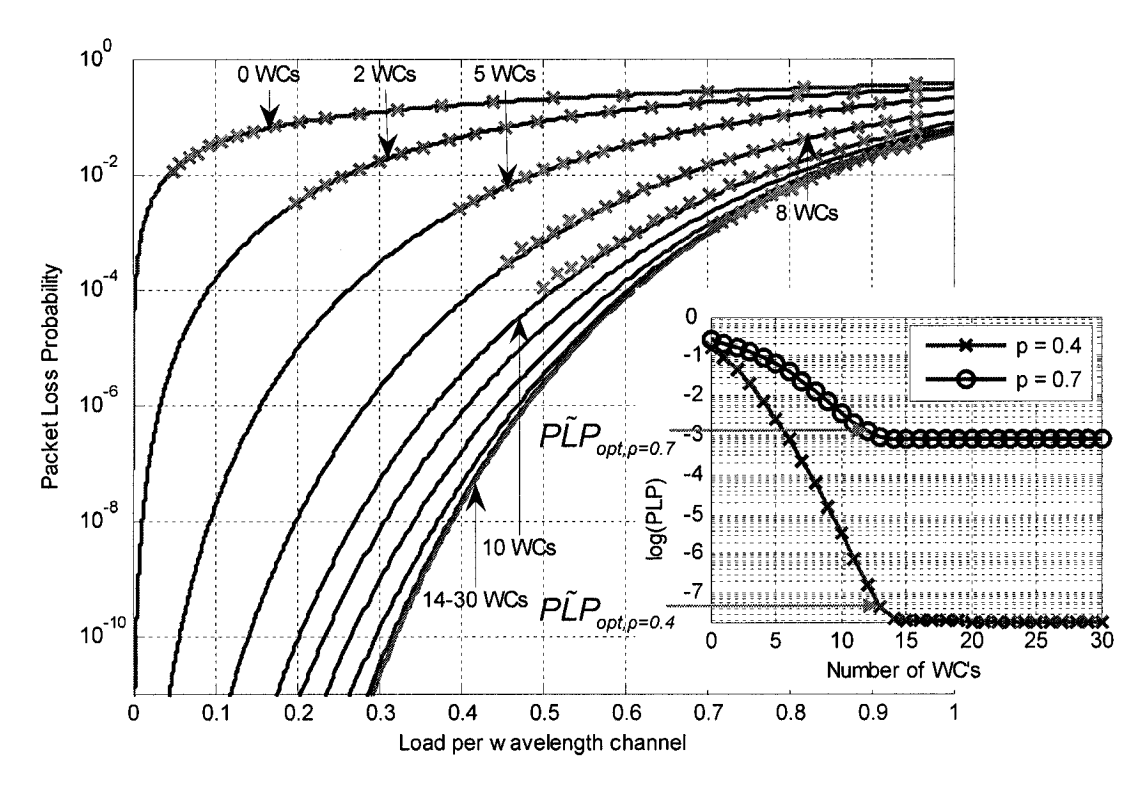


Figure 4.7: PLP vs load for a 4×4 switch with 31 wavelengths per fiber with reduced sets of FRWC's under uniform traffic. Inset: PLP vs WC's at a load of 0.4 and 0.7.

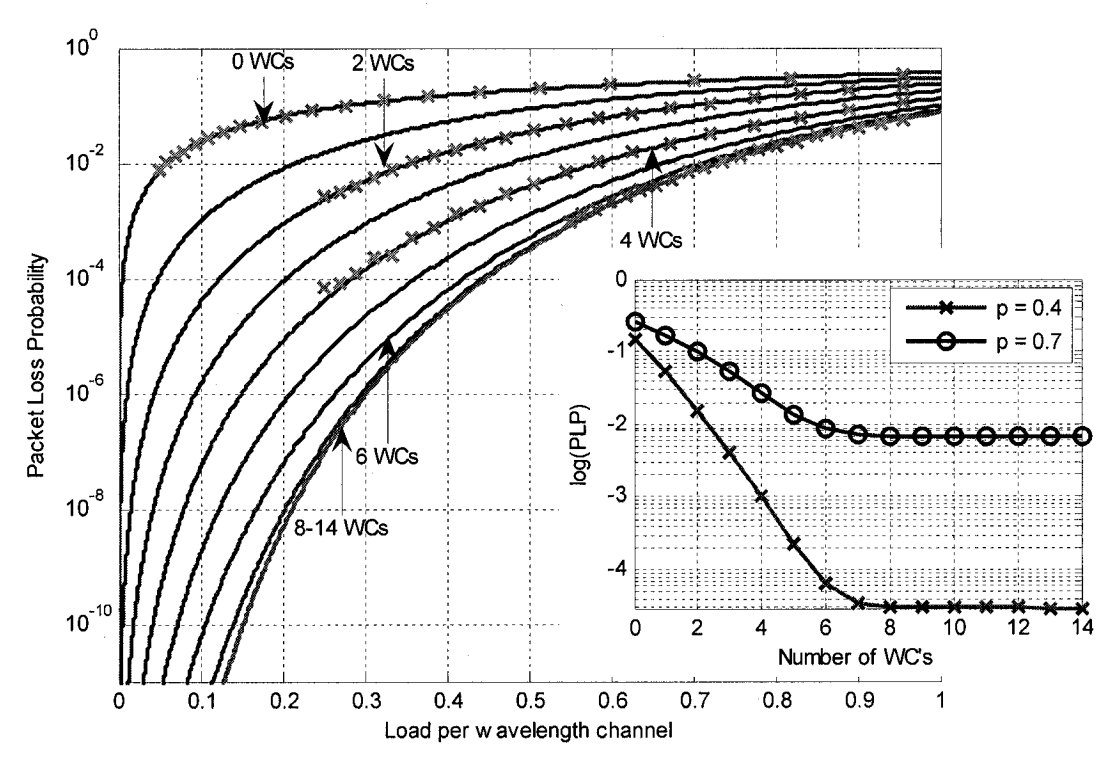


Figure 4.8: PLP vs load for an 8×8 switch with 15 wavelengths per fiber with reduced sets of FRWC's under uniform traffic. Inset: PLP vs WC's at a load of 0.4 and 0.7.

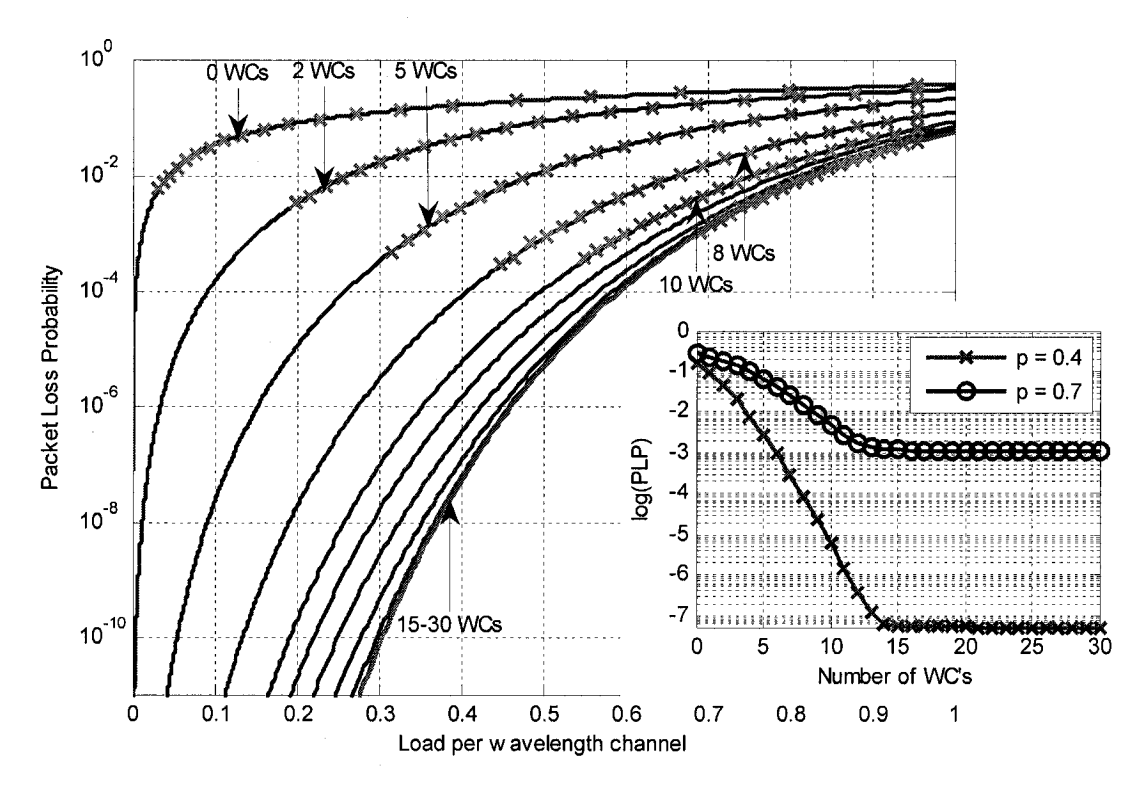


Figure 4.9: PLP vs load for an 8×8 switch with 31 wavelengths per fiber with reduced sets of FRWC's under uniform traffic. Inset: PLP vs WC's at a load of 0.4 and 0.7.

#### 4.1.7 Observations and Discussion

In the above plots, the MC trials agree well with the theoretical PLP results. In all plots, a PLP reduction by employing sets of FRWC's in an SPOF architecture is clearly observed. Other important observations are summarised below:

- PLP is markedly improved at lower loads using WC's as observed in the insets of all plots. For example, the optimal PLP ( $PLP_{opt}$ ) for a complete set of FRWC's in Figure 4.7 at  $\rho = 0.4$  is four orders of magnitude lower than at  $\rho = 0.7$ .
- When the number of fibers in the switch, N, is increased (for constant n), there are more possible packets in the switch (nN), but the load directed at one output fiber decreases (ρ/N). The values counter each other, and in moving from N = 4 to N = 8, very slight PLP degradation is observed. This is illustrated in Figure 4.7 for a 4×4 switch and Figure 4.9 for an 8×8 switch where n = 31.
- As *n* increases (for constant *N*), there are more packets in the switch and PLP increases when FRWC's are not used. However, PLP decreases markedly when employing sets of FRWC's. In Figure 4.7 where 31 wavelengths are used, the

optimal PLP at  $\rho = 0.4$  is five orders of magnitude lower than that achieved with seven wavelengths in Figure 4.5.

#### 4.1.7.1 Discussion

In the theoretical development of this section, we considered that the number of contentions m could range from [0,j-1] for  $j \le n$ . However through simplification of the combination equations, it can be shown that for up to n wavelengths per fiber entering the switch, the maximum number of contentions occurring is

$$m_{\text{max}} = \left| n - \frac{n}{N} \right| \tag{4.14}$$

For  $m > m_{max}$ ,  $K_{N,n}(j,m)$  is zero. Thus for  $L = L_{opt} = m_{max}$  FRWC's per output fiber,  $PLP_{opt}$  will be obtained as with a complete set of n-1 FRWC's. However, at a given load, PLP values for switches with considerably fewer than  $m_{max}$  FRWC's often closely match the PLP when  $m_{max}$  FRWC's are used. We term this "near optimal PLP" ( $P\tilde{L}P_{opt}$ ), and say that the PLP for L FRWC's ( $PLP_L$ ) is nearly optimal if the difference between  $PLP_L$  and  $PLP_{opt}$  is of the same order as  $PLP_{opt}$ . In this case, we say  $L = \tilde{L}_{opt}$ . Given a load  $\rho$ , this can be expressed mathematically as

If 
$$\left[\log_{10}\left(PLP_L - PLP_{opt}\right)\right] = \left[\log_{10}\left(PLP_{opt}\right)\right]$$
 (4.15)

then  $P\tilde{L}P_{opt}$  is achieved using  $\tilde{L}_{opt}$  FRWC's at the given load.

For example, as shown in the inset of Figure 4.7, the 4×4 switch with 31 wavelengths has  $m_{max} = 23$ , but  $P\tilde{L}P_{opt}$  is achieved with 12 FRWC's at  $\rho = 0.7$ , and 13 FRWC's at  $\rho = 0.4$ . The values of  $\tilde{L}_{opt}$  and  $m_{max}$  for each switch configuration considered in this section are summarised in Table 4.2.

Table 4.2: Number of FRWC's required to reach optimal, and near optimal PLP.

N. sayo	n	Figure	$L_{opt} = m_{\rm max}$	$\tilde{L}_{opt,\rho=0.4}$	$ ilde{L}_{opt, ho=0.7}$
4	7	Figure 4.5	5	3	1
4	15	Figure 4.6	11	6	5
4	31	Figure 4.7	23	13	12
8	15	Figure 4.8	13	6	5
8	31	Figure 4.9	27	13	9

In summary, excellent data throughput improvements are made using sets of FRWC's, negating the need for optical buffers. By using reduced (rather than complete) sets, cost and complexity savings are made while maintaining optimal PLP.

# 4.2 Multiple Slot (Bursty) Analysis of Traffic Flow in a Bufferless Space Switch with Reduced Sets of FRWC's

A more realistic model of traffic flow through a switch employing FRWC's is one that accounts for bursty data traffic patterns [8]. In this context, bursty traffic refers to payloads containing varied numbers of slots, where the payload length corresponds to an underlying probability distribution. Using this bursty traffic assumption, the transmission success of the payload as a whole (comprising multiple slots) must be considered. Intuitively, the throughput results will be poorer than the single slot analysis of Section 4.1.

## 4.2.1 Bursty Traffic Arrival Process

A standard assumption is that the payload length (number of slots) is geometrically distributed with mean burst length  $\beta$  [8, 56]. If B is a Geometric RV denoting the packet length, then P(B=b) is given by

$$P(B=b) = \frac{1}{\beta} \left(1 - \frac{1}{\beta}\right)^{b-1}$$
 (4.16)

Using this assumption and further assuming the number of active sources in each slot is correlated to the number active in the previous slot, each of the nN possible input wavelengths can be modelled as an ON-OFF source as shown in Figure 4.10. In this figure,  $r_{01}$  is the probability of going from the OFF to ON state, while  $r_{10}$  is the probability of the reverse process. As discussed in [8, 57], the idle and active packet lengths of each user are geometrically distributed with means  $1/r_{01}$  and  $\beta$  respectively.

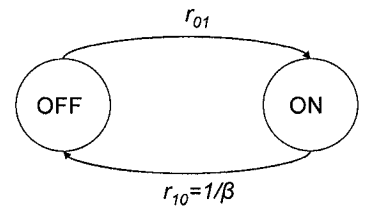


Figure 4.10: ON-OFF model of the nN identical bursty traffic sources to the switch.  $\beta$  is the mean burst length.

From the single slot analysis, the load of each source directed at one output fiber is  $\rho/N$ . Using Figure 4.10, the probability a source is active is given by [8] and must equal this value. That is

$$P(\text{source active}) = \frac{r_{01}}{r_{01} + r_{10}} = \frac{\rho}{N}$$
 (4.17)

Thus for a given load  $\rho$  and mean burst length  $\beta$ ,  $r_{01}$  is found from (4.17) as

$$r_{01} = \frac{\frac{\rho}{N} \frac{1}{\beta}}{1 - \frac{\rho}{N}} \tag{4.18}$$

To determine the state transition probabilities for the number of active sources in a time slot, recall that a maximum of nN sources can be active in any slot. For correlated traffic, given i sources are active in a time slot, the probability of having j sources active in the next slot can be found following the approach in [8]. This can alternatively be thought of as the probability of moving from state i to state j in two consecutive time slots. This probability,  $A_{i,j}$ , is shown in [8] to be

$$A_{i,j} = \sum_{k=\max(0,i-j)}^{\min(i,nN-j)} \left[ \binom{i}{k} r_{10}^{k} \left( 1 - r_{10} \right)^{i-k} \right] \left[ \binom{nN-i}{k-i+j} r_{01}^{k} \left( 1 - r_{01} \right)^{nN-k-j} \right]$$
(4.19)

Using (4.16)-(4.19) the correlated bursty arrival traffic is now fully modelled. The next stage of the model is to determine the PLP over a complete payload, where a similar method to the approach on wireless CDMA channel modelling in [56] is used.

#### 4.2.2 Finding the PLP

We begin by defining a variable  $\alpha_{ij}$  to denote the joint conditional probability of successful transmission of the current and previous slots given j active sources in the current slot and i active sources in the previous slot.  $\alpha_{ij}$  is complemented by defining  $\alpha_{0j}$  as the probability of success in the 1<sup>st</sup> slot given j active sources in that slot.

We further define  $R_b(j)$  as the probability of success of *all* slots in a packet up to and including the  $b^{th}$  slot, given j active sources in that slot. Looking at the first slot,  $R_I(j)$  is defined as

$$R_1(j) = \alpha_{0j} P(J=j) \tag{4.20}$$

where P(J=j) is found from (4.2).

For a payload containing b slots,  $R_b(j)$  is found recursively from  $R_{b-1}(j)$  as

$$R_{b}(j) = \sum_{i=0}^{nN} R_{b-1}(i) A_{i,j} \alpha_{ij}$$
 (4.21)

The only unknowns in (4.20) and (4.21) are  $\alpha_{0j}$  and  $\alpha_{ij}$ . From the work on uniform traffic, it follows that  $\alpha_{0j}$  is expressed as

$$\alpha_{0j} = \frac{n - \overline{\lambda}_j}{j} = \frac{n - \sum_{m} P(M = m \mid J = j) \lambda_{j,m}}{j}$$
(4.22)

where  $\lambda_{j,m}$  and the probabilities P(M = m | J = j) are found from (4.6) and (4.8).

Before evaluating  $a_{ij}$ , we assume that given the bufferless constraint, the number of successful transmissions in the  $(b-1)^{th}$  slot will not affect the number of successes in the  $b^{th}$  slot. Thus, when calculating  $a_{ij}$ , information from the previous slot need not be included. That is,

$$\alpha_{ii} = \alpha_{0i} \tag{4.23}$$

The probability of success of all slots up to and including slot b given j active sources in the  $b^{th}$  slot,  $R_b(j)$ , has now been determined. To remove the condition of j active sources in the  $b^{th}$  slot, we sum over all possible j sources to find  $R_b$ ,

$$R_b = \sum_{j=0}^{nN} R_b \left( j \right) \tag{4.24}$$

The overall PSP is found by summing (4.24) over all payload lengths multiplied by the probability of a payload of each length occurring as dictated by the Geometric distribution in (4.16):

$$PSP = \sum_{b=1}^{\infty} R_b P(B=b)$$
 (4.25)

For computer implementation, the  $\infty$  upper limit in (4.25) is replaced by the term  $b_{max}$ , where

$$P(B = b_{\text{max}}) < \varepsilon$$

$$\Rightarrow b_{\text{max}} = \left[ 1 + \ln(\beta \varepsilon) / \ln(1 - 1/\beta) \right]$$
(4.26)

where  $\lceil x \rceil = ceil(x)$ , the smallest integer  $\geq x$ . In (4.26),  $\varepsilon$  is a limit that determines the run-time of the program. By selecting  $\varepsilon$  to be  $10^{-11}$ , (4.26) is a very accurate approximation of (4.25).

The PLP is found from the PSP as

$$PLP = 1 - PSP \tag{4.27}$$

Finally, it should be noted that by setting  $\beta = 1$  in (4.16), the multiple slot (bursty) analysis presented in this section reduces to the single slot (uniform) analysis of the previous section. The uniform model is simply a special case of the more general bursty traffic model.

#### 4.2.3 Monte-Carlo Simulation and Model Verification

As in Section 4.1, MC simulation is required to verify the bursty traffic model. This algorithm modifies the arrival process of the flowchart in Figure 4.3 and accounts for multiple slots in each trial. Due to its similarity to Figure 4.3, the bursty model flowchart is presented in Appendix A.

#### 4.2.4 Results

This section compares the results of the theoretical analysis and MC simulation for bursty traffic flow in a switch with reduced sets of FRWC's. The scenarios considered and

corresponding plots are indicated in Table 4.3. In all simulations, 15,000-25,000 MC simulations were used with mean burst lengths of two and four.

Table 4.3: Bursty traffic switch scenarios modelled. For each scenario, the corresponding plots are given.

Number of fibers N	Codes per fiber n	Mean burst length: β	Figure
4	15	2	Figure 4.11
4	15	4	Figure 4.12
8	15	2	Figure 4.13

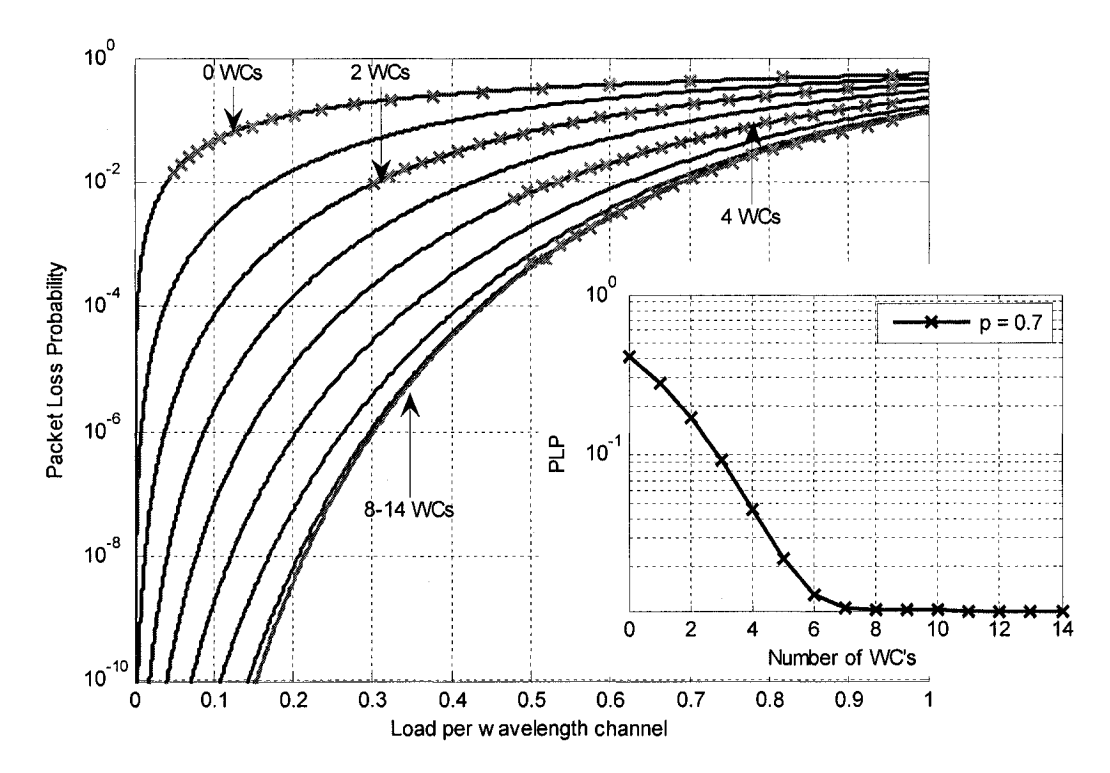


Figure 4.11: PLP vs load for a  $4\times4$  switch with 15 wavelengths per fiber with reduced sets of FRWC's under bursty traffic with  $\beta=2$ . Inset: PLP vs WC's at a load of 0.7.

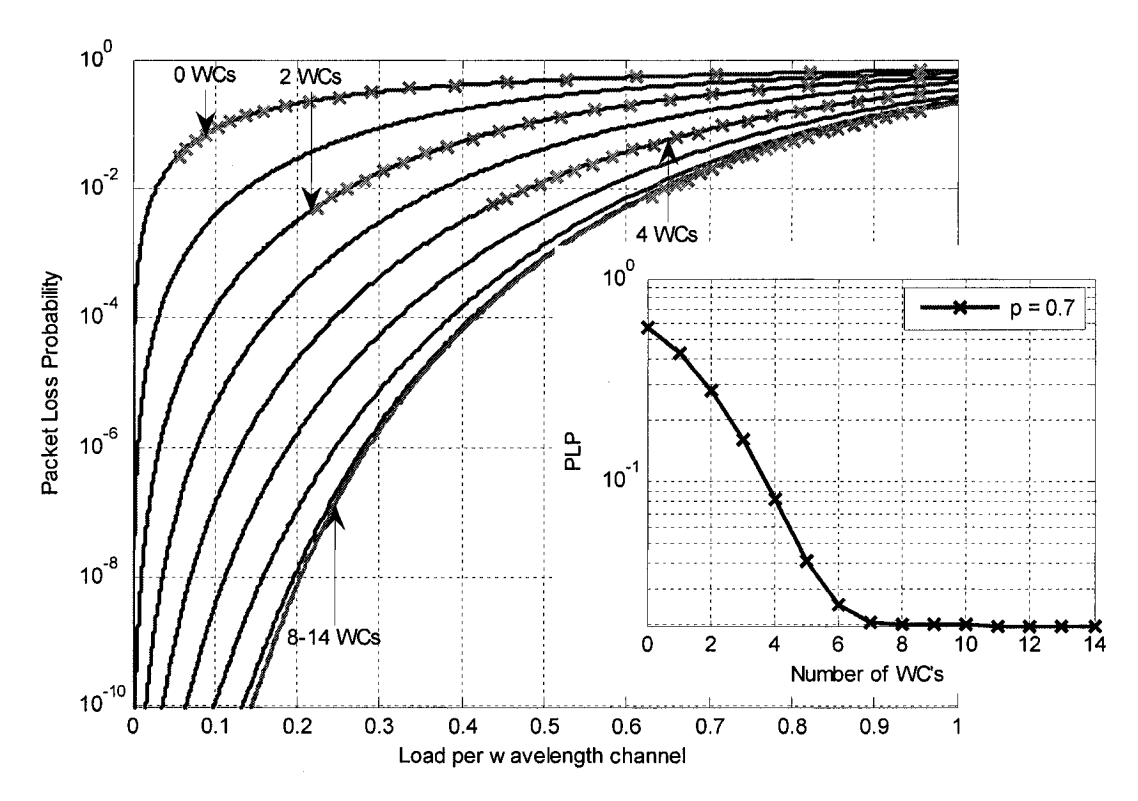


Figure 4.12: PLP vs load for a 4×4 switch with 15 wavelengths per fiber with reduced sets of FRWC's under bursty traffic with  $\beta$  = 4. Inset: PLP vs WC's at a load of 0.7.

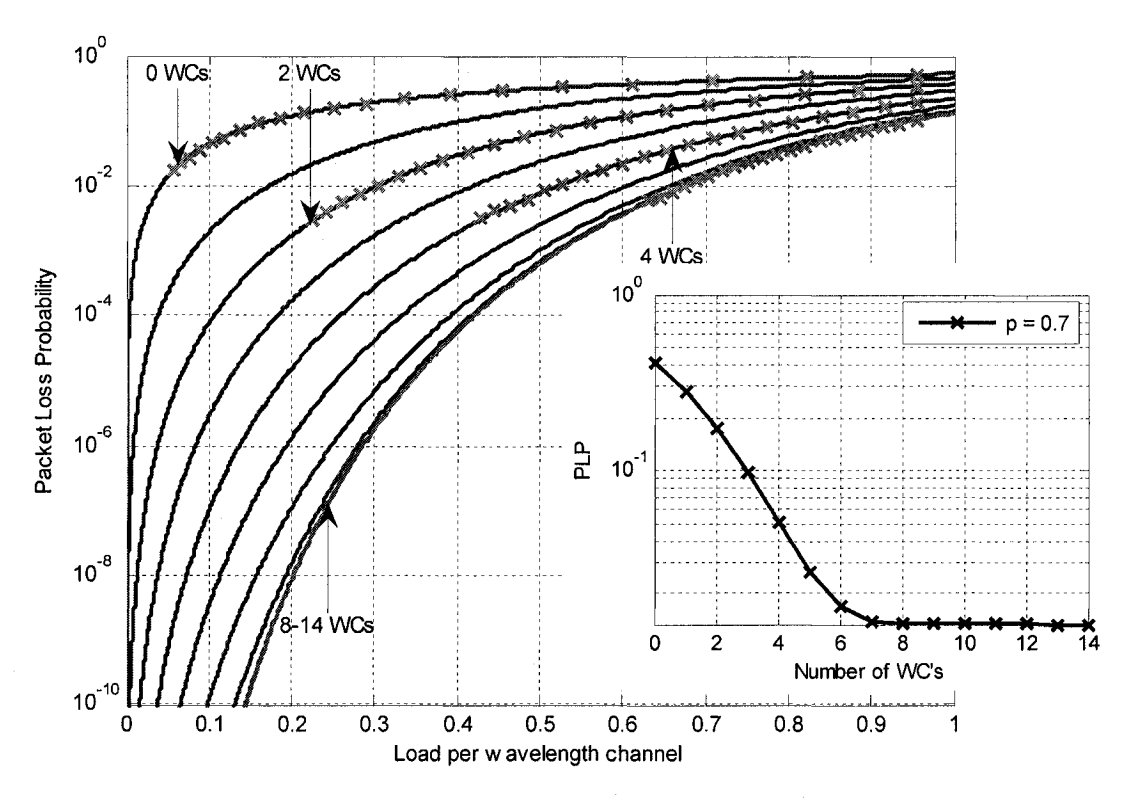


Figure 4.13: PLP vs load for an 8×8 switch with 15 wavelengths per fiber with reduced sets of FRWC's under bursty traffic with  $\beta = 2$ . Inset: PLP vs WC's at a load of 0.7.

#### 4.2.5 Observations

Once again the MC simulations agree well with the theoretical results. The plots of this section indicate that as the mean burst length increases, PLP increases accordingly for constant n. For example, for  $\beta = 1$  (uniform) in the 4×4 switch with n = 15 of Figure 4.6,  $PLP_{opt}$  at  $\rho = 0.7$  is  $5 \times 10^{-3}$ . This increases to  $1 \times 10^{-2}$  for  $\beta = 2$  in Figure 4.11 and to  $2 \times 10^{-2}$  for  $\beta = 4$  in Figure 4.12. This is intuitive, as for a higher  $\beta$ , each payload contains on average more slots, reducing the chance of successful transmission of the entire packet.

When N is increased, the PLP degradation due to an increased number of packets in the switch is partially offset by a decreased load directed at each output fiber, causing this degradation to be slight (as observed for uniform traffic). This can be observed in Figure 4.11 and Figure 4.13 where  $PLP_{opt}$  at  $\rho = 0.7$  moves from  $1 \times 10^{-2}$  for N = 4 to  $1.3 \times 10^{-2}$  for N = 8.

To summarise, increasing  $\beta$  has a detrimental effect on throughput in that a lower load is required to achieve the same PLP as for uniform traffic. Given that current networks transport payloads at least 1500 bytes long (maximum Ethernet payload size), unrealistically low loads would be required for acceptable PLP in our optical MPLS network. However, by increasing the number of wavelengths and using sets of WC's to exploit the wavelength domain, the effects of bursty traffic can be negated. For example, referring to Figure 4.5 where seven wavelengths are used with uniform traffic, a load of less than 0.083 is required to achieve a PLP of  $10^{-8}$ . By increasing the number of wavelengths to 15, and now considering bursty traffic with  $\beta = 4$  (Figure 4.12), a PLP of  $10^{-8}$  can be achieved at the higher load of 0.2. That is, although mean burst length has increased from one to four, adding more wavelengths and using WC's allows the same PLP to be achieved at higher loads, negating the detrimental effects of bursty traffic.

# 4.3 General Analysis of Traffic Flow in a Bufferless Space Switch with Reduced Sets of LRWC's

As discussed in Chapter 3, the physical limitations on wavelength conversion make it important to study the impacts of a limited-range conversion constraint. This constraint,

combined with the possibility of reduced sets of WC's per output fiber, gives rise to a wavelength matching problem in the switch in each time slot. To demonstrate this problem, consider the scenario shown in Figure 4.14, where six packets (from several input fibers) request transmission to one output fiber. In this example, five wavelengths are used and WC's are limited to convert to only one wavelength above or below the input wavelength.

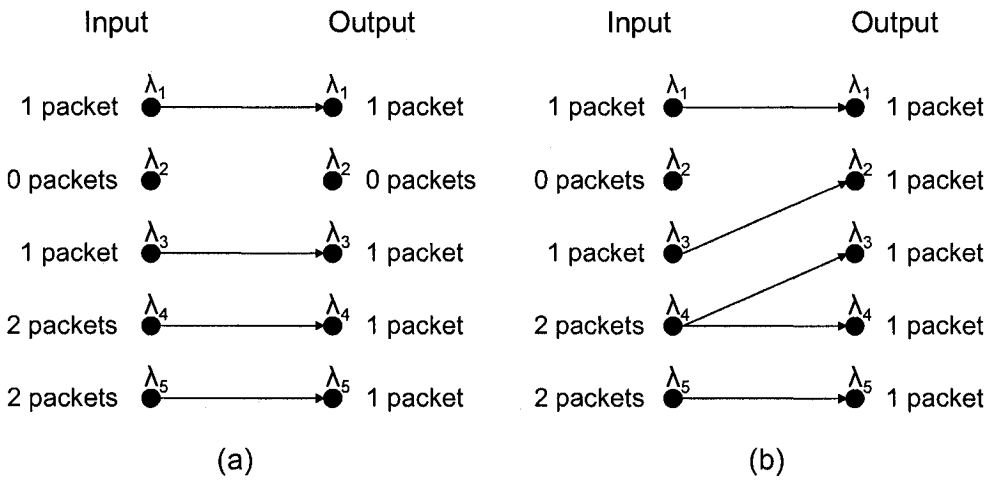


Figure 4.14: Matching problem in a space switch. The WC's are assumed to have a limited range conversion constraint described above. The matching shown in (a) requires 0 conversions and transmits 4 packets, while that shown in (b) requires 2 conversions but transmits 5 packets.

As observed in Figure 4.14, different wavelength matchings can yield different throughputs. Obviously the matching in Figure 4.14(b) is optimal as it has higher throughput. However, if in this example, only one WC was available on the output fiber, the matching in (b) would be illegal and matching (a) would be optimal. This example illustrates that the matching problem is an optimization problem where the throughput is to be maximised under the constraints of limited-range wavelength conversion and reduced numbers of WC's. This is in contrast to the previous analyses with FRWC's, where any input wavelength was matched to any output wavelength.

To solve this matching problem, we implement a Random Matching Algorithm (RMA), Optimum Matching Algorithm (OMA) and a Brute Force Matching Algorithm (BFMA) in the switch control block. An explanation of the algorithms, as well as their efficiency and ability to maximise throughput are discussed.

## 4.3.1 Random Matching Algorithm

This simple algorithm is adapted from [7], and is described as follows. When one or more active sources arrive on each input wavelength, the RMA randomly selects one packet to forward to the same wavelength (without conversion). It then randomly moves through all wavelengths where a contention has arisen. For each contending packet, the RMA randomly chooses an available output wavelength within the conversion range (CR). Once the maximum number of conversions has been reached, or every packet has been matched to an output wavelength, the algorithm terminates. The RMA requires at most  $\min(j-1,n-1)$  iterations.

The simplicity of this algorithm makes it very attractive. The RMA performs well but is sensitive to WC CR.

# 4.3.2 Optimum Matching Algorithm

To optimise a matching, we attempt to find the "best" solution in the matching problem of a bipartite graph, where the input subset is the wavelengths entering the switch, and the output subset is the available wavelengths at the output. The bipartite graph can be denoted G = [V, E], where V denotes the graph vertices (wavelengths) in both the input and output subsets (as observed in Figure 4.14), and E is the subset of edges (connections between input and output wavelengths) in the matching. A legal matching arises if the following conditions are met:

- There are no contentions on each output wavelength.
- Any conversions taking place must obey the constraints of the LRWC.
- The total number of conversions is less than or equal to the number of WC's on the output fiber.

A matching satisfying the above constraints and containing the maximum number of edges (highest throughput) is an optimal matching. There are often many different optimal matchings for a given bipartite graph G.

In our OMA, Munkres (Hungarian) algorithm [58] is used to solve this optimization problem with the following modifications: Initially, the OMA creates a  $j \times n$  rectangular

input matrix M, where each row corresponds to an input wavelength requesting access to the output fiber, and each column corresponds to an output wavelength. For each input wavelength, the columns of M within its CR are assigned a cost of 1, while all other columns in that row have  $\cos \infty$ , ensuring an input wavelength will be assigned within its CR. The standard steps of the Munkres algorithm are then followed [59]. However, once the maximum number of conversions is reached, remaining input wavelengths are matched to the same wavelength (if available), or dropped.

The OMA will always return a maximum matching with  $\min(j,n)$  edges for complete sets of LRWC's. However, accounting for the constraint of a reduced number of conversions, sub-optimal matchings may be returned. The computational complexity of the Hungarian algorithm is upper bound by  $O(\min(j,n)^2 \times \max(j,n))$  [60]. From (4.2), the mean number of packets requesting access to an output fiber, E(J), in each time slot is  $n\rho$ . The mean computational complexity of the OMA is thus upper bound by  $O((n\rho)^2 n)$ . However, the simplicity of the bipartite graph G and corresponding binary valued matrix M suggests that the complexity of the OMA will be considerably lower than this bound.

Although the OMA is less efficient than the RMA, its optimised matchings can make it advantageous in scenarios where PLP insensitivity to CR is required. By combining both the RMA and OMA into a single algorithm, the most optimal matchings will be achieved at the expense of running time.

#### 4.3.3 Brute-Force Matching Algorithm

To measure how close the RMA and OMA algorithms are to providing optimum matchings, the BFMA is used. This algorithm populates a tree with all possible wavelength matchings in the bipartite graph and searches each path for the matching that provides the maximum edges. This algorithm will always give the maximum (optimal) matching, and has been optimised to minimise memory usage and the number of searched branches by identifying illegal matchings at an early stage. However, due to the nature of tree searching, the runtime is still exponentially dependant on the number of vertices, |V|, and can only be used to benchmark the performance of the RMA and OMA.

### 4.3.4 Limited-Range Wavelength Conversion Scenarios

In this thesis, we define limited-range conversion in terms of translation from an input wavelength to a set of wavelengths below (down), or both above and below (up and down) the input [55, 61]. An "up only" conversion analysis is excluded due to the ER penalties for up conversion associated with XGM, as discussed in Chapter 3.

To express these scenarios mathematically, consider a CR of k, where  $k \in [0, n-1]$ . The output sets of wavelengths to which an input wavelength  $\lambda_i$  ( $i \in [1, n]$ ) can be converted for each scenario is shown in Table 4.4.

Table 4.4: Output wavelength set for each conversion scenario given input wavelength  $\lambda_i$  an(4.28)d CR k.

Input λ	Scenario	Output Wavelength Set
$\lambda_i$	Down	$\{\max(\lambda_1,\lambda_{i-k}),,\lambda_i\}$
$\lambda_i$	Up & Down	$\{\max(\lambda_1, \lambda_{i-k}),, \min(\lambda_n, \lambda_{i+k})\}$

In the down conversion scenario, for  $k \in [\min(i+1,n),n]$ , the output wavelength set will not change, resulting in no throughput improvement. For example, the input wavelength  $\lambda_l$  could not be converted to any other output wavelengths regardless of the CR. As a result, when complete sets of fully down converting WC's are used, the PLP will not be as low as that achievable for complete sets of FRWC's in the up and down scenario (where all output wavelengths can be available).

#### 4.3.5 Results

As always a closed form analysis is preferred, however the various matching algorithms in this section render a mathematical approach intractable. Consequently, these results are based purely on MC simulation due to its ability to cope with arbitrarily complex systems. Using this approach, however, low PLP's cannot be measured with high precision due to the massive number of MC trials required [62]. As a result, all PLP's measured in this section are greater than 10<sup>-4</sup>. Although not practical in a realistic communication system, these simulations clearly demonstrate the effects of limited-range conversion with reduced sets of WC's.

The scenarios considered and their associated plots are summarised in Table 4.5. All simulations use a single slot (uniform) analysis with 15,000-20,000 MC trials. As observed in the previous section, a bursty traffic assumption will gradually degrade the PLP as  $\beta$  increases, and is thus not included in this analysis.

In the plots for up and down conversion, the horizontal dashed black line indicates the optimum (theoretical) PLP achievable using a complete set of FRWC's. For down conversion only, the optimum theoretical PLP using a complete set of FRWC's and assuming all output wavelengths are available is listed. This highlights the sub-optimal throughput in a down conversion only assumption.

Table 4.5: Reduced sets of LRWC scenarios. For each scenario, the corresponding plots are given.

Number of fibers	Wavelengths per fiber n	Load ρ	Matching Algorithm	Conversion Scenarios	Figure
4	15	0.7	RMA or OMA	Down	Figure 4.15
4	15	0.7	RMA and OMA	Down	Figure 4.16
4	31	0.7	RMA and OMA	Down	Figure 4.17
4	31	0.7	RMA or OMA	Up & Down	Figure 4.18
4	31	0.7	RMA and OMA	Up & Down	Figure 4.19
8	31	0.7	RMA and OMA	Up & Down	Figure 4.20

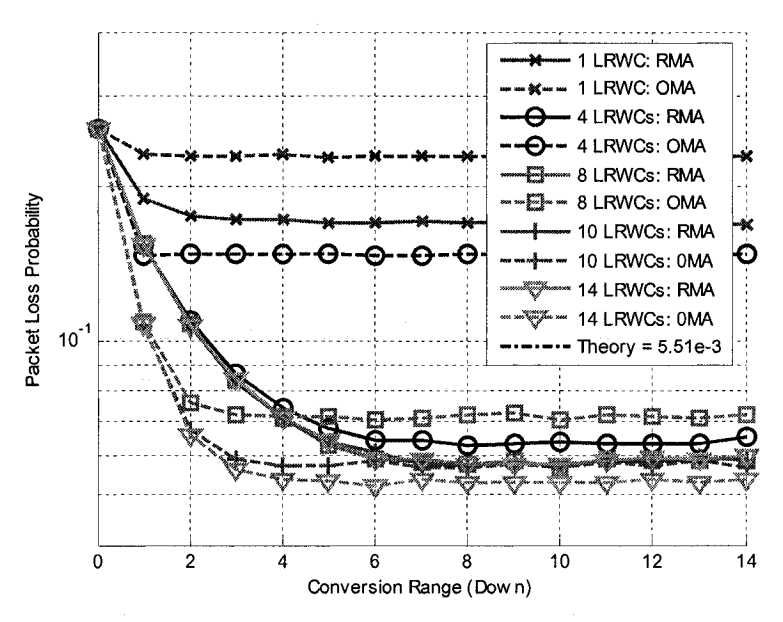


Figure 4.15: PLP vs CR for a 4×4 switch with 15 wavelengths per fiber with reduced sets of LRWC's under uniform traffic with  $\rho = 0.7$ . The RMA (solid lines) and OMA (dashed lines) are used separately and *down conversion* is considered. The optimum PLP with a complete set of FRWC's assuming all output wavelengths are available is  $5.51 \times 10^{-3}$ .

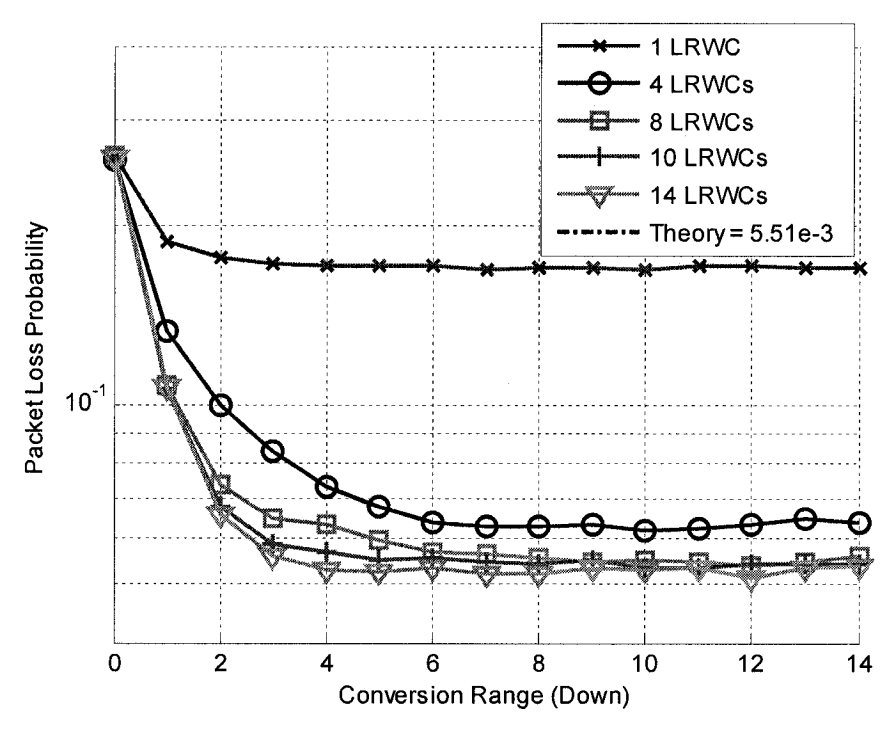


Figure 4.16: PLP vs CR for a 4×4 switch with 15 wavelengths per fiber with reduced sets of LRWC's under uniform traffic with  $\rho=0.7$ . The RMA and OMA are used together and *down conversion* is considered. The optimum PLP with a complete set of FRWC's assuming all output wavelengths are available is  $5.51 \times 10^{-3}$ .

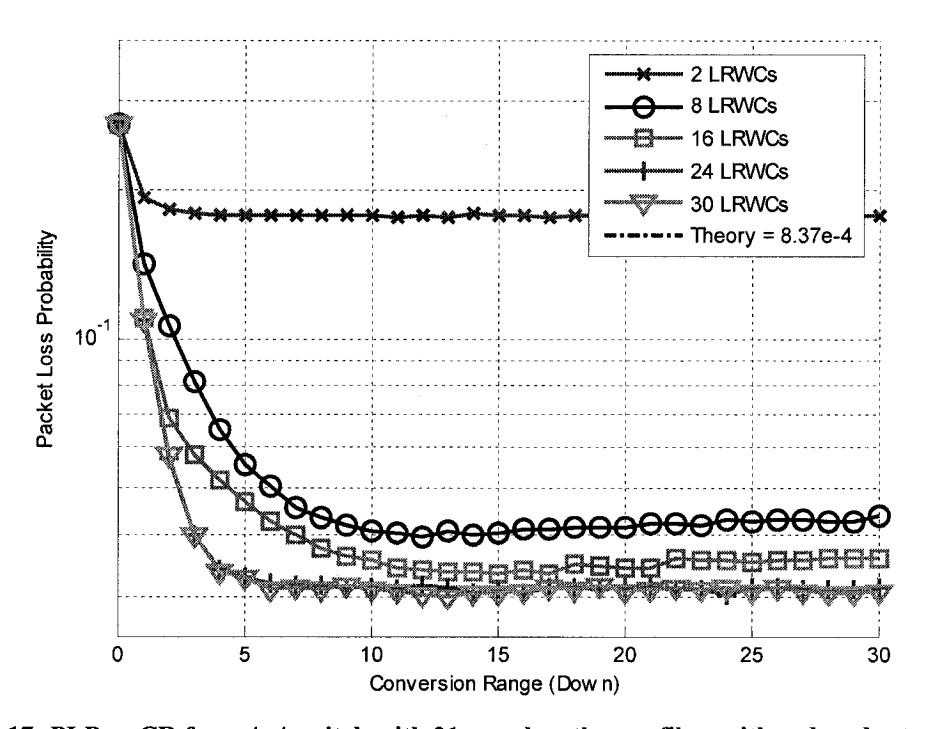


Figure 4.17: PLP vs CR for a 4×4 switch with 31 wavelengths per fiber with reduced sets of LRWC's under uniform traffic with  $\rho$  = 0.7. The RMA and OMA are used together and *down conversion* is considered. The optimum PLP with a complete set of FRWC's assuming all output wavelengths are available is  $8.37 \times 10^{-4}$ .

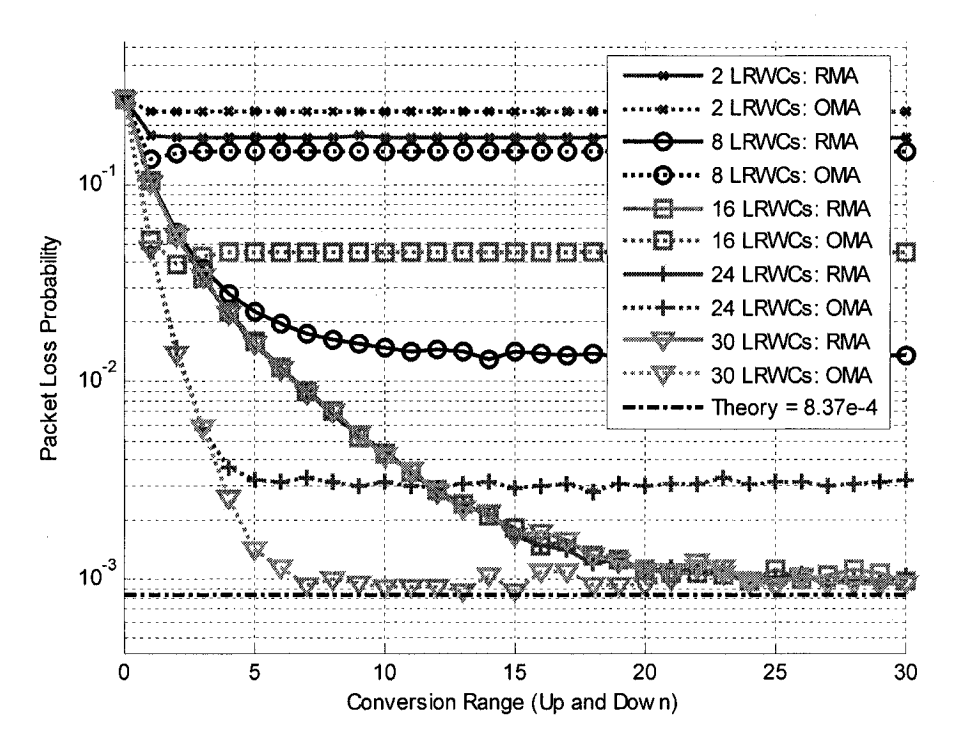


Figure 4.18: PLP vs CR for a 4×4 switch with 31 wavelengths per fiber with reduced sets of LRWC's under uniform traffic with  $\rho = 0.7$ . The RMA (solid lines) and OMA (dashed lines) are used separately and up and down conversion is considered.

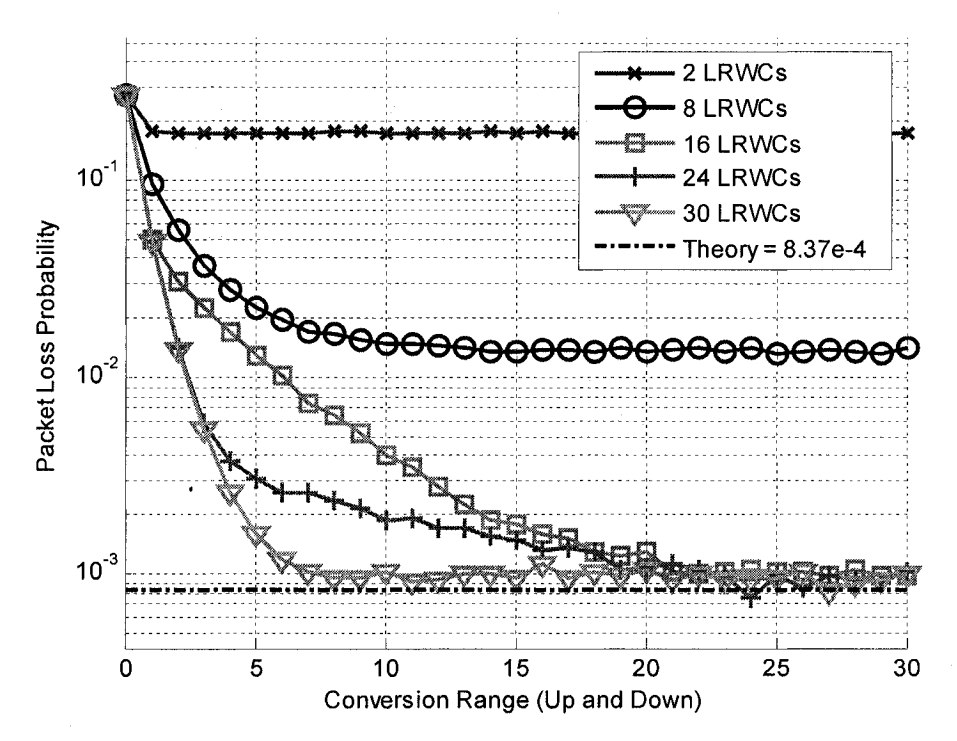


Figure 4.19: PLP vs CR for a 4×4 switch with 31 wavelengths per fiber with reduced sets of LRWC's under uniform traffic with  $\rho = 0.7$ . The RMA and OMA are used together and up and down conversion is considered.

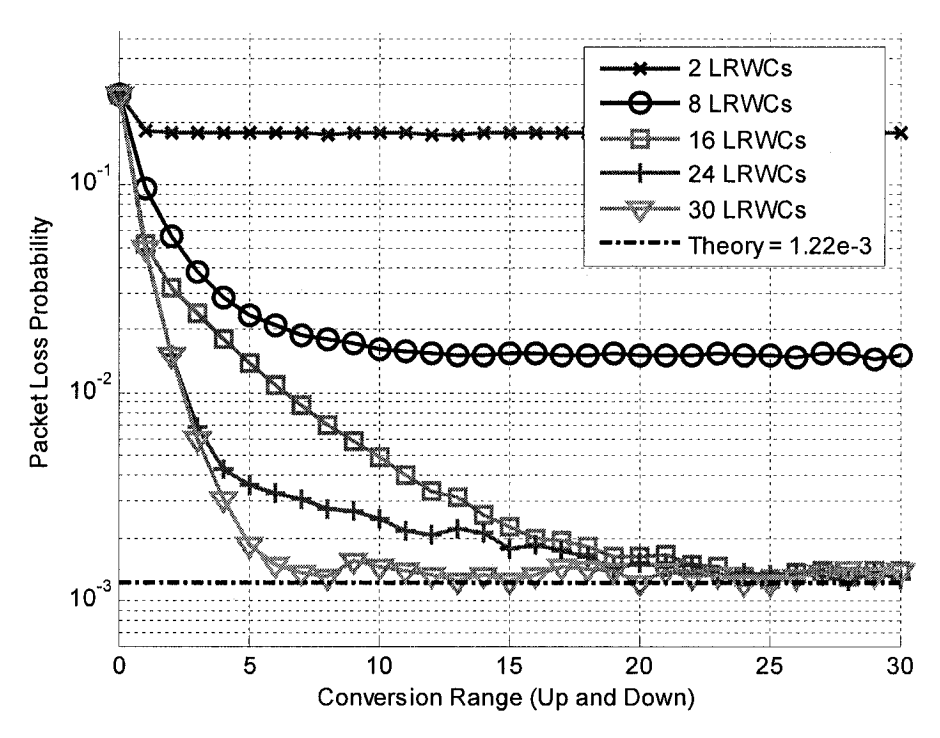


Figure 4.20: PLP vs CR for an 8×8 switch with 31 wavelengths per fiber with reduced sets of LRWC's under uniform traffic with  $\rho = 0.7$ . The RMA and OMA are used together and up and down conversion is considered.

#### 4.3.6 Observations

The plots of the previous section provide a strong insight into the performance of reduced sets of LRWC's with the various conversion scenarios. The observations made are presented in the following sub-sections.

### 4.3.6.1 Comparing Down to Up and Down Conversion

For down conversion only (Figure 4.15 to Figure 4.17), the optimal PLP's predicted by the FRWC results of Section 4.1.6 are not reached even for full downward conversion. The results of the up and down conversion assumption are always better than for down only conversion. For example, in Figure 4.17, the optimal PLP achieved with down conversion is  $3.08 \times 10^{-2}$  whereas the theoretical optimum with up and down conversion is  $8.37 \times 10^{-4}$  for the same switch configuration.

## 4.3.6.2 Comparing RMA to OMA

In all plots, the OMA decreases to a PLP floor quickly and stays constant at this level, even though these values are generally poorer than for the RMA. Examining the RMA,

we refer to the  $4\times4$  switch with n=31 of Figure 4.18 at  $\rho=0.7$ . In this plot, as CR increases, the PLP approaches the levels given by the PLP vs number of FRWC curves (inset of Figure 4.7) at  $\rho=0.7$ . In this inset,  $P\tilde{L}P_{opt}$  is reached for 12 FRWC's. Thus for greater than or equal to 12 LRWC's, the PLP vs CR curves of Figure 4.18 will decrease to  $P\tilde{L}P_{opt}$  (or  $PLP_{opt}$ ) as CR increases.

To achieve optimal PLP with CR insensitivity, we combine the RMA and OMA into a single control algorithm. For up and down conversion, the PLP (for increasing CR) will approach that given by the ideal PLP vs  $\rho$  curves of Section 4.1.6 (for a given load and number of FRWC's). For greater than or equal to  $\tilde{L}_{opt}$  LRWC's, the PLP will approach  $P\tilde{L}P_{opt}$  (or  $PLP_{opt}$ ), reaching this value faster (at a lower CR) for more LRWC's. To demonstrate this, consider again the 4×4 switch with n=31, where the RMA and OMA are used simultaneously in Figure 4.19. Recalling from Figure 4.7 that  $\tilde{L}_{opt}=12$  for  $\rho=0.7$ , the CR's required to reach  $PLP_{opt}$  for greater than  $\tilde{L}_{opt}$  LRWC's are shown in Table 4.6.

Table 4.6: Number of LRWC's and corresponding CR required to reach  $PLP_{opt}$  for the  $4 \times 4$  switch with n = 31 and up and down conversion as shown in Figure 4.19.

# LRWC's	CR to reach PLPopt
16	23
24	19
30	7

A comparison of the combined RMA-OMA to the FAA of [55] is presented in Figure 4.21. In this plot, a  $16 \times 16$  switch with n=32 is analysed, and is compared to the overlaid results of simulations for identical parameters using the FAA from Figure 18 of [55]. Using the FAA, for  $L \le 24$ , PLP increases (or does not monotonically decrease) to a floor with increasing CR, and optimal PLP is reached only for a complete set of LRWC's. In contrast, the PLP curves using our algorithm decrease monotonically for all L, with equal or lower PLP than achieved with the FAA (up to two orders of magnitude lower for L=16). Note that equal PLP at k=0  $\forall L$ , and similar PLP for  $L \ge 31$  confirm identical simulation environments for our comparison.

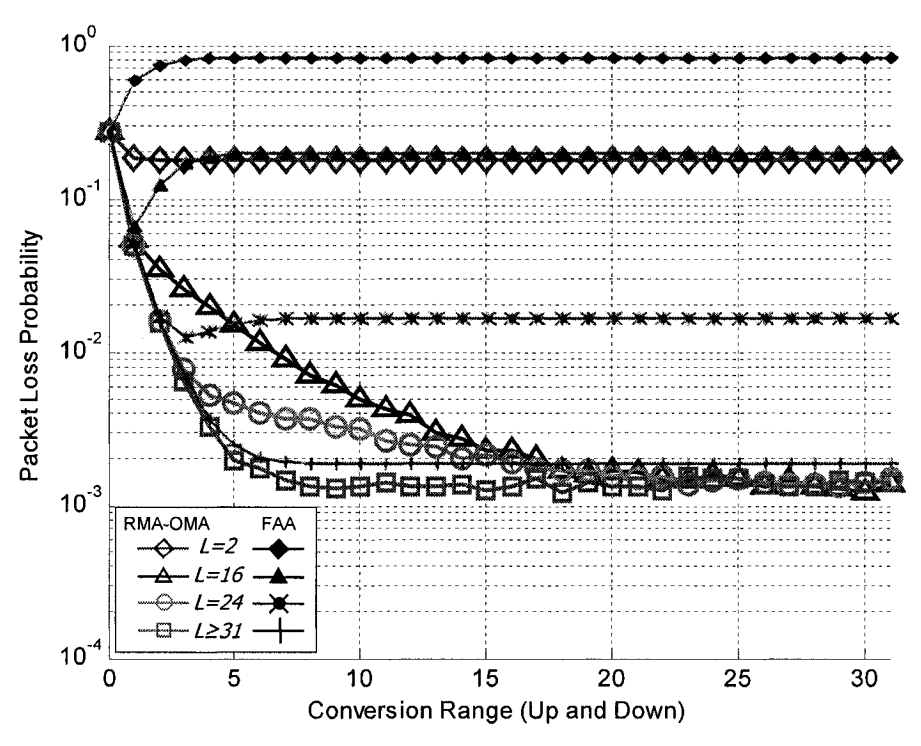


Figure 4.21: PLP vs CR for a  $16\times16$  switch with 32 wavelengths per fiber with reduced sets of LRWC's at  $\rho=0.7$  assuming up and down conversion. A combined RMA-OMA is used and compared to the overlaid FAA results from Figure 18 of [55].

#### 4.3.6.3 Increasing N or n

As N is increased (N = 8 in Figure 4.20), very similar results to the N = 4 cases are observed. This was expected from the plots of uniform traffic flow with FRWC's, where varying N made only a minor difference to PLP. As n increases from 15 to 31, lower  $PLP_{opt}$  is achieved using the LRWC's as seen by comparing Figure 4.16 and Figure 4.17.

#### 4.3.6.4 **Summary**

The main results of this section are summarised by the following points.

- The up and down conversion scenario always outperforms the down only assumption.
- The OMA reduces PLP sensitivity to CR, but is often outperformed by the RMA, especially for few LRWC's.
  - o In these cases, the RMA, with its lower computational complexity is a more attractive choice for the switch control algorithm.

- The RMA and OMA combined yield a lower PLP floor than the FAA for an identical switch configuration. This is at the expense of computational complexity.
- Using up and down conversion with both RMA and OMA simultaneously, a throughput of  $P\tilde{L}P_{opt}$  is reached for greater than or equal to  $\tilde{L}_{opt}$  LRWC's as CR increases.
  - o For more LRWC's, the CR required to reach this throughput is lower.

## 4.4 Software Package

Based on the work of Sections 4.1-4.3, a software package was built in MATLAB to model WDM data payload traffic flow in a NN with various switch configurations using reduced sets of LRWC's in an SPOF architecture. The program was designed to be operated using the simple GUI shown in Figure 4.22.

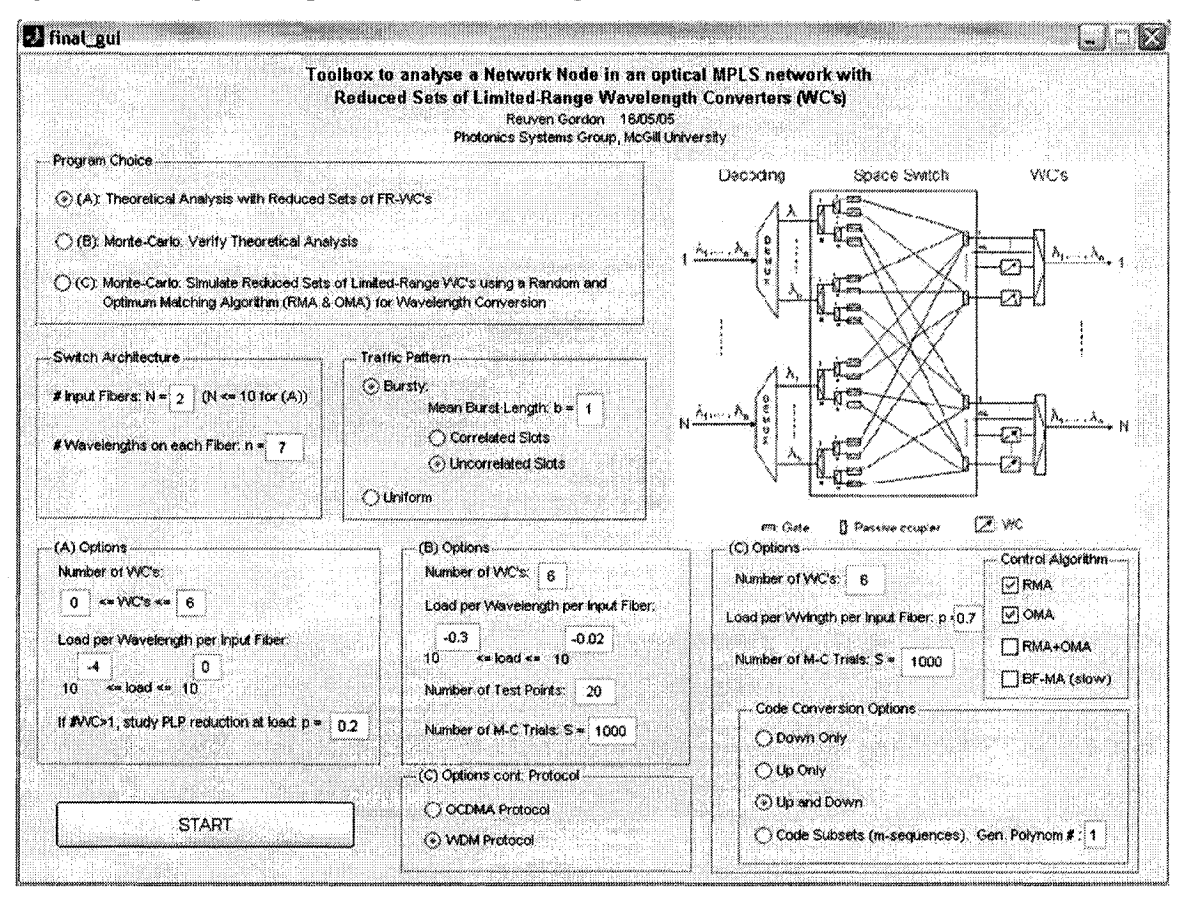


Figure 4.22: Software package GUI to analyse throughput in a NN of an optical MPLS network.

The program, containing some 35 individual files and over 4,000 lines of code, allows the user to specify all switch parameters and types of simulations to perform (GUI programs (A)-(C)) as discussed in this chapter. Any theoretical curve can be easily verified with MC simulation. Some innovative functions in this package include:

- Comprehensive error handling to ensure legal switch configurations.
- All results written (or appended) to an output file for future reference.
- Intuitive curve plotting to integrate theoretical and MC simulation results.

It is expected that this program will be used to determine required numbers of realistic WC's to meet throughput requirements as discussed in the following section.

#### 4.5 Discussion and Cost Considerations

In this chapter, we examined the dependency of PLP on many parameters in a space switch employing WC's. By generalising and improving upon previous studies, our analysis on reduced sets of FRWC's and LRWC's under bursty traffic, the use of Munkres algorithm in the OMA and the combined RMA and OMA in the switch control block are currently novel research. The main highlights of this analysis are summarised below.

- A complete set of FRWC's is not required to obtain near optimal PLP under either traffic assumption.
- Payloads containing multiple slots (bursty traffic) degrade PLP as the packet length increases. This can be negated by using more wavelengths and sets of WC's.
- Accounting for the limited-range conversion constraint, a wavelength matching
  algorithm must be used to achieve the best PLP for a given number of LRWC's.
  This added constraint reduces the ability of LRWC's to achieve optimal PLP.
  - A down only conversion assumption will not yield optimal PLP even for complete sets of WC's as no wavelengths above the input wavelength are available for conversion.

• The OMA does not suffer from increasing PLP with increasing CR as observed in certain cases with the FAA. Combining the RMA with the OMA provides a control algorithm that yields the most CR insensitive and optimal PLP.

A trade-off arises when selecting the number of WC's per output fiber when each WC has limited conversion capability. Ideally, the minimum number of realistic WC's should be used to obtain a desired threshold PLP,  $PLP_{th}$ , to minimise cost and switch complexity.

Very simply, the PLP for any switch configuration could be expressed as

$$PLP = f(N, n, \beta, \rho, CR, WC's)$$
(4.29)

where  $f(\cdot)$  is some mapping function specific to the configuration. To choose the minimum number of FRWC's to achieve a  $PLP_{th}$  (given N, n,  $\beta$  and  $\rho$ ), one would refer to PLP vs FRWC curves similar to those of Sections 4.1 and 4.2. Realistically, depending on the CR of the WC's, optimal performance would no longer be obtained, and the number of LRWC's used would need to be increased.

Recalling that CR is technology dependant, an empirical cost function depending on CR and number of WC's could be defined as

$$C = g\left(CR, WC's\right) \tag{4.30}$$

In this case, (CR, WC's) "pairs" could be chosen from simulation curves similar to those of Section 4.3 to ensure the PLP threshold is satisfied. If these pairs made up the set  $\{CR, WC's\}_{th}$ , a pair (CR, WC's) could be chosen from this set to minimise the cost function of (4.30). That is,

$$C_{\min} = \min \left\{ g\left(CR, WC's\right) \right\} \quad \text{where } (CR, WC's) \in \left\{CR, WC's\right\}_{th}$$
 (4.31)

This method would minimise switch cost whilst ensuring a threshold throughput was maintained for a given switch configuration.

Finally, the analysis of this chapter is applicable not only to networks with wavelength multiplexed data channels, but also to OCDMA networks, where each user packet is transmitted on a code. By considering code, rather than wavelength contentions in the space switch, the above analysis can be applied. It should be noted that depending on the code family choice and coding domain, the limited-range wavelength conversion definitions of Section 4.3.4 may not apply. For example, up or down only conversion assumptions may not be realistic for spectral codes comprising several wavelengths in a given range.

# 5 Demonstration of an All-Photonic, Spectral, Label Switching Photonic Code Converter

As discussed in Chapter 2, label processing (extraction, recognition and switching) is a fundamental task of the NN. In the previous chapter, we examined the data throughput improvement by incorporating realistic single WC's (converting one wavelength to another) into the space switch of a NN. To date, single WC's have been demonstrated [11, 50, 63] as well as multicasting systems (converting one wavelength to several others) [64, 65]. However, considerably less work has been performed on concurrent, multiple wavelength to multiple wavelength conversion. This technology is required to switch spectral OCDMA coded labels.

In this chapter, we demonstrate successful all-photonic label code conversion of (7,4) spectral m-sequences based on XGM in a SFRL. An all-photonic system avoids costly Optical-Electronic-Optical conversion and simplifies implementation due to the absence of electronics. An example of this conversion is shown in Figure 5.1, where initially the label switcher, also referred to as a photonic code converter (PCC) is considered as a black box.

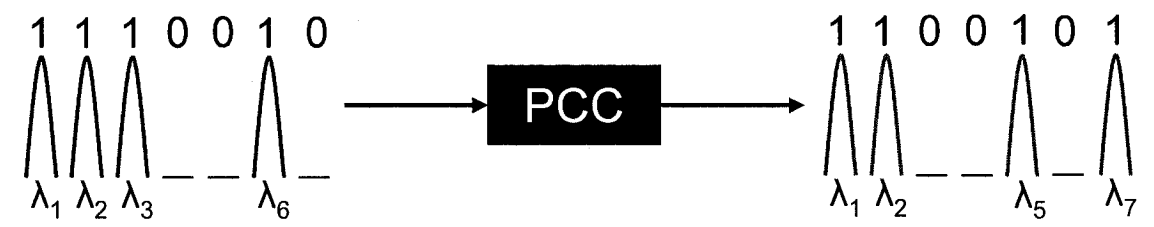


Figure 5.1: Conversion from input to output code using a PCC.

Section 5.1 introduces the experimental setup used and the principle of operation of the PCC. The operating parameters are also discussed. In Section 5.2, input-output code spectra and static transfer characteristics are illustrated for the cases of 0, 1 and 2 wavelength overlap between input and output codes. The step response of the PCC is used to measure the ability to convert label codes and is discussed in Section 5.3. A summary of the PCC and its limitations are presented in Section 5.4.

## 5.1 Building the PCC

#### 5.1.1 Experimental Setup

The experimental setup for the all-photonic, spectral PCC is shown in Figure 5.2 (laboratory pictures are shown in Appendix D). The PCC converts (7,4) m-sequence label codes and performs concurrent, quad-wavelength conversion. In this setup, the four wavelengths for input label code i ( $\lambda_{i1},...,\lambda_{i4}$ ) are generated from four tunable laser sources (TLS) each with their own polarization control (PC) before being combined into the control arm. An electro-optic modulator (MOD) is driven by a function generator to impress a low frequency square wave onto code i. This is used to measure the step response of the PCC. An erbium-doped fiber amplifier (EDFA) and variable optical attenuator (VOA) are used to amplify and set the power of code i before injection into the PCC via an optical circulator (OC<sub>A</sub>).

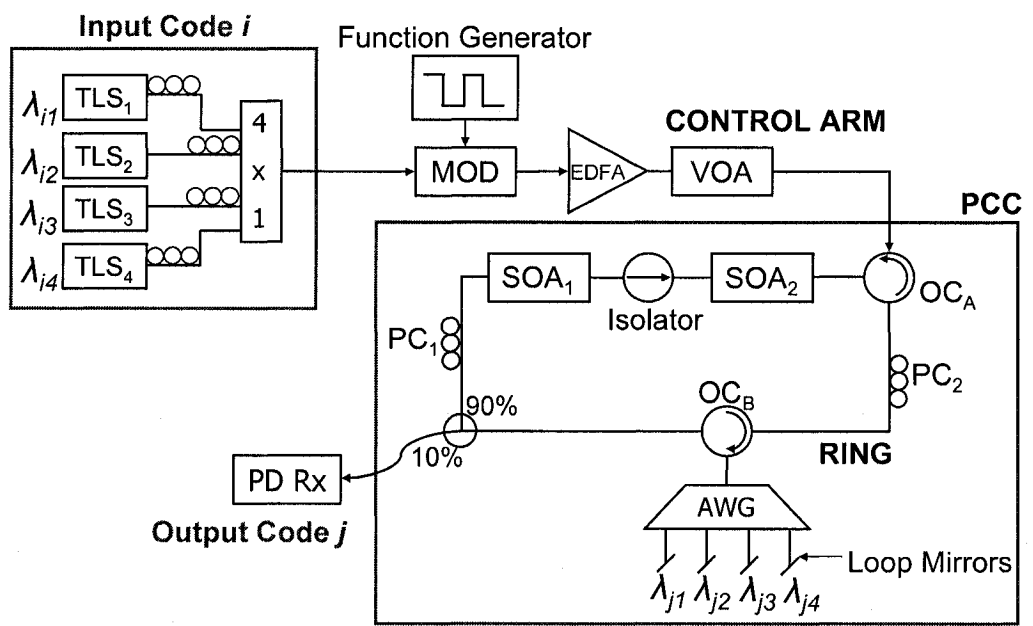


Figure 5.2: Experimental setup for the quad-wavelength, all-photonic PCC using XGM in an SOA.

The PCC is based on a multi-wavelength SFRL. The output wavelengths  $(\lambda_{j1},...,\lambda_{j4})$  comprise the output code (code j) and are defined by an arrayed waveguide grating (de)multiplexer (AWG) whose corresponding output ports are connected to fiber loop mirrors. Each AWG port is spaced by 100GHz and has a varying length of fiber between input and output. As a result, the loop mirror lengths are carefully set to ensure the length of fiber traveled by each wavelength in the SFRL is within 8mm of the other

wavelengths for a total round trip length of approximately 57.5m. This ensures that the round trip propagation time of each wavelength is within 0.01% of the others. Although not necessary for label switching (due to the low frequency input code modulation), this is essential for other applications including all-optical clock recovery discussed in Appendix B.

Superimposed fiber Bragg gratings (SI-FBG's) with reflection peaks at each wavelength in code *j* could be used in place of the AWG. Using SI-FBG's, the ring round trip lengths of each wavelength are equal and fiber splicing is not required. However the reflection response of each grating must be closely matched to ensure the reflected wavelengths can be made to have equal lasing powers in the ring.

Two Avanex SOA's are used in the PCC and are biased to optimise PCC response. SOA<sub>1</sub> is biased slightly above its transparent point to provide some small gain and counter the losses of the double pass through the AWG. Conversely, SOA<sub>2</sub> is highly biased and used for XGM to achieve code conversion. The isolator ensures that only SOA<sub>2</sub> sees the injected input code *i*. Polarization controllers PC<sub>1</sub> and PC<sub>2</sub> account for the polarization dependent gains of the SOA's and allow equalization of the lasing powers for all wavelengths in the ring. A 10-90% output coupler is used, and the 10% output port is connected to a 125MHz InGaAs NewFocus photo-receiver (PR) with constant conversion gain. The PR is used to detect output code *j* and remove high frequency noise components from the SOA's and other apparatus in the ring.

#### 5.1.2 Principle of Operation

When the injected input code (counter-propagating with the lasing signals of the SFRL) is ON (logical "1"), SOA<sub>2</sub> becomes saturated. As a result, the four wavelengths  $\lambda_{j1},...,\lambda_{j4}$  experience little or no gain in SOA<sub>2</sub> and do not have sufficient net gain to lase. That is, the output power is OFF (logical "0") and there is no conversion from code i to code j. When the input code is OFF, the four wavelengths experience gain in SOA<sub>2</sub> and reestablish lasing. The output power goes ON and code conversion occurs. Since the PCC is based on XGM, code conversion will result in an inverted output signal. However, as the PCC does not perform data conversion, this is not seen as a limitation.

#### 5.1.3 Experimental Parameters

The output code j is defined by the AWG as  $\{1,1,1,0,1,0,0\}$  and operates with 200GHz spaced wavelengths at 1536.54, 1538.11, 1539.69 and 1542.85nm. Three input codes are used to test the PCC and are documented in Table 5.1. The input codes have a varying number of wavelength overlaps with output code j corresponding to different core network scenarios. The PCC response will vary according to the number of overlaps.

The first input code has no wavelength overlaps with code j and represents label switching between different code families (not necessarily m-sequences). The second input code has one wavelength overlap with code j and represents switching between two families of m-sequences on different wavelength ranges. The third input code has two wavelength overlaps with code j and corresponds to conversion between two m-sequence label codes from the same code set and wavelength range. This is arguably the most important case as it corresponds to label switching in a network operating with one label code set.

In addition to defining the input and output codes, Table 5.1 specifies all experimental parameters. These were determined via an iterative approach to ensure optimal PCC response in all cases of input-output code combinations. The modulator is biased at  $V_{\pi}$  with the largest possible peak to peak voltage swing from the function generator to ensure the input code has maximum ER. The ring fundamental frequency for each wavelength  $f_{0,\lambda j}$ , was determined by varying the input modulation frequency  $f_{mod}$ , and observing the trace of each output wavelength on the communications signal analyser (CSA). When  $f_{mod}$  matched a harmonic of  $f_{0,\lambda j}$ , a "clean" output signal was observed, with  $f_{0,\lambda j}$  corresponding to the frequency difference between consecutive harmonics. By varying  $f_{mod}$  over several harmonics and averaging the differences, an accurate value of  $f_{0,\lambda j}$  could be found. Given  $f_{0,\lambda j}$ , the ring length seen by each wavelength,  $L_j$ , is found from (5.1) where a fiber refractive index of n = 1.5 is assumed, and c is the speed of light in a vacuum.

$$L_j = \frac{c}{nf_{0,\lambda_j}} \tag{5.1}$$

Finally, the value  $f_{0,mean}$  refers to the mean fundamental frequency of all output wavelengths.

Table 5.1: Experimental Parameters.

Table 5.1: Experimental Parameters.						
Parameter	Symbol	Value Value				
Control Arm						
Input Code 1	i <sub>1</sub>	{1,1,1,0,0,1,0} - 1533.40,1534.98,1535.76,1541.28nm				
Input Code 2	$i_2$	{1,1,1,0,0,1,0} - 1533.40,1534.98,1536.54,1541.28nm				
Input Code 3	i <sub>3</sub>	{1,1,0,1,0,0,1}- 1536.54,1538.11,1541.28,1546.03nm				
VOA		8.8-9.4dB				
EDFA		20%				
Modulator Bias Voltage	$V_{\it bias}$	$6.27V = V_{\pi}$				
Function Generator						
Modulation Frequency	f <sub>mod</sub>	12.8kHz square wave				
Peak-to-Peak Voltage	$V_{p-p}$	2V (maximum)				
Offset Voltage	$V_{th}$	0V				
PCC						
Output Code	j	{1,1,1,0,1,0,0} - 1536.54,1538.11,1539.69, 1542.85nm				
SOA₁ Bias Current	I <sub>SOA,1</sub>	36.17mA				
SOA <sub>2</sub> Bias Current	I <sub>SOA,2</sub>	138.9mA				
Ring Length for $\lambda_{i1}$	$L_{j1}$	57.577 ±0.001m				
Ring Length for $\lambda_{j2}$	$L_{j2}$	57.575 ±0.001m				
Ring Length for λ <sub>j3</sub>	$L_{j3}$	57.569 ±0.001m				
Ring Length for $\lambda_{j4}$	$L_{j4}$	57.572 ±0.001m				
Ring Fundamental Freq.	f <sub>0,mean</sub>	3.47MHz				

## 5.2 Spectral and Static Transfer Characteristics

In this section, an optical spectrum analyser (OSA) presents a snapshot of the inputoutput code spectra. This demonstrates the number of wavelength overlaps between input and output codes. In these plots, the output code peak power is approximately 15dB lower than the input code peak power. This is due to the relatively high AWG losses in the ring (9.2dB per round trip) reducing ring lasing powers and the fact that only 10% of the lasing power is coupled out of the ring.

In addition to the spectral plots, a static transfer function (TF) for each input-output code combination is presented. These characteristics plot peak output power of each wavelength in code *j* against total input power. Measurements are made by turning the function generator off and varying the input power by manually adjusting the VOA in the control arm. In the plots of this section, we use ER to define the input code total power ratio between ON to OFF states:

$$ER = 10\log_{10}\left(\frac{P_{ON,in}}{P_{OFF,in}}\right) \tag{5.2}$$

#### 5.2.1 Zero Wavelength Overlap

Figure 5.3 illustrates the input-output code spectra for zero wavelength overlap.

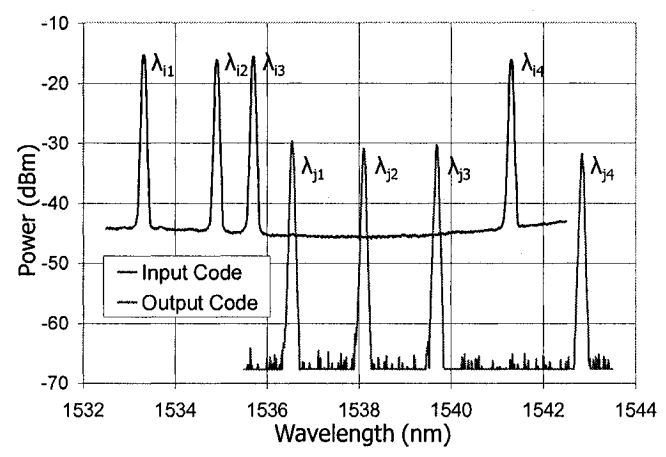


Figure 5.3: Input-output code spectra for zero wavelength overlap.

Using the SOA bias currents indicated in Table 5.1, the static TF for the PCC is obtained in Figure 5.4 by plotting the peak power of each output wavelength in code *j* against the total input power of code *i*. From this characteristic, all output wavelengths have a very similar behaviour as a function of input power, with a sharp, step like transition and limiting functionality at both low and high input powers. It was found experimentally that the position of the XGM step depends on the losses in the ring and bias current in the SOA. Increasing ring losses by using a higher percentage output coupler or including a VOA in the ring moves the step left (to lower input powers), as does decreasing the bias current.

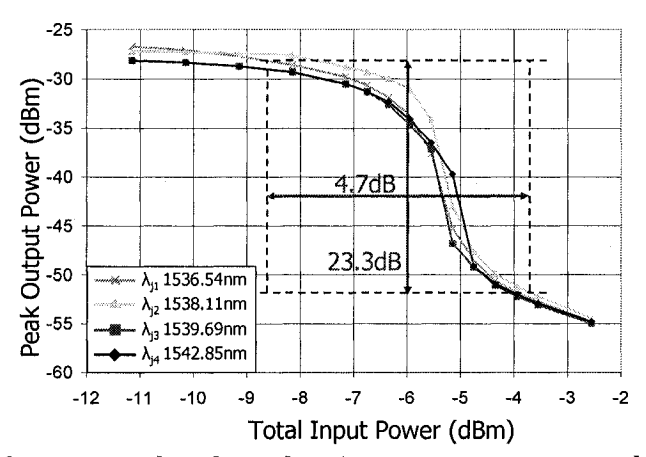


Figure 5.4: Static TF for zero wavelength overlap. A power meter measures the total input power.

In Figure 5.4, an input code with a 4.7dB ER (corresponding to the transition width) positioned around the TF step yields an output signal with an amplified peak power swing of 23.3dB. Furthermore, noise on the "0" and "1" levels of the input code (due to previous transmission through lengths of fiber) would not be transferred to the PCC output due to the flat (limiting) regions of the TF. For a slowly modulated label code, the PCC would provide 2R regeneration capability. If the label code is not modulated, as is the case for the spectral m-sequences we consider in this thesis, Figure 5.4 highlights that a large input power swing from ON to OFF states is not required to achieve code conversion.

#### 5.2.2 One Wavelength Overlap

The input-output code spectra for the one wavelength overlap case are illustrated in Figure 5.5. Ideally, wavelength overlap should not affect the output code in terms of peak power swing degradation. Realistically however, there is a finite SOA facet reflectivity and possible crosstalk between the same counter-propagating wavelengths in the SOA. These SOA reflections will cause a reduced power input code signal to be reflected and co-propagate with the output code. Although this input code power could be reduced by up to 40dB, it will experience gain in the SOA's and will in turn reduce the peak power swing on these overlapping output wavelengths.

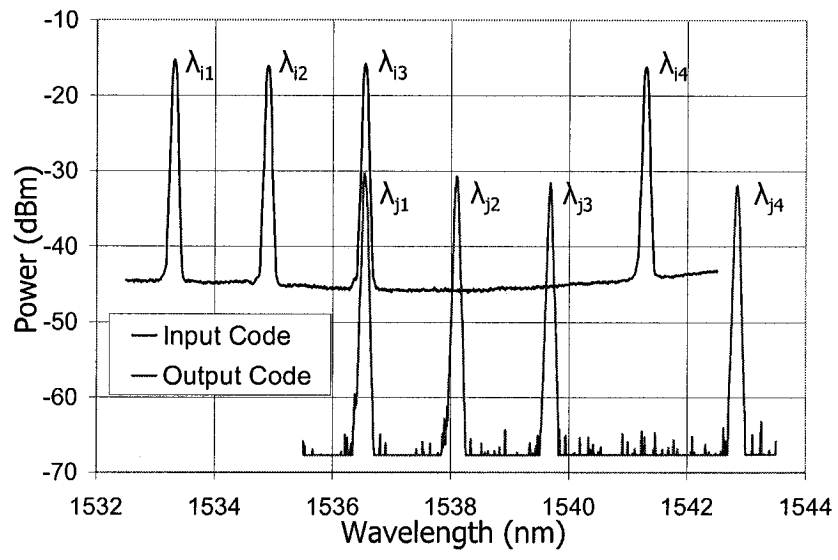


Figure 5.5: Input-output code spectra for one wavelength overlap.

In the static TF of Figure 5.6, peak power swing degradation is observed when the input code is ON. In this case,  $\lambda_{jl}$  has a peak power floor at -40dBm compared to the other wavelengths with a peak power below -50dBm. For example, an input code with 4.7dB ER positioned around the TF step will yield an output code with a peak power swing of 25dB on the non-overlapping wavelengths but just 12dB on  $\lambda_{jl}$ .

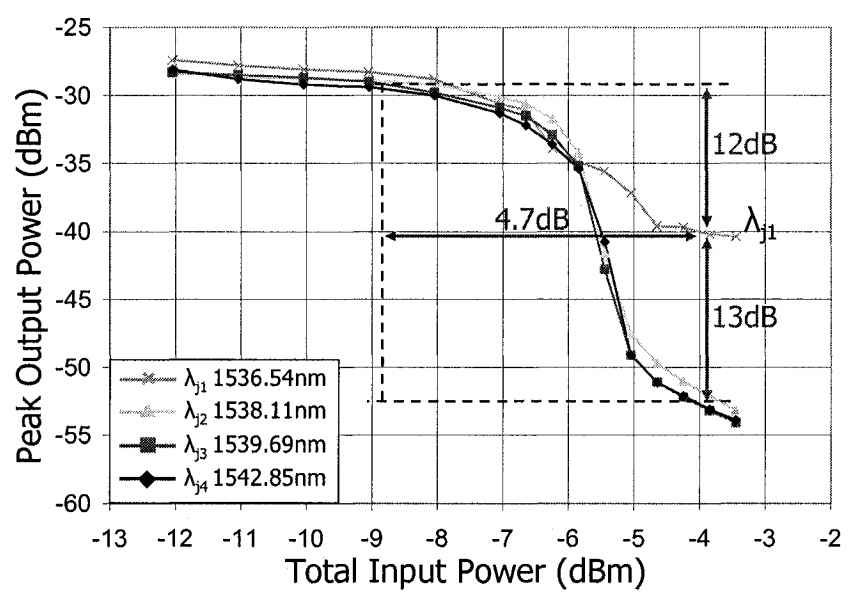


Figure 5.6: Static TF for one wavelength overlap.

#### 5.2.3 Two Wavelength Overlap

The spectra for the conversion between two m-sequences from the same code set are shown in Figure 5.7 where two wavelength overlaps occur.

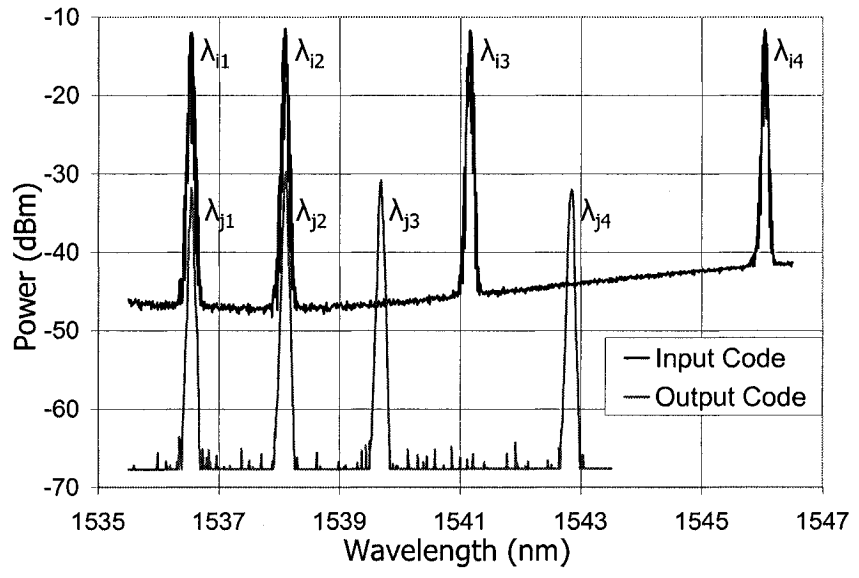


Figure 5.7: Input-output code spectra for two wavelength overlap.

The corresponding static TF is illustrated in Figure 5.8. When the input signal is ON, output wavelengths  $\lambda_{j1}$  and  $\lambda_{j2}$  have a peak power floor at -42dBm while the non-overlapping wavelengths have a peak power below -54dBm. In this case, an input code with a larger ER is required to maintain limiting functionality at low input powers.

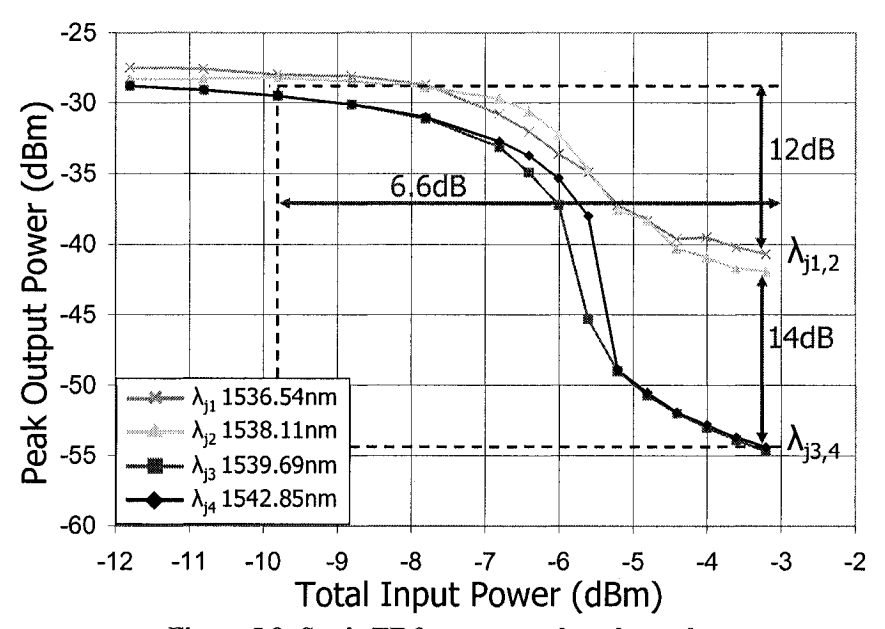


Figure 5.8: Static TF for two wavelength overlap.

## 5.3 Step Response

The step response of the PCC is a good indicator of its performance as it simulates the conversion of a label code. To measure the step response, a 12.8kHz low frequency (slowly modulated) square wave from the function generator is used. This is far lower than the ring fundamental frequency of approximately 3.5MHz and ensures active harmonic mode-locking does not occur in the ring, which would result in a pulsed output [66]. The input signal is measured by the CSA optical module, while the output signal is sent to the external NewFocus PR to remove high frequency noise components and then to the CSA electrical module.

In the plots of this section, we define the contrast ratio (C/R) as a measure of the quality of the signal in the time domain as

$$C/R = 10\log_{10}\left(\frac{P_{ON}}{P_{OFF}}\right) dB$$
 (5.3)

where P is optical power. For a PR, the output voltage  $V_{out}$  corresponds to a scaled version of the input optical power

$$V_{out} = G.P_{in} \tag{5.4}$$

where G is the conversion gain. The conversion gain is a product of the PR responsivity R (which depends on quantum efficiency and wavelength), amplifier gain  $A_g$ , and input impedance  $R_{in}$ . Thus G is expressed as

$$G = R.A_{\sigma}.R_{in} \tag{5.5}$$

Based on the 125MHz NewFocus PR datasheet [67], the responsivity is approximately constant at 1.0A/W over the small PCC output wavelength range (1536.54 - 1542.85nm). The low total PCC output optical power (maximum of 12 $\mu$ W to the PR for zero wavelength overlap) is below the listed PR saturation power of 55 $\mu$ W, ensuring it remains in the linear regime. Given linear operation and the small wavelength range,  $A_g$ , and thus G are assumed to be constant. Experimentally, G was measured to be relatively constant at  $3.8 \times 10^4 V/W$  over the wavelength range and power variations of the PCC.

Given a constant PR conversion gain, the C/R of the measured electrical signal from the PR is equivalent to (5.3) and given by

$$C/R = 10\log_{10}\left(\frac{P_{ON}}{P_{OFF}}\right) = 10\log_{10}\left(\frac{V_{ON}/G}{V_{OFF}/G}\right) = 10\log_{10}\left(\frac{V_{ON}}{V_{OFF}}\right) dB$$
 (5.6)

The following sub-sections present the time domain step response plots where all wavelengths of code *j* are measured simultaneously. The re-amplifying capability and rise and fall times are examined to measure the effectiveness of the PCC.

#### 5.3.1 Zero Wavelength Overlap

The step response of the PCC for conversion from code  $i_l$  to j is plotted in Figure 5.9. In this plot, the left y-axis measures the input code optical power in blue, while the right y-axis measures the output code voltage after the PR in red. In this step response, an input code with 4.7dB C/R results in an amplified inverted output code with a C/R of 17.8dB. There is negligible overshoot and no ringing in the response.

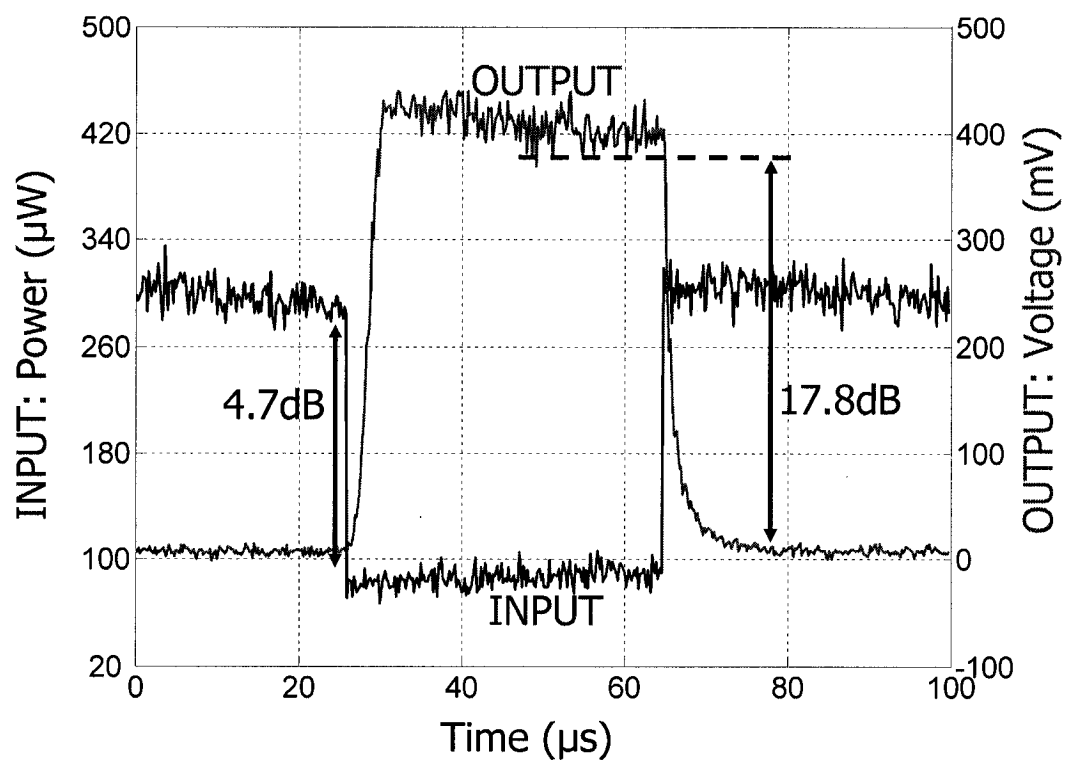


Figure 5.9: Step response for conversion from code  $i_1$  to j (zero wavelength overlap).

In Figure 5.10, we zoom in on the previous step response plot to view the transient behaviour of the PCC and measure the turn on and off delays  $(t_{DI}$  and  $t_{D2})$  as well as 10-90% rise and fall times  $(t_R$  and  $t_F)$ . These timing metrics are listed in Table 5.2 under the column  $i_I \rightarrow j$ .

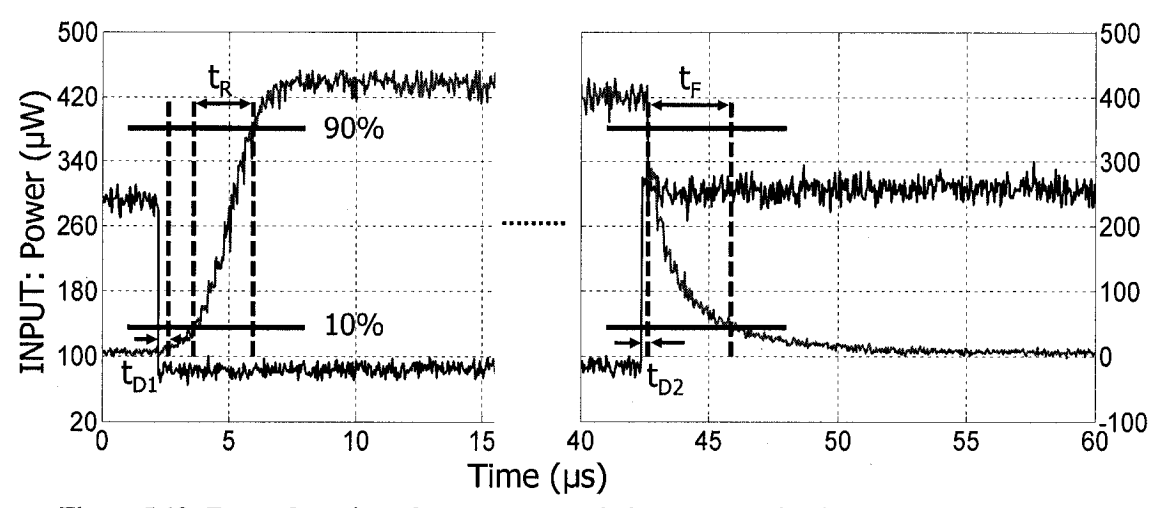


Figure 5.10: Zoomed version of step response of Figure 5.9 to highlight transient behaviour.

Table 5.2: Turn on/off delays and 10-90% rise/fall times for all input-output code combinations.

	Symbol	14→1	Time (μs) I₂→j	<i>i₃</i> →j
Turn On Delay	$t_{D1}$	0.4	0.24	0.2
10-90% Rise Time	$t_R$	2.32	1.94	2.22
Turn Off Delay	$t_{D2}$	0.26	0.04	0.08
90-10% Fall Time	$t_{\digamma}$	3.22	2.6	1.47

Bearing in mind there is approximately 57.5m of fiber in the ring, a 280ns turn on/off delay is expected when measuring input and output signals on the same scope. In the worst case, the PCC requires up to 3.22µs to convert the coded packet label for zero wavelength overlap.

## 5.3.2 One Wavelength Overlap

The step response for conversion from input code  $i_2$  to j with one wavelength overlap is shown in Figure 5.11. As expected, the output C/R is reduced compared to the case of zero wavelength overlap, where in this case an input code with 4.7dB C/R yields an output code with a C/R of 13.8dB. The transient timing metrics are given in column  $i_2 \rightarrow j$  of Table 5.2. These times are marginally improved over the zero wavelength overlap case.

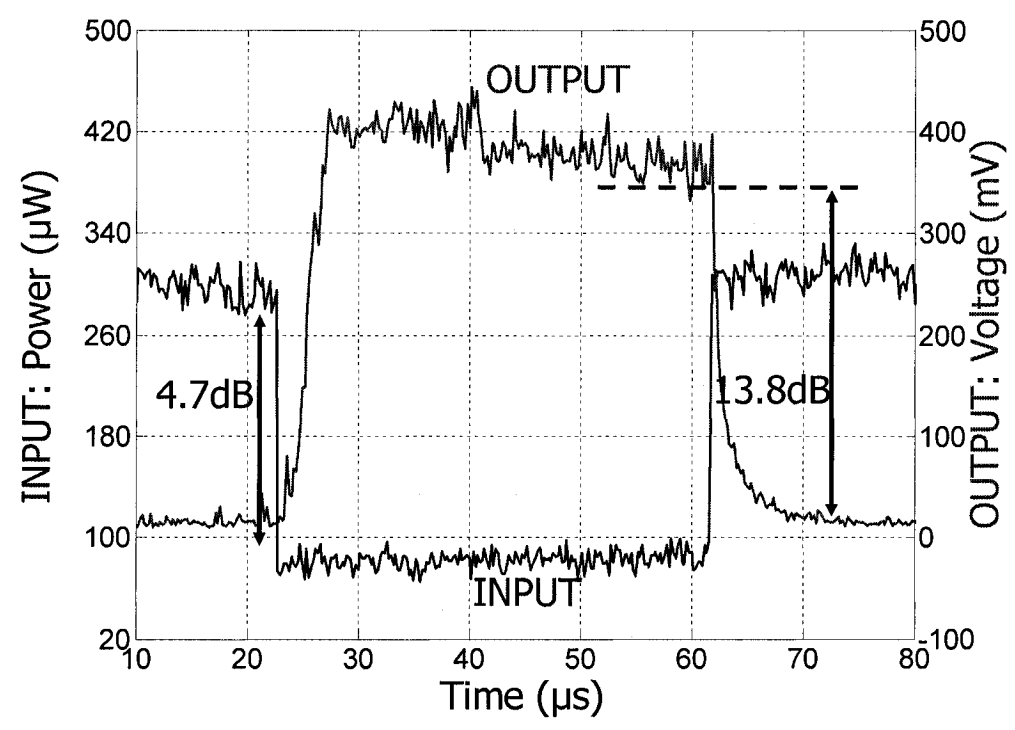


Figure 5.11: Step response for conversion from code  $i_2$  to j (one wavelength overlap).

#### 5.3.3 Two Wavelength Overlap

For the final case of two wavelength overlap, the step response is shown in Figure 5.12, with the transient timing metrics given in column  $i_3 \rightarrow j$  of Table 5.2. As predicted in the static TF of Figure 5.8 and illustrated in the step response, although re-amplifying is still observed, a larger input C/R is required to obtain an output signal with a similar C/R as for the previous cases. The timing metrics are again reduced compared to the zero wavelength overlap case, and may be explained from the fact that several wavelengths in the output code already exist. In such multi-wavelength overlap cases, inversion does not need to be established in SOA<sub>2</sub> for the overlapping wavelengths, resulting in faster conversion.

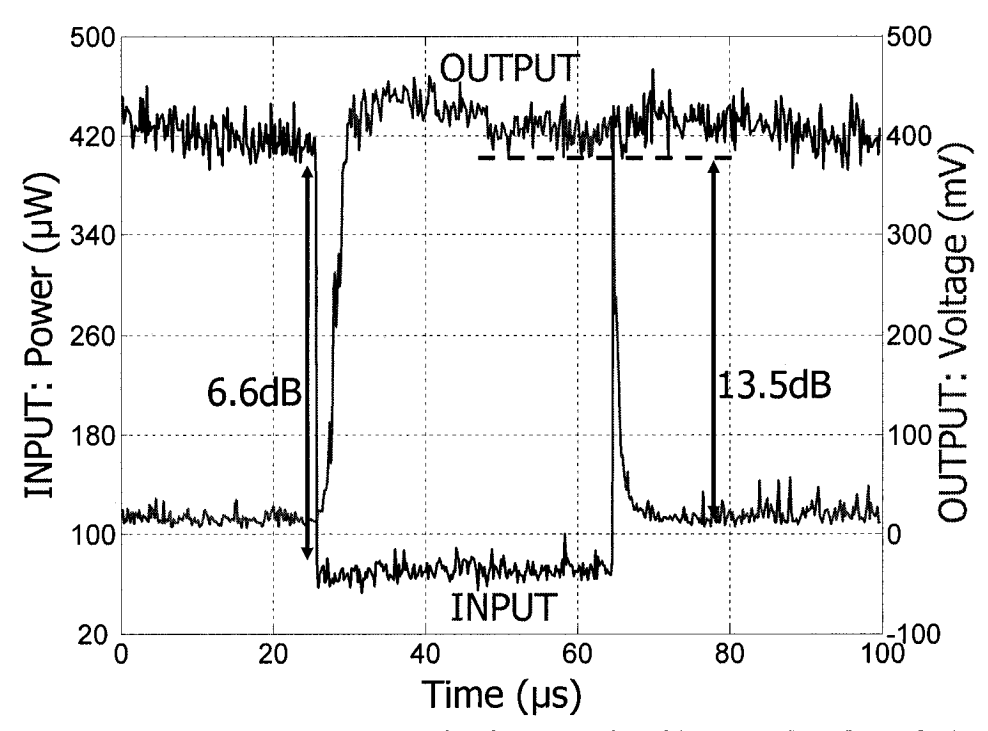


Figure 5.12: Step response for conversion from code  $i_3$  to j (two wavelength overlap).

#### 5.4 Discussion

In this chapter, successful, all-photonic OCDMA coded packet label switching was demonstrated for (7,4) m-sequences. The PCC was built using commercially available products and achieved simple and stable operation. From the step response, C/R improvement was observed for slowly modulated labels. The limiting functionality in the static transfer characteristics indicated that the lasing powers on each output wavelength are equalized, and that noise or ER degradation on the input signal would be negated.

Although this PCC converts from any incoming code to the output code defined by the wavelength ports selected in the AWG, tuneable code conversion is possible using tuneable wavelength selective components such as a wavelength selective Micro-Opto-Electro-Mechanical Systems (MOEMS) switch in the SFRL.

In addition to performing label code switching in a NN, the viability of a label switching network depends on the ability to perform clock and data recovery (CDR) [68]. In this network, it is infeasible to send a global clock signal to every end user. Ideally, the end user should be able to recover the clock from the incoming data stream and proceed with data processing. By making some simple modifications to this PCC, we achieved all-photonic clock recovery of a return-to-zero (RZ) data payload signal. This modified PCC could multicast the clock onto several output wavelengths defined by the AWG. A discussion of this work and preliminary results are presented in Appendix B.

#### 5.4.1 Limitations

In this thesis, the spectral labels are assumed to be CW. Given the 10-90% rise and fall times are of the order of  $\mu$ s, a packet entering the NN would require payload buffering in a fixed length of fiber delay line until the switching was complete to allow simultaneous transmission of payload and label. These times could be reduced by using shorter cavity lengths.

Furthermore, although a simple configuration for a weight four code, difficulties would be encountered for longer length (and higher weight) codes in equalising and stabilising the lasing wavelength powers in the ring (currently achieved by the PC's). This could be resolved by developing packaging solutions to minimise ring instabilities or by using multiple PCC's in parallel, where each PCC converts a set of wavelengths defining a section of the code.

Finally, to negate label inversion arising from XGM in the PCC, a simple modification to the PCC setup could be made as shown in the block diagram of Figure 5.13. In this diagram, spectral label i is input to an XGM based multiple-input to single-output WC. The output control wavelength ( $\lambda_c$ ) is sent to a PCC modified to accept a single input. By

using a dedicated control channel in the intermediate step with sufficient power to saturate  $SOA_2$ , wavelength overlap (and thus ER degradation) would not occur in switching between label i and label j.

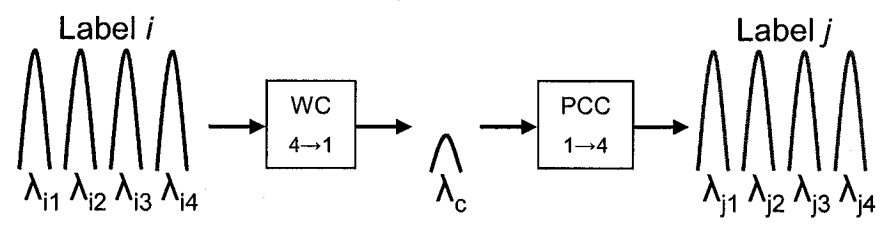


Figure 5.13: Negating label inversion by switching from label i to j using an intermediate step with dedicated control wavelength  $\lambda_c$ .

## 6 Conclusions

## 6.1 Summary

This thesis studied optical MPLS networks. We were concerned with data payload and label processing in a NN as a packet transits through the core network. Our study comprised a theoretical analysis of data traffic throughput improvement achievable using reduced sets of realistic WC's in a space switch, and a practical demonstration of a spectral label switching PCC in the laboratory.

In Chapters 1 and 2, we motivated the need for optical access networks and presented an optical MPLS network where packet payloads were wavelength multiplexed and labels spectrally OCDMA coded. At a NN, data payload wavelength contentions were discussed and various space switch and WC architectures were introduced to mitigate these contentions and improve throughput.

In Chapter 3, several common wavelength conversion technologies were contrasted to demonstrate their limited-range conversion capability (for WC's), and also to assess their applicability for all-photonic label switching systems.

In Chapter 4, we presented a rigorous theoretical analysis to model uniform and bursty data traffic flow in a bufferless NN with reduced sets of FRWC's. All results were verified by MC simulation. We further used MC analysis to model the realistic scenario of reduced sets of LRWC's with various matching algorithms in the switch control block. These analyses made up a software package allowing a user to determine the number of WC's required in a NN to achieve a desired PLP threshold given data traffic statistics and limitations on CR. The main results of this chapter are summarised below.

- Optimal throughput can be achieved using reduced sets of FRWC's in a NN.
   Savings of greater than half the complete set of FRWC's can often be made, resulting in considerable complexity and cost reductions.
- Bursty traffic PLP degradation can be mitigated by increasing the number of wavelengths in the network and using sets of WC's.

- The constraint of limited-range conversion reduces the effectiveness of reduced sets of LRWC's in achieving optimal throughput in a NN. However, by using optimal matching algorithms, the sensitivity of PLP to CR is reduced. In this case a trade-off between CR and number of LRWC's must be made to achieve a desired PLP.
  - o The ability to account for bursty traffic and LRWC's with various matching algorithms generalises previous studies.
- In contrast to previous work, by combining the random and Munkres matching algorithms introduced in this thesis into the switch control block, lower PLP is obtained than when using the FAA discussed in [55]. The RMA and OMA ensure the PLP always decreases monotonically to a PLP floor as CR increases. These results are further distinguished from the FAA matching algorithm where PLP can *increase* to a PLP floor as CR increases. The trade-off for this improved performance is an increased computational complexity.

Having examined the advantages of resolving payload wavelength contentions, we studied another fundamental aspect of the NN, label processing. Chapter 5 demonstrated successful label code switching of (7,4) spectral m-sequences using a setup built from commercially available optical components. Cases of zero, one and two wavelength overlaps between input and output codes were examined corresponding to various network scenarios. The thresholding behaviour of the static transfer characteristics indicated that pulse re-shaping would occur, while the step response plots showed significant re-amplification. These results verified that the PCC is capable of 2R-regeneration for slowly modulated labels. For the CW spectral labels considered in this thesis, noise and ER degradation on the input label is negated, while output wavelength lasing powers are equalized. Furthermore, our PCC could be modified to perform all-photonic clock recovery from the data payload as discussed in Appendix B.

The significance of this work lies firstly in the cost and complexity savings to be made by recognizing that reduced sets of realistic WC's can be incorporated into a space switch in the NN to resolve data wavelength contentions. Secondly, the PCC label switching

system demonstration solves a key label processing issue in the NN. Ultimately, this work brings optical MPLS networks a step closer to practical deployment.

#### 6.2 Future Directions

Although the software package modelling traffic flow in a NN with reduced sets of LRWC's is comprehensive, improvements could be made by including additional wavelength matching algorithms in the switch control block. A detailed algorithm comparison study (in terms of computational complexity and performance) could be used to aid optical MPLS network engineering.

In relation to the practical demonstration of a label switching PCC, considerable future work remains. Firstly, an investigation of other techniques to achieve label code conversion could be performed using the technologies of Chapter 3. This would allow conclusions to be drawn as to the overall suitability of each technology to concurrent multiple wavelength conversion.

Secondly, as discussed in Section 2.1, realistic labels will have longer lengths than the (7,4) m-sequences studied in this thesis, and thus conversion between longer label codes could be explored. As mentioned in Chapter 5, this could be achieved by running multiple PCC's in parallel or by developing improved packaging techniques to enhance ring stability.

Finally, there is considerable work to be done on the all-photonic clock recovery setup of Appendix B. Based on the success of the preliminary results presented, we plan to use an RZ source rather than simulating RZ pulses with an NRZ pattern generator. Additionally, the use of SI-FBG's rather than an AWG in the ring will equalise round trip times of each wavelength and minimise interference effects at harmonics of the fundamental ring frequency.

## 7 References

- [1] A. Stok and E. H. Sargent, "Lighting the Local Area: Optical Code-Division Multiple Access and Quality of Service Provisioning," *IEEE Network*, pp. 42-46, Nov/Dec 2000.
- [2] C. A. Brackett, "Dense wavelength division multiplexing networks: Principles and applications," *IEEE Journal on Select. Areas in Comms.*, vol. 8, pp. 948, 1990.
- [3] P. E. Green, L. A. Coldren, K. M. Johnson, J. G. Lewis, and C. M. Miller, "Alloptical packet-switched metropolitan-area network proposal," *J. Lightwave Technol.*, vol. 11, no.5, pp. 754, 1993.
- [4] K. Kitayama, "Code division multiplexing lightwave networks based on optical code converter," *IEEE Journal on Select. Areas in Comms.*, vol. 16, no.7, pp. 1309, 1998.
- [5] D. Norte and A. E. Willner, "All-optical data format conversions and reconversions between the wavelength and time domains for dynamically reconfigurable WDM networks," *J. Lightwave Technol.*, vol. 14, no.6, pp. 1170, 1996.
- [6] V. Eramo and M. Listanti, "Packet Loss in a Bufferless Optical WDM Switch Employing Shared Tunable Wavelength Converters," *J. Lightwave Technol.*, vol. 18, no.12, pp. 1818-1833, Dec 2000.
- [7] V. Eramo, M. Listanti, and M. D. Donato, "Performance Evaluation of a Bufferless Optical Packet Switch With Limited-Range Wavelength Converters," *IEEE Photon. Technol. Lett.*, vol. 16, no.2, pp. 644-646, Feb 2004.
- [8] S. L. Danielsen and C. Joergensen, "Analysis of a WDM Packet Switch with Improved Performance Under Bursty Traffic Conditions Due to Tuneable

- Wavelength Converters," *J. Lightwave Technol.*, vol. 16, no.5, pp. 729-734, May 1998.
- [9] J. He, X. Wang, and K. T. Chan, "Tunable All-Optical Wavelength Conversion and 2R Regeneration Based on Semiconductor-Fiber Ring Laser," presented at LEOS, 2001.
- [10] K. Obermann and S. Kindt, "Performance Analysis of Wavelength Converters Based on Cross-Gain Modulation in Semiconductor-Optical Amplifiers," *J. Lightwave Technol.*, vol. 16, no.1, pp. 78-85, Jan 1998.
- [11] M. Asghari, I. H. White, and R. V. Penty, "Wavelength Conversion Using Semiconductor Optical Amplifiers," *J. Lightwave Technol.*, vol. 15, no.7, pp. 1181-1190, July 1997.
- [12] R. E. Gordon and L. R. Chen, "Demonstration of All-Photonic Code Conversion in a Semiconductor Fiber Ring Laser for OCDMA Networks," presented at OSA Topical Meeting on Information Photonics, Charlotte, NC, Jun 2005.
- [13] R. E. Gordon, L. R. Chen, and M. Coates, "Analysis of a WDM Packet Switch with a Reduced Set of Limited-Range Wavelength Converters," presented at OSA Topical Meeting on Information Photonics, Charlotte, NC, Jun 2005.
- [14] Y. G. Wen, Y. Zhang, and L. K. Chen, "On Architecture and Limitation of Optical Multiprotocol Label Switching (MPLS) Networks Using Optical-Orthogonal-Code (OOC)/Wavelength Label," *Optical Fiber Technology*, vol. 8, pp. 43-70, 2002.
- [15] "Diagram of an MPLS packet." http://commons.wikimedia.org/wiki/Image:MPLS packet.png, June 2005.
- [16] A. Leon-Garcia and I. Widjaja, Communications Networks: Fundamental Concepts and Key Architectures, 2001.

- [17] S. LaRochelle, L. A. Rusch, A. Leon-Garcia, L. R. Chen, and D. V. Plant,

  "Packet-switched networks with photonic code-based processing," NSERC-CIPI
  NCE Project #IT2.
- [18] M. Y. Jeon, Z. Pan, J. Cao, Y. Bansal, and J. Taylor, "Demonstration of all-optical packet switching routers with optical label swapping and 2R regeneration for scalable optical label switching network applications," *J. Lightwave Technol.*, vol. 21, no.11, pp. 2723-2733, Nov 2003.
- [19] S. Aleksic and V. Krajinovic, "Comparison of optical code correlators for alloptical MPLS networks," presented at European Conference on Optical Communications, 2002.
- [20] H. Sotobayashi, "Transparent virtual optical code/wavelength path network," *IEEE Journal on Select. Topics in Quantum Electron.*, vol. 8, no.699-704, 2002.
- [21] J. Faucher, R. Adams, L. R. Chen, and D. V. Plant, "Multiuser OCDMA System Demonstrator With Full CDR Using a Novel OCDMA Receiver," *IEEE Photon. Technol. Lett.*, vol. 17, no.5, May 2005.
- [22] A. Li and D. V. Plant, "A Broadband PLL solution for Burst-mode Clock and Data recovery in All-Optical networks," presented at OSA Topical Meeting on Information Photonics, Charlotte, NC, Jun 2005.
- [23] G. Brochu, S. LaRochelle, and R. Slavik, "Modeling and Experimental Demonstration of Ultracompact Multiwavelength Distributed Fabry-Pérot Fiber Lasers," *J. Lightwave Technol.*, vol. 23, no.1, pp. 44-53, 2005.
- [24] J. E. McGeehan, M. C. Hauer, A. B. Sahin, and A. E. Willner, "Multiwavelength-Channel Header Recognition for Reconfigurable WDM Networks Using Optical Correlators Based on Sampled Fiber Bragg Gratings," *IEEE Photon. Technol. Lett.*, vol. 15, no.10, pp. 1464-1466, Oct 2003.

- [25] D. J. Blumenthal, P. R. Prucnal, and J. R. Sauer, "Photonic Packet Switches: Architectures and experimental implementations," *IEEE Commun. Mag.*, vol. 82, no.11, pp. 1650, 1994.
- [26] T. Fjelde, A. Kloch, and D. Wolfson, "Novel scheme for efficient label-swapping under simple XOR gate," presented at European Conference on Optical Communications, 2000.
- [27] S. J. B. Yoo, "Wavelength Conversion Technologies for WDM Network Applications," *J. Lightwave Technol.*, vol. 14, pp. 955-966, Jun 1996.
- [28] N. Wada and F. Kubota, "Cutting-Edge Technologies on Broadband and Scalable Photonic Network-Packet switched networks based on all-optical label processing," *Optical Review*, vol. 11, no.2, pp. 106-112, 2004.
- [29] A. Teixera, P. Andre, P. Monteiro, M. Lima, R. Nogueira, and J. da Rocha, "All optical routing based on OCDMA headers," presented at European Conference on Optical Communications. Paper ThEE4, 2003.
- [30] A. Teixera, M. Lima, P. Andre, and J. da Rocha, "All optical time-wavelength Code Router for Optical CDMA networks," presented at LEOS Annual Meeting. Paper ML3, 2001.
- [31] K. Kitayama, "Architectural Considerations for Photonic IP Router Based upon Optical Code Correlation," *J. Lightwave Technol.*, vol. 18, no.12, pp. 1834-1843, Dec 2000.
- [32] N. Karafolas and D. Uttamchandani, "Optical Fiber Code Division Multiple Access Networks: A Review," *Optical Fiber Technology*, vol. 2, pp. 149-168, 1996.
- [33] R. M. H. Yim, J. Bajcsy, and L. R. Chen, "A New Family of 2-D Wavelength—Time Codes for Optical CDMA With Differential Detection," *IEEE Photon. Technol. Lett.*, vol. 15, no.1, pp. 165-167, Jan 2003.

- [34] J.-K. Liang, "Merged m-sequence Codes for Hybrid Time-Spreading/ Wavelength-Hopping Optical CDMA System," in *Department of Electrical Engineering*. Tianan: National Cheng Kung University, 2003, pp. 49.
- [35] A. A. Hassan, J. E. Hershey, and G. J. Saulnier, "Perspectives in Spread Spectrum," Boston, 1998.
- [36] G. Contestabile, M. Presi, and E. Ciaramella, "Multiple Wavelength Conversion for WDM Multicasting by FWM in an SOA," *IEEE Photon. Technol. Lett.*, vol. 16, no.7, pp. 1775-1777, July 2004.
- [37] G. N. Rouskas, "Optical Layer Multicast- Rational, building blocks and challenges," *IEEE Network*, vol. 17, pp. 60-65, Jan/Feb 2003.
- [38] D. K. Hunter, M. C. Chia, and I. Andonovic, "Buffering in optical packet switches," *J. Lightwave Technol.*, vol. 16, no.12, pp. 2081-2094, Dec 1998.
- [39] F. Masetti, P. Gavignet, D. Chiaroni, and G. DaLoura, "Fiber delay lines optical buffer for ATM photonic switching applications," presented at IEEE Infocom, San Francisco, CA, Mar 1993.
- [40] S. L. Danielsen, P. B. Hansen, and K. E. Stubkjaer, "Wavelength Conversion in Optical Packet Switching," *J. Lightwave Technol.*, vol. 16, no.12, pp. 2095-2108, Dec 1998.
- [41] V. Eramo, M. Listanti, and P. Pacifici, "A Comparison Study on the Number of Wavelength Converters Needed in Synchronous and Asynchronous All-Optical Switching Architectures," *J. Lightwave Technol.*, vol. 21, no.2, pp. 340-355, Feb 2003.
- [42] V. Eramo and M. Listanti, "Performance Evaluation of Optical Cross Connect Architectures Under an Efficient Wavelength Assignment," *IEEE Comms. Lett.*, vol. 6, no.7, pp. 294-296, July 2002.

- [43] T. Durhuus, B. Mikkelsen, and C. Joergensen, "All-Optical Wavelength Conversion by Semiconductor Optical Amplifiers," *J. Lightwave Technol.*, vol. 14, pp. 942-954, Jun 1996.
- [44] K. Inoue and H. Toba, "Wavelength conversion experiment using fiber four-wave mixing," *Photonics Technology Letters, IEEE*, vol. 4, no.1, pp. 69, 1992.
- [45] B. E. Olsson, P. Ohlen, L. Rau, and D. J. Blumenthal, "A simple and robust 40-Gb/s wavelength converter using fiber cross-phase modulation and optical filtering," *Photonics Technology Letters, IEEE*, vol. 12, no.7, pp. 846, 2000.
- [46] L. Rau, R. Doshi, S. Rangarajan, C. Yijen, D. J. Blumenthal, and J. E. Bowers, "Analog performance of an ultrafast sampled-time all-optical fiber XPM wavelength converter," *Photonics Technology Letters, IEEE*, vol. 15, no.4, pp. 560-562, 2003.
- [47] J. M. H. Elmirghani and H. T. Mouftah, "All-optical wavelength conversion: technologies and applications in DWDM networks," *Communications Magazine*, *IEEE*, vol. 38, no.3, pp. 86-92, 2000.
- [48] J. Mork, M. L. Nielsen, and T. W. Berg, "The Dynamics of Semiconductor Optical Amplifiers: Modeling and Applications," *Optics & Photonics News*, vol. 6, pp. 43-48, July 2003.
- [49] D. Mahgerefteh, P. Cho, J. Goldhar, and G. L. Burdge, "Technique for Suppression of Pattern Dependence in a Semiconductor-Optical-Amplifier Wavelength Converter," *IEEE Photon. Technol. Lett.*, vol. 9, no.12, pp. 1583-1585, Dec 1997.
- [50] H. Ishikawa, S. Watanabe, and H. Kuwatsuje, "Wavelength Conversion Technologies for Photonic Network Systems," *Fujitsu Sci. Tech.*, vol. 35, pp. 126-138, Feb 1999.

- [51] B. Ramamurthy and B. Mukherjee, "Wavelength Conversion in WDM Networking," *IEEE Journal on Select. Areas in Comms.*, vol. 16, no.7, pp. 1061-1073, Sept. 1998.
- [52] G. P. Agrawal, Nonlinear Fiber Optics: Academic Press, 2001.
- [53] S. L. Danielsen, B. Mikkelsen, C. Joergensen, T. Durhuus, and K. E. Stubkjaer, "WDM Packet Switch Architectures and Analysis of the Influence of Tuneable Wavelength Converters on the Performance," *J. Lightwave Technol.*, vol. 15, no.2, pp. 219-226, Feb 1997.
- [54] V. Eramo and M. Listanti, "Input Wavelength Conversion in Optical Packet Switches," *IEEE Comms. Lett.*, vol. 7, no.6, pp. 281-283, June 2003.
- [55] V. Eramo, M. Listanti, and M. Spaziani, "Resources Sharing in Optical Packet Switches With Limited-Range Wavelength Converters," *J. Lightwave Technol.*, vol. 23, no.2, pp. 671-687, Feb 2005.
- [56] J. Landman, "Modelling a DS-CDMA Fading Channel with Bursty Traffic Arrivals." Cape Town: University of Cape Town, Sept 2003.
- [57] A. K. Wong, "Traffic Modeling and buffer dimensioning in an ATM switch with shared-memory end-grids," presented at ISS, Yokohama, Japan, Oct 1992.
- [58] D. B. West, *Introduction to Graph Theory*, 2 ed: Prentice Hall, 2001.
- [59] R. A. Pilgrim, "Munkres Assignment Algorithm: http://216.249.163.93/bob.pilgrim/445/munkres.html," 2004.
- [60] F. Burgeios and J. C. Lassalle, "An extension of munkres algorithm for the assignment problem to rectangular matrices," *Comm. of the ACM 14:802*, 1971.
- [61] G. Shen, S. K. Bose, T. H. Cheng, C. Lu, and T. Y. Chai, "Performance Study on a WDM Packet Switch With Limited-Range Wavelength Converters," *IEEE Comms. Lett.*, vol. 5, no.10, pp. 432-434, Oct 2001.

- [62] P. J. Smith, M. Shafi, and H. Gao, "Quick Simulation: A Review of Importance Sampling Techniques in Communications Systems," *IEEE Journal on Select.*Areas in Comms., vol. 15, no.4, pp. 597-613, May 1997.
- [63] Z. G. Lu, S. A. Boothroyd, and J. Chrostowski, "Tunable Wavelength Conversion in a Semiconductor-Fiber Ring Laser," *IEEE Photon. Technol. Lett.*, vol. 11, no.7, pp. 806-808, July 1999.
- [64] K. K. Chow and C. Shu, "All-optical wavelength conversion with multicasting at 6x10Gbit/s using electroabsorption modulator," *Electronics Letters*, vol. 39, no.19, pp. 1395-1397, 2003.
- [65] K. K. Chow and C. Shu, "All-optical signal regeneration with wavelength multicasting at 6x10 Gb/s using a single electroabsorption modulator," *Optics Express*, vol. 12, no.13, pp. 3050-3054, 2004.
- [66] J. He and K. T. Chan, "Wavelength-switchable all optical clock recovery at 10Gbit/s based on semiconductor fiber ring laser," *Optics Express*, vol. 13, no.1, pp. 327-335, Jan 2005.
- [67] Datasheet, "NewFocus InGaAs 125MHz Photoreceiver, Model 1811-FC," <a href="http://www.newfocus.com/product/model.cfm?productlineid=3&modelgroupid=1">http://www.newfocus.com/product/model.cfm?productlineid=3&modelgroupid=1</a> 054&modelno=1811%2DFC.
- [68] R. Adams, "Analysis and implementation of a two-dimensional wavelength-time optical code-division multiple-access system." Montreal: McGill University, 2005, pp. 64.

# 8 Appendix A: Monte-Carlo Algorithm Flowcharts

# 8.1 Bursty Traffic in a Switch with Reduced Sets of FR-PCC's

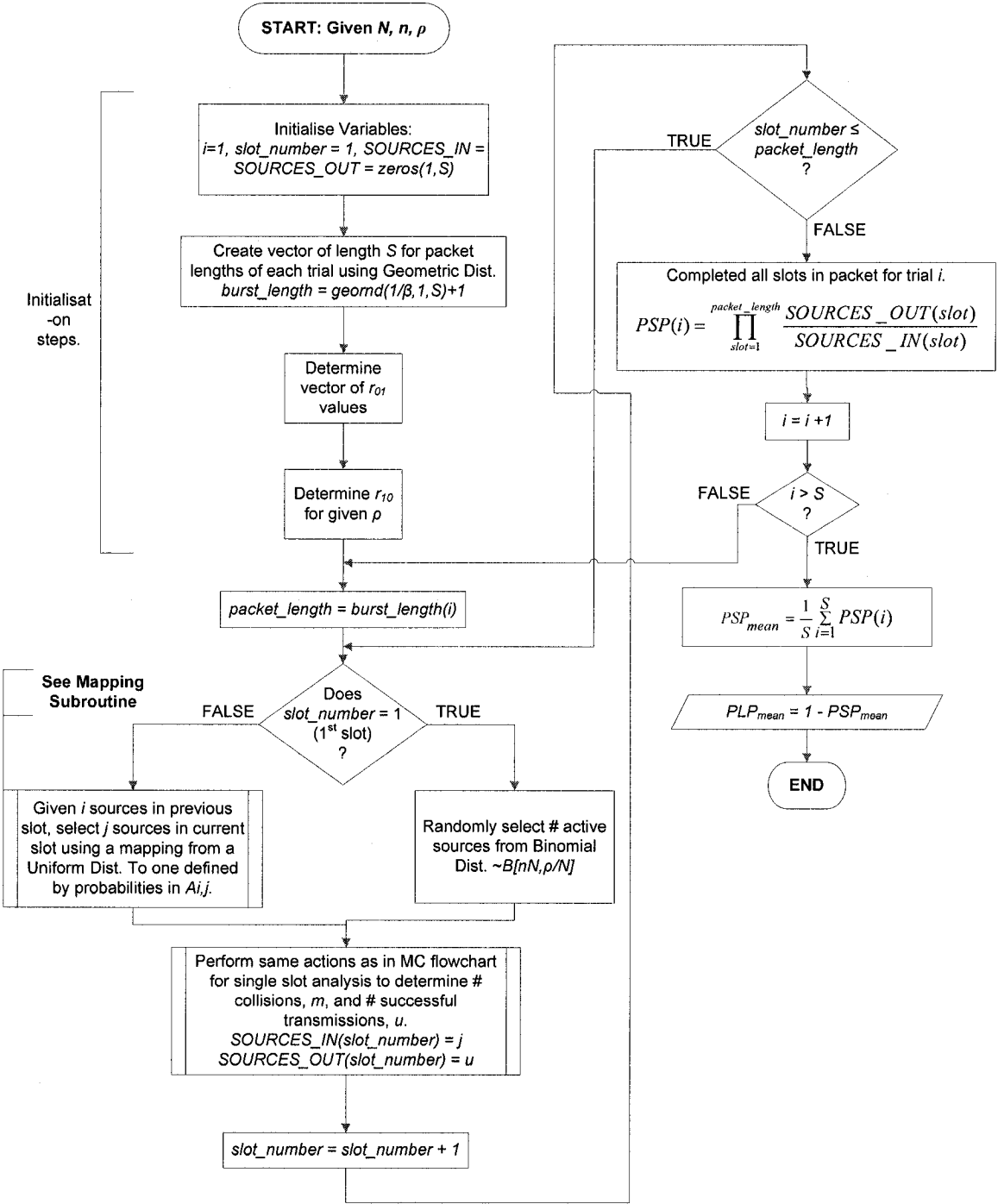


Figure 8.1: Flowchart to implement MC algorithm for bursty (multiple slot) traffic presented in Section 4.2. The Mapping subroutine is illustrated in Figure 8.2.

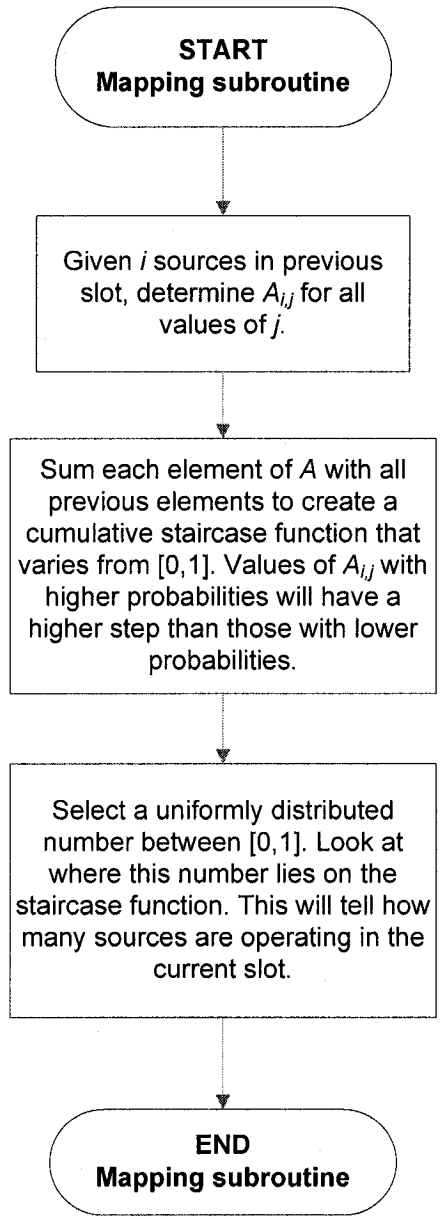


Figure 8.2: Mapping subroutine from Figure 8.1.

# 9 Appendix B: All-Photonic Clock Recovery

#### 9.1 Introduction

The importance of CDR was discussed in Section 5.4. In an optical network, the ability to perform all-photonic CDR removes an electronic processing bottleneck at the end user stage and promotes the attractiveness of optical networks in the marketplace. In this appendix, all-photonic clock recovery is demonstrated for an RZ data signal at modulation frequencies above 2GHz. We consider the cases of single and multiple input data wavelengths, and extract the clock onto single and multiple output wavelengths (i.e. clock multicasting).

#### 9.2 Laser Setup

To achieve all-photonic clock recovery from the data payload, the PCC setup of Figure 5.2 is used, where the function generator is replaced by an RZ source. As an RZ source was unavailable during testing, we used a bit error rate tester (BERT) to generate a square, non-return-to-zero (NRZ) pseudo-random bit sequence (PRBS). By modifying the BERT's hex file to pad each bit of the NRZ PRBS with *n* zeros, we could simulate an RZ PRBS with

$$f_{RZ} = \frac{f_{\text{mod}}}{n+1} \tag{9.1}$$

where  $f_{RZ}$  is the RZ modulation frequency and  $f_{mod}$  is the modulation frequency of the NRZ PRBS. The duty cycle of the RZ PRBS is given by

$$DC = \frac{1}{n+1} \times 100\% \tag{9.2}$$

If the RZ data signal arrives on one wavelength, only one TLS is used in the control arm of Figure 5.2. The number of AWG ports connected to fiber loop mirrors corresponds to the number of wavelengths the recovered clock is to be multicast over. As discussed in Section 5.1.1, the loop mirror lengths were carefully spliced to ensure the ring round trip times for each wavelength were closely matched.

## 9.3 Principle of Operation

As for code conversion, when a "1" (or "0") bit enters the PCC from the control arm, lasing is cut-off (or established) on the output wavelengths due to XGM in SOA<sub>2</sub>. However, by setting  $f_{RZ}$  of the data signal to equal a harmonic of the fundamental ring frequency,  $f_0$ , active harmonic mode locking in the ring occurs, resulting in a pulsed output on the wavelengths selected by the AWG. This is the recovered clock with frequency  $f_{RZ}$ . If  $f_{RZ}$  does not match a harmonic of  $f_0$ , mode locking will not occur and the output will be unintelligible.

# 9.4 Preliminary Results

This section presents preliminary results for all-photonic clock recovery from an RZ data signal on to one and four output wavelengths.

### 9.4.1 One Input Wavelength to One Output Wavelength

For this measurement, the RZ data signal is carried (and the clock is recovered) on a single wavelength. The parameters for this setup are shown in Table 9.1. From these values,  $f_{RZ} = 2.22$ GHz and corresponds to the 638<sup>th</sup> harmonic of  $f_0$ .

Table 9.1: Experimental parameters for clock recovery of an RZ data signal on one wavelength.

,		8
Parameter	Symbol	Value
RZ Input PRBS		·
Input Wavelength	$\lambda_i$	1541.28nm
Padded zeros	n	1
Duty Cycle	DC	50%
Mark Ratio	MR	50%
Length	L	2 <sup>14</sup> -1
NRZ Modulation Freq.	f <sub>mod</sub>	4.442GHz
RZ Modulation Freq.	$f_{RZ}$	2.223GHz
Clock Recovery		,
Output Wavelength	$\lambda_{j1}$	1536.54nm
Ring Length	$L_{j}$	57.44m
Ring Fundamental Freq.	$f_0$	3.482MHz
EDFA after 10% Coupler	EDFA <sub>out</sub>	15%

A CSA trace of the input RZ PRBS is presented in Figure 9.1, with the recovered clock on output wavelength  $\lambda_{jl}$  given in Figure 9.2. In both plots, sample acquisition mode was used in the CSA.

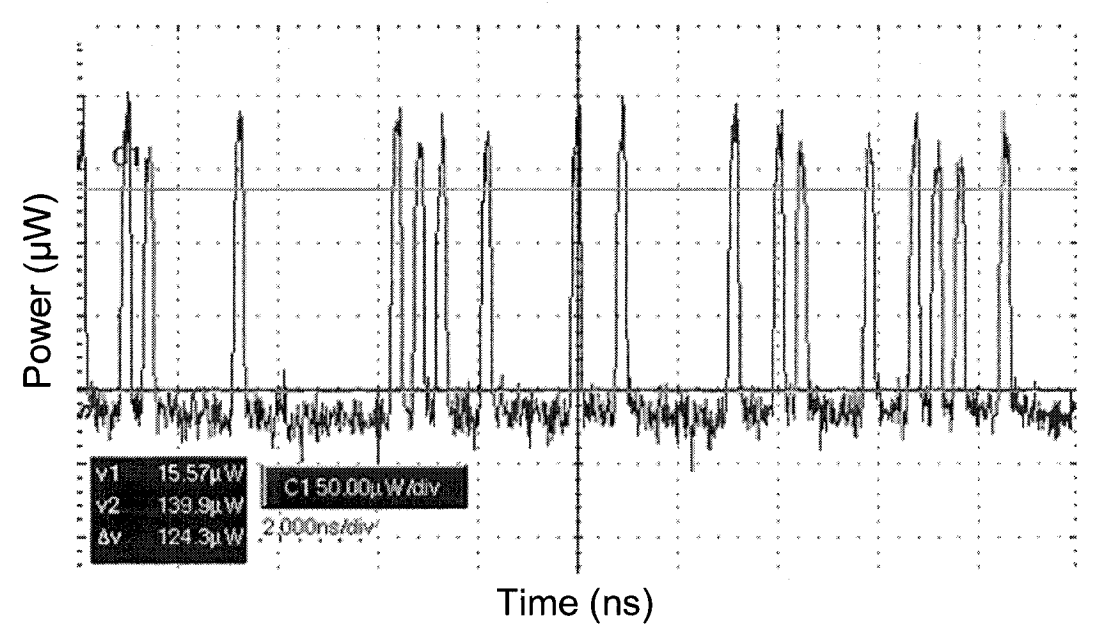


Figure 9.1: Input RZ PRBS operating on  $\lambda_i$  and modulated at 2.22GHz = 638f<sub>0</sub>.

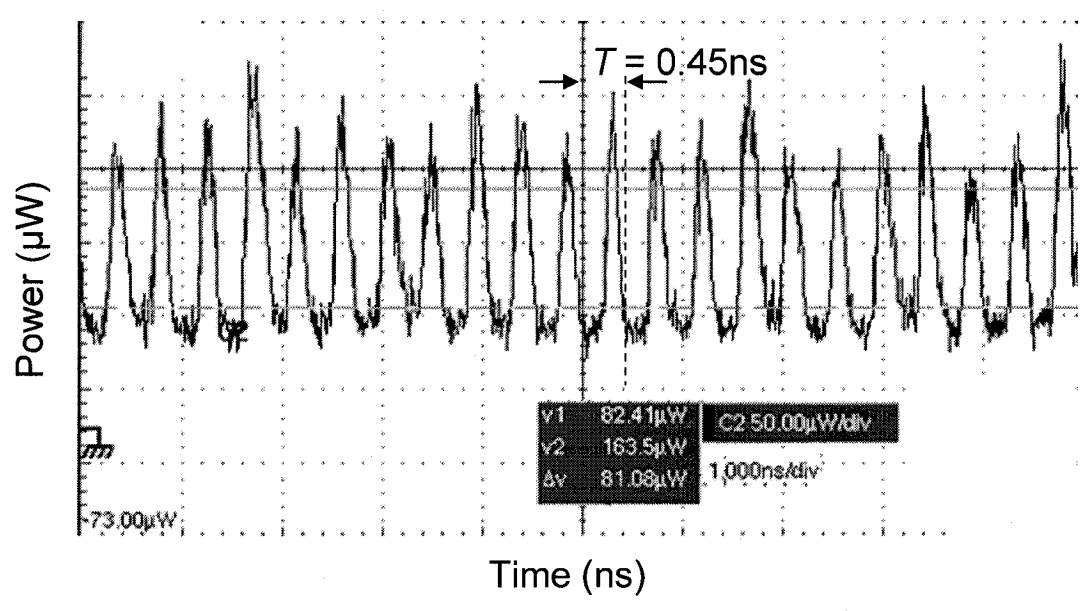


Figure 9.2: Recovered clock on  $\lambda_{jl}$ . Sample mode acquisition used in the CSA.

From Figure 9.2, the recovered clock is reasonably clean, with a period of 0.45ns corresponding to a clock frequency of 2.22GHz, matching  $f_{RZ}$ . A C/R degradation occurs in the recovery process, from 5.6dB at the input to 3dB at the output. This degradation arises as a result of an EDFA stage at the 10% coupler output to boost the recovered clock power allowing it to be detected at the CSA optical module. Due to the nonlinear EDFA gain curve, lower clock powers ("0" level) receive more gain than higher powers

("1" level), reducing C/R. The EDFA amplified spontaneous emission (ASE) noise also degrades OSNR.

## 9.4.2 Four Input Wavelengths to Four Output Wavelengths

In this setup, the RZ data signal arrives on four wavelengths defined by code  $i_1$ . The clock is recovered and multicast on four output wavelengths defined by output code j. Both codes are defined in Table 5.1. The parameters for this setup are shown in Table 9.2.

Table 9.2: Experimental parameters for clock recovery of an RZ data signal on four wavelengths.

The state of the s			
Parameter	Symbol	Value	
RZ Input PRBS			
Input Wavelengths (code i <sub>1</sub> )	λ <sub>i1-4</sub>	1533.40,1534.98,1535.76,1541.28nm	
Padded zeros	n	1	
Duty Cycle	DC	50%	
Mark Ratio	MR	50%	
Length	L	2 <sup>14</sup> -1	
NRZ Modulation Freq.	f <sub>mod</sub>	1.125GHz	
RZ Modulation Freq.	$f_{RZ}$	562.758MHz	
Clock Recovery			
Output Wavelengths (code j)	λ <sub>j1-4</sub>	1536.54,1538.11,1539.69,1542.85nm	
Ring Length	$L_i$	57.57m	
Ring Fundamental Freq.	$f_0$	3.474MHz	
EDFA after 10% Coupler	<b>EDFA</b> <sub>out</sub>	15%	
Photoreceiver		NewPort 818-BB-31: 1.5GHz bandwidth	

For this setup, the lower RZ data rate corresponds to the  $162^{nd}$  ring harmonic. In this case, a 1.5GHz external PR was used after the output EDFA and connected to the CSA electrical module. CSA traces with  $16\times$  averaging for the input and recovered clock are shown in Figure 9.3.

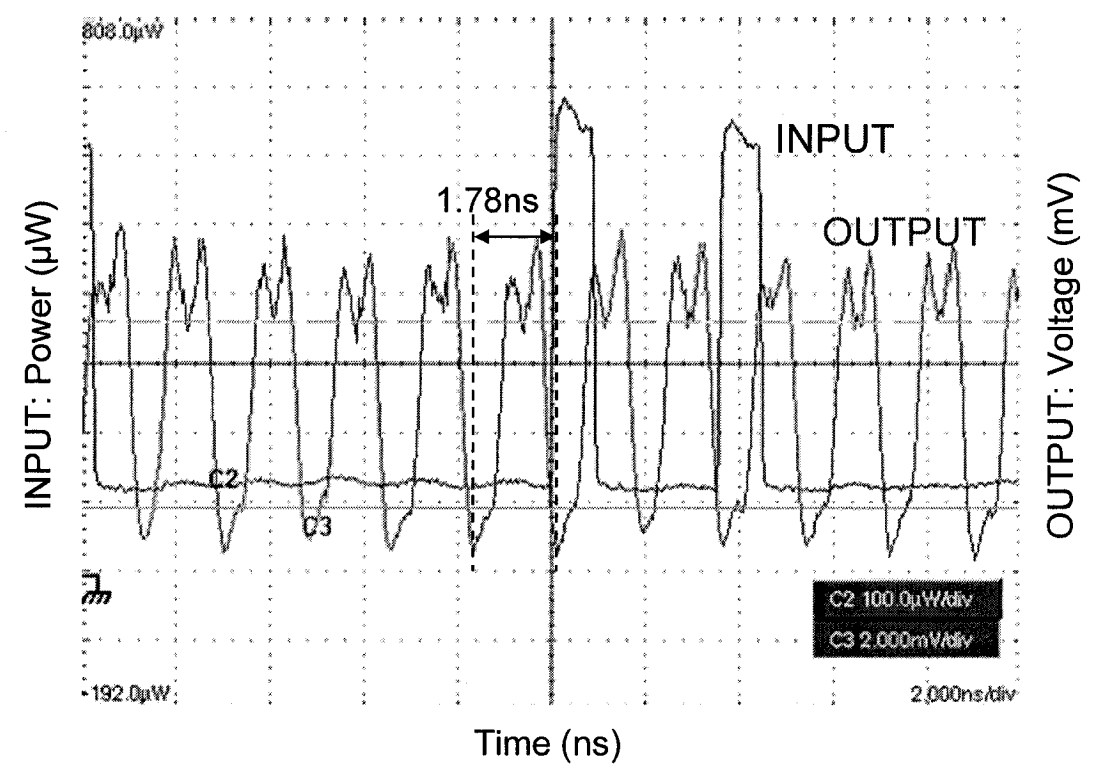


Figure 9.3: CSA trace (16x sampling) for input RZ PRBS (blue) and recovered clock output (red). The clock of the incoming data on four wavelengths defined by code  $i_1$  is multicast to four wavelengths defined by code j.

In these traces, the recovered clock has a period of 1.78ns corresponding to a frequency of 561.8MHz and closely matches  $f_{RZ}$ . Again C/R degradation is observed and arises for the same reasons as the previous case. The interference pattern in the output signal is due to the mismatches in round trip lengths of each lasing wavelength resulting in marginally different fundamental frequencies. In this case, the slightly differing frequencies of the  $162^{\text{nd}}$  harmonic for each wavelength in code j caused this interference. This was verified with a TO-BPF at the ring output to confirm that all wavelengths in code j were present and had approximately equal C/R's and modulation frequencies.

### 9.5 Discussion

We have demonstrated preliminary results for all-photonic clock recovery using the simple PCC configuration of Chapter 5. The ability to multicast the clock to several wavelengths makes it a promising technology for optical MPLS networks and could form a component of an all-photonic 3R-regeneration system. Further research will focus on

reducing ring sensitivity to path-length misalignments between wavelengths, a timing jitter assessment on the recovered clock, and methods to improve the output C/R.

# 10 Appendix C: Publications accepted for conferences

The following are the two publications accepted for conference presentations.

- R. E. Gordon and L. R. Chen, "Demonstration of All-Photonic Code Conversion in a Semiconductor Fiber Ring Laser for OCDMA Networks," presented at OSA Topical Meeting on Information Photonics, Charlotte, NC, Jun 2005 [12].
- R. E. Gordon, L. R. Chen, and M. Coates, "Analysis of a WDM Packet Switch with a Reduced Set of Limited-Range Wavelength Converters," presented at OSA Topical Meeting on Information Photonics, Charlotte, NC, Jun 2005 [13].

# Demonstration of All-Photonic Code Conversion in a Semiconductor Fiber Ring Laser for OCDMA Networks

#### Reuven E. Gordon and Lawrence R. Chen

Photonic Systems Group, Department of Electrical and Computer Engineering, McGill University 3480 University Street, Montréal, Québec, Canada, H3A 2A7
E-mail:rgordon@photonics.ece.mcgill.ca

**Abstract:** We demonstrate all-photonic code conversion for OCDMA network applications based on cross-gain modulation in a semiconductor fiber ring laser. The code converter translates weight four spectral sequences and is capable of providing 2R regeneration.

©2005 Optical Society of America

OCIS codes: (060.2330) fiber optics communication, (060.4510) optical communications

#### 1. Introduction

Optical code division multiple access (OCDMA) has been proposed as a protocol to satisfy the ever increasing capacity requirements of local area and optical access networks. In contrast with time and wavelength division multiplexed access (TDM and WDM), OCDMA operates asynchronously, does not require central control and efficiently utilizes bandwidth under bursty traffic [1].

An OCDMA network comprised of many inter-connected sub-networks will often have the same code-set in use in different sub-networks. In this configuration, code contentions may arise when a user requests transmission between sub-networks at a network node. Conversely, if a user requests transmission to a sub-network operating with a different code-set (and possibly at different wavelengths), conversion would be required to a new code (and wavelengths) within that set. These contentions or required conversions can be resolved by incorporating photonic code converters (PCCs) into the network nodes, thereby resulting in a significant increase in throughput. For one-dimensional (1-D) spectral photonic codes, conversion involves translating a code defined by one set of k wavelengths to another defined by a different set of k wavelengths, where k is the Hamming weight of the code family [1]. In essence, a 1-D spectral PCC extends the capability of a wavelength converter in WDM networks by performing concurrent multiple-wavelength conversion.

Common wavelength conversion technologies demonstrated for WDM networks include four-wave mixing (FWM) or cross-gain and cross-phase modulation (XGM, XPM) in semiconductor optical amplifiers (SOAs). Of these three technologies, XGM is the simplest, provides the highest conversion efficiency, does not require on-chip integration for stability, and allows 2R (re-amplifying and re-shaping) regeneration capability [2].

In this paper, we demonstrate all-photonic code conversion based on XGM in a semiconductor fiber ring laser (SFRL). The steady-state transfer characteristics demonstrate that our PCC is capable of 2R regeneration.

#### 2. Experimental Setup and Principle of Operation

The experimental setup is shown in Fig. 1. In our demonstration, we consider the conversion of 1D spectral codes of length 7 and weight 4, defined by m-sequences [3]. The incoming code (code i) is denoted  $\{1,1,1,0,0,1,0\}$  with wavelengths 1533.4 nm, 1534.98 nm, 1535.76 nm and 1541.28 nm; this code is to be converted to the output code j denoted by  $\{1,1,1,0,1,0,0\}$  operating on wavelengths 1536.54 nm, 1538.11 nm, 1539.69 nm and 1542.85 nm. Note that these two m-sequences are not cyclically shifted versions of each other, but are created from different generator polynomials [4]. This could correspond to a scenario in which a user requests access to a sub-network with a different code set at different wavelengths.

The four wavelengths for code i ( $\lambda_{il}...\lambda_{id}$ ) are generated from four tunable laser sources (TLS) before being combined into the control arm. An electro-optic modulator (MOD) driven by a pulse pattern generator (PPG) produces the corresponding data signal. An erbium-doped fiber amplifier (EDFA) and variable optical attenuator (VOA) are used to amplify and set the power of the input signal code i before injection into the PCC via an optical circulator (OC<sub>A</sub>).

The PCC is based on a multi-wavelength SFRL. The output wavelengths  $(\lambda_{j1}...\lambda_{j4})$  correspond to the output code (code j) and are defined by an arrayed waveguide (AWG) grating whose corresponding output ports are connected to fiber loop mirrors. The lengths of the loop mirrors are set to ensure that the round trip propagation times for each wavelength in the SFRL are within 1%. Two SOAs are used: SOA<sub>1</sub>, which is biased slightly above its transparent point to provide some small gain, and SOA<sub>2</sub>, which is highly biased and used for XGM to achieve

code conversion. The isolator ensures that only the highly biased  $SOA_2$  sees the injected input signal code *i*. Polarization controllers ( $PC_1$  and  $PC_2$ ) are used to account for the polarization dependent gains of the SOAs.

The principle of operation of the PCC is as follows. When the injected input code (counter-propagating with the lasing signals of the SFRL) is ON (logical "1"),  $SOA_2$  becomes saturated. As a result, the four wavelengths  $(\lambda_{j1}...\lambda_{j4})$  experience little or no gain in  $SOA_2$  and do not have sufficient net gain to lase, i.e. the output power is OFF (logical "0") such that there is no conversion from code i to code j. On the other hand, when the input code is OFF, the four wavelengths experience gain in  $SOA_2$  and consequently re-establish lasing, i.e. the output power is ON such that there is code conversion. Note that since the PCC is based on XGM, code conversion will result in data inversion.

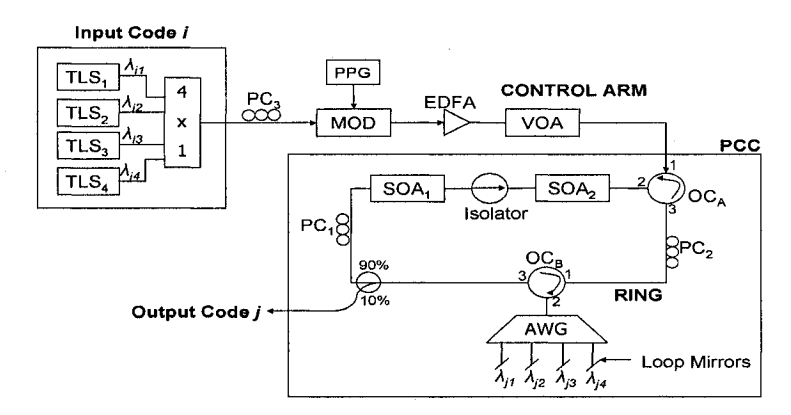


Fig. 1. Experimental setup for a quad-wavelength all-optical PCC using XGM in an SOA.

#### 3. Results

In Fig. 2, we show the static input/output power transfer characteristics of the PCC for bias currents  $I_{SOAI} = 36.2$  mA and  $I_{SOA2} = 135.5$  mA. Since all four output wavelengths  $(\lambda_{j1}...\lambda_{j4})$  have the same behavior as a function of input power, proper code conversion can take place and the code converted output signal has equal power at all four wavelengths. Furthermore, the sharp, step-like transition in the transfer characteristics (i.e. thresholding and limiting functionality) shows that the PCC is capable of 2R regeneration. In particular, if the extinction ratio (ER) of the input signal at code i is greater than the slope width of the transfer characteristics ( $\approx 6$  dB), then the output signal at code j will have a significantly improved ER (more than 30 dB).

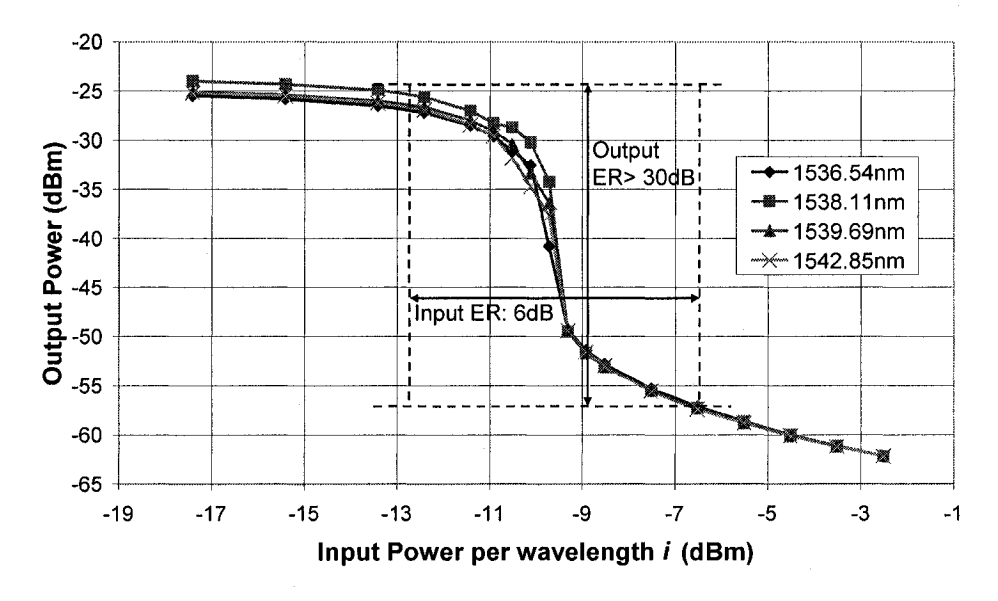


Fig. 2. Static transfer characteristic of PCC (output power vs. total average input power). An SOA<sub>1</sub> bias current of 36.2 mA and an SOA<sub>2</sub> bias current of 135.5 mA are used.

Figs. 3(a) and (b) show the spectra of the input code i with peak powers (per wavelength) of -12.8 dBm ("0") and -6.8 dBm ("1"); the ER is 6 dB. Figs. 3(c) and (d) show the corresponding output from the PCC: the power at all four output wavelengths are approximately equal and take values of -26.3 dBm when code i is off and -56.7dBm when code i is ON. The average ER at the output is 30.4 dB. Further experimental results will be presented at the conference.

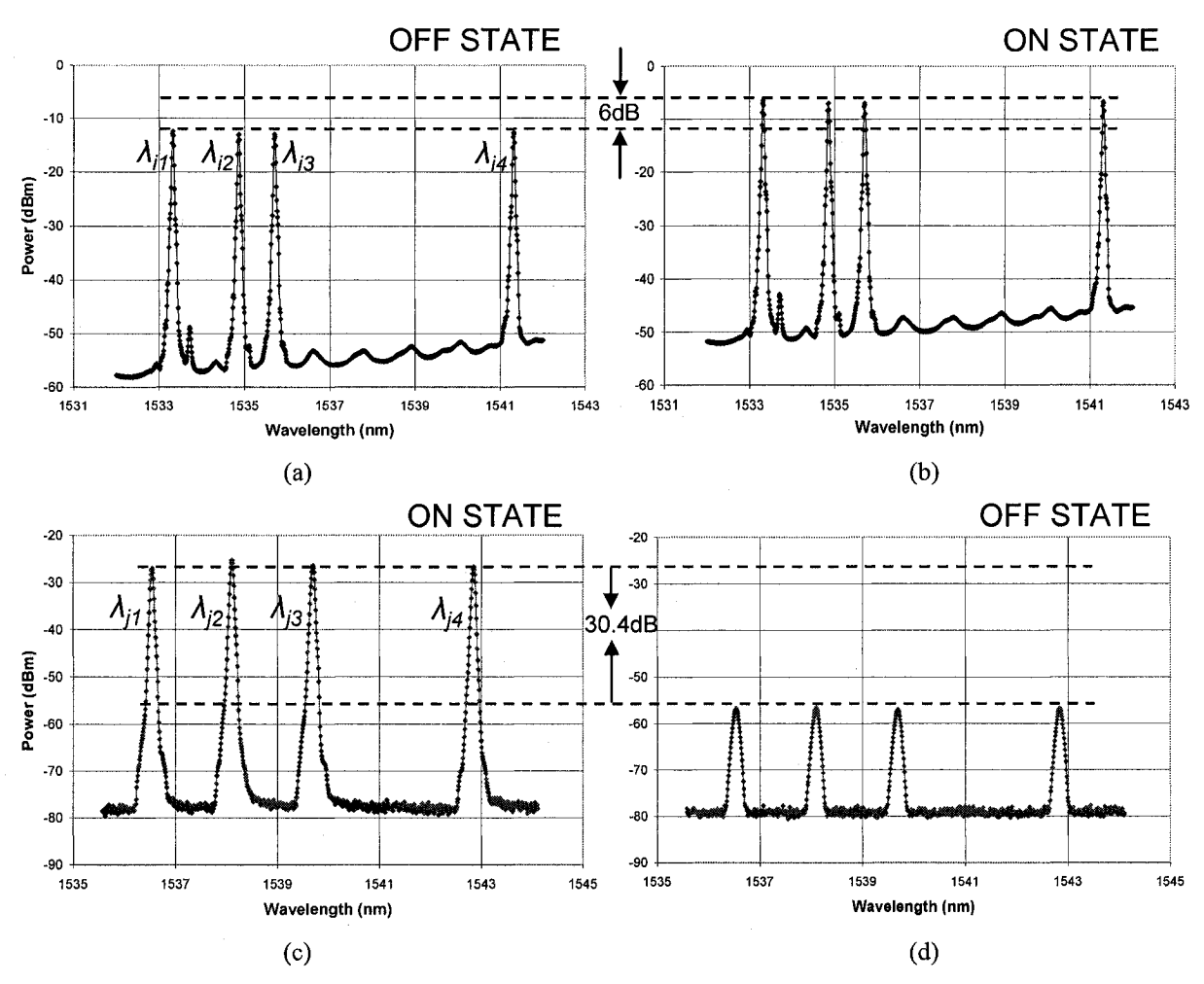


Fig. 3. Spectra of input code i for (a) "0" and (b) "1" power levels. Corresponding SFRL output at code j: (c) "0" and (d) "1" level for code i.

#### 4. Summary

In summary, we have demonstrated all-photonic code conversion of length 7, weight 4 spectral codes using XGM in a SFRL. The static characteristics exhibit thresholding and limiting such that the PCC is capable of 2R regeneration. Further improvements in the output power of the code converted signal should be possible by optimizing the fiber laser cavity. Tunable code conversion should also be possible by using tunable wavelength selective components (for example, a wavelength-selective MOEMS switch) in the SFRL.

#### References

- [1] A. Stok and E. H. Sargent, "Lighting the Local Area: Optical Code-Division Multiple Access and Quality of Service Provisioning," *IEEE Network*, pp. 42-46, 2000.
- [2] S. J. B.Yoo, "Wavelength Conversion Technologies for WDM Network Applications," J. Lightwave Technol., vol. 14, pp. 955-966, June 1996.
- [3] M. Kavehrad and D. Zaccarin, "Optical Code-Divison Multiplexed Systems Based on Spectral Encoding of Noncoherent Sources," J. Lightwave Technol., vol. 13, pp. 534-545, 1995.
- [4] J.-K. Liang, "Merged m-sequence Codes used for Hybrid Time-Spreading / Wavelength-Hopping Optical CDMA System." Taiwan: National Cheng Kung University, 2003, pp. 26-28.

# Analysis of a WDM Packet Switch with a Reduced Set of Limited-Range Wavelength Converters

#### Reuven E. Gordon, Lawrence R. Chen, and Mark Coates

Photonic Systems Group, Department of Electrical and Computer Engineering, McGill University 3480 University Street, Montréal, Québec, Canada, H3A 2A7

E-mail:rgordon@photonics.ece.mcgill.ca

**Abstract:** We analyze the performance of a packet switch in a wavelength division multiplexed network employing reduced sets of limited-range wavelength converters. Optimal operation is achieved by trading off conversion range and number of converters.

©2005 Optical Society of America

OCIS codes: (060.2330) fiber optics communication, (060.4510) optical communications

#### 1. Introduction:

Wavelength division multiplexing (WDM) is a highly flexible method of implementing all-optical packet-switched networks [1]. Using tunable optical wavelength converters (TOWC's), the WDM protocol can solve packet contentions in a switch, while providing high throughput and transparency, making the technology especially promising. The studies in [2-4] suggest that an output buffered switch equipped with a complete set of full-range TOWC's (FRWC's) can reduce the packet loss probability (PLP) by several orders of magnitude over a switch with no conversion capability. (A complete set of TOWC's implies each wavelength channel has its own TOWC, while full-range implies that each TOWC can convert from one wavelength to any other). Moreover, the added wavelength dimension in WDM allows TOWC's to provide a "logical buffer", where practical PLP floors can be obtained without any tunable delay lines [3]. This is desirable as delay lines comprise long lengths of fiber and cause scheduling and complexity issues in the switch.

Recently, studies have focused on the throughput of WDM switches with reduced (shared) sets of FRWC's [5,6]. Results show, that switches using fewer, shared, FRWC's can often achieve the same throughput as switches with complete sets of FRWC's [6]. Other studies have accounted for the physical limitations of popular wavelength conversion technologies (i.e. four wave mixing, cross-gain and cross-phase modulation in semiconductor optical amplifiers) and examined switches with complete sets of limited-range wavelength converters (LRWC's) [7,8]. In [7], it was found that when each channel has access to a LRWC with even a small conversion range, throughputs close to that of a switch employing complete sets of FRWC's can be obtained. (The conversion range refers to the number of wavelengths, above and below, that each LRWC can convert to from a given wavelength).

In this paper, we analyze the throughput of a slotted, bufferless, WDM switch in the most general (and previously unstudied) case of reduced sets of LRWC's. Both uniform and bursty traffic patterns are considered. The Shared Per (Output) Line switch architecture [5] is used and shown in Fig. 1. Each of the N input fibers carries n wavelengths. Each output fiber has a bank of L LRWC's and n-L direct lines combined into the passive coupler. L can vary from 0 (no conversion capability) to n-1 (complete set). The space switch requires  $nN \times nN$  gates. An electronic control system assumed to extract packet headers and control routing and wavelength conversion is not shown in the switch.

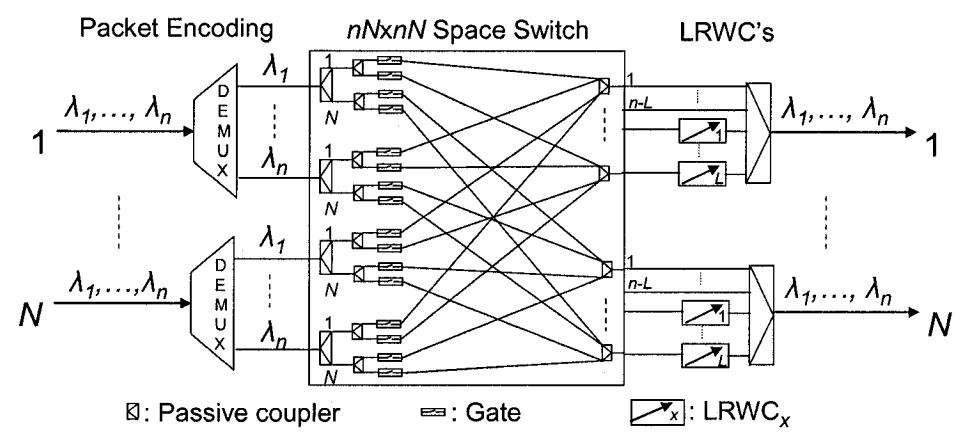


Fig. 1. Slotted WDM packet switch using optical gates for the space switch. Each output fiber has a bank of L LRWC's.

#### 2. WDM Packet Switch Model with Reduced Sets of LRWC's

The different WDM switch scenarios we consider are summarized in Fig. 2. All systems using FRWC's are modeled analytically and verified through Monte-Carlo (M-C) simulation. Systems using LRWC's are modeled by M-C simulation only.

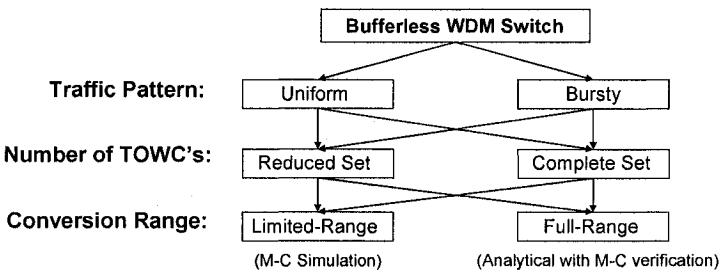


Fig. 2. WDM switch configurations.

For uniform input traffic, each of the nN input channels are modeled as Bernoulli random variables with time independent load  $\rho$ . Assuming a packet has an equal probability of going to any output fiber, the channel load directed at one output is  $\rho/N$ . The bursty traffic model considers each of the nN input channels to be an ON-OFF source [2], and assumes the number of active channels in the current slot are correlated to the number active in the previous slot.

The theoretical analysis of a switch with reduced sets of FRWC's involves developing equations to model the mean number of unused wavelengths per output fiber per time-slot, and the conditional probability for i contentions occurring given j active channels (where  $i \in [0, \min(j-1, n-1)]$  due to the bufferless constraint, and  $j \in [0, nN]$ ). For bursty traffic, an expression for probability of success of *all* slots in a packet up to and including the k<sup>th</sup> (final) slot is required. (The probability of a packet containing k slots is governed by the geometric distribution with mean burst length  $\beta$ . For  $\beta = 1$ , the bursty model reduces to a uniform model). These expressions result in an analytical equation for PLP (to be presented).

For systems with reduced sets of LRWC's, users on each wavelength contend for transmission to a given output fiber, and may only be converted to other wavelengths within their conversion range. This problem is further constrained by a reduced number of conversions allowed in each time slot. Thus a wavelength matching problem between input and output wavelength sets arises. To solve this problem, random and optimum matching algorithms (RMA and OMA) are used by the switch.

When one or more users arrive on an input wavelength, the RMA, modified from [7], randomly selects one user to forward to the same wavelength (without conversion). It then randomly moves through all wavelengths where a contention has arisen. For each contending user, it randomly chooses an available output wavelength (within the conversion range) to convert to. Once the maximum number of conversions are reached (or every user has been matched to an output wavelength), the algorithm ends.

The OMA attempts to find the optimal solution in the rectangular matching problem of a bipartite graph G, where the input subset is the wavelengths entering the switch, and the output subset is the available wavelengths at the output [7]. A legal matching occurs if (1) there are no contentions in the output wavelength set, (2) all conversions taking place obey the constraints of the LRWC, and (3) the total number of conversions is less than or equal to the number of LRWC's on the output fiber. A matching that satisfies these conditions and contains the maximum number of edges (highest throughput) is an optimal matching. There are often many optimal matchings for a given bipartite graph G. Using Munkres (Hungarian) algorithm, the OMA will always return an optimal matching for complete sets of LRWC's. However, with the added constraint of a reduced number of conversions, sub-optimal matchings may be returned.

#### 3. PLP results and Model Verification

The results of a study of a 4×4 switch with 15 wavelengths per fiber under bursty traffic with  $\beta=2$  are presented. Fig. 3(a) shows the analytical PLP curves versus channel load for a switch with reduced sets of FRWC's. These results are verified by M-C simulations with 10,000 trials. Based on these values, PLP is plotted against number of FRWC's for a load  $\rho=0.7$  in the inset of Fig. 3(a). The M-C simulations results agree well with the analytical curves. There are also several orders of magnitude improvement in PLP between a switch with a complete set of FRWC's and one with none at all, especially for lower loads. From the inset in Fig. 3(a), for 8 or more FRWC's, there is negligible reduction in PLP. In general, near-optimal PLP's can be obtained with far fewer FRWC's than the complete set.

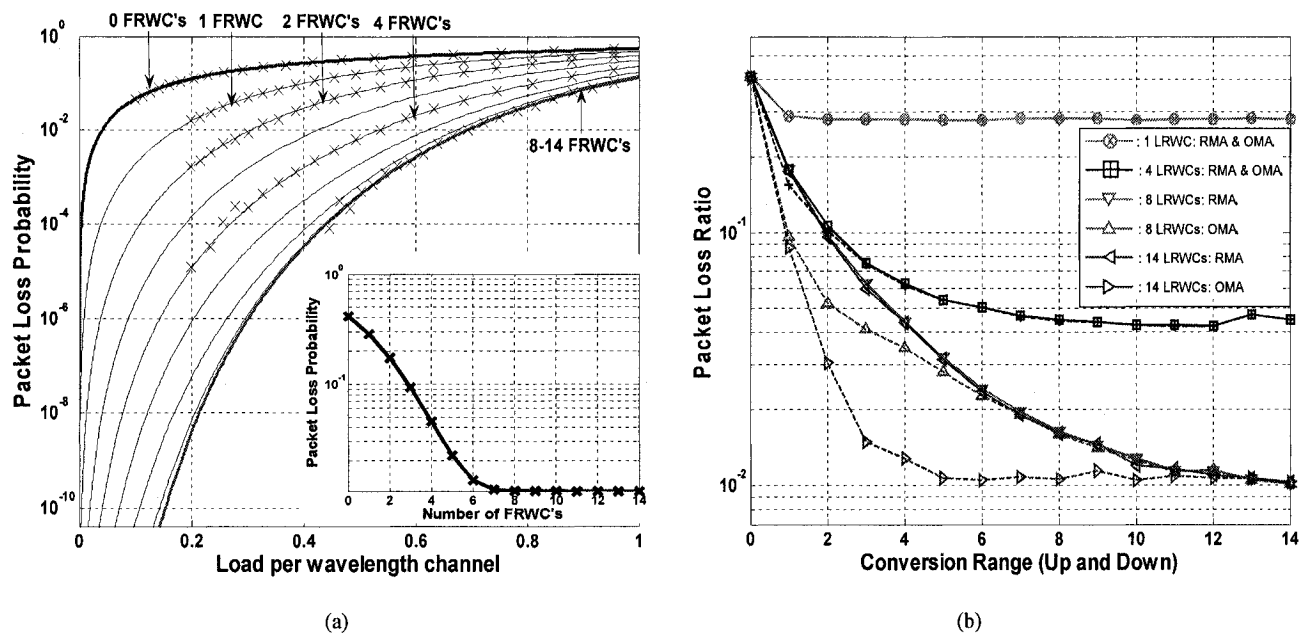


Fig 3(a) PLP vs channel load for a 4×4 switch with 15 wavelengths on each fiber with reduced sets of FRWC's under bursty traffic ( $\beta = 2$ ). × denote M-C simulation results. Inset: PLP vs number of FRWC's for  $\rho = 0.7$ . (b) PLP vs conversion range (up and down) for a 4×4 switch with 15 wavelengths on each fiber for reduced sets of LRWC's. Bursty traffic flow ( $\beta = 2$ ), with  $\rho = 0.7$ .

Fig. 3(b) plots PLP against conversion range for a switch with reduced sets of LRWC's at load  $\rho=0.7$ , where each simulation uses 10,000 M-C trials. The results of both the RMA and OMA are shown. With one LRWC per output line, a conversion range of 1 gives the same PLP as a conversion range of 14 (i.e. FRWC). When a complete set of LRWC's are used (14 LRWC's in Fig. 4), the OMA yields much lower PLP than the RMA. In fact, a complete set of LRWC's with a conversion range of 5 gives the same PLP as a complete set of FRWC's. Recall from the inset in Fig. 3(a) that 8 or more FRWC's yield an optimal PLP; this is not the case when the conversion range is reduced (see PLP for 8 LRWC's in Fig. 3(b)). In these scenarios, the OMA is not as effective when the constraint of a reduced number of conversions is added, and is only marginally better than the RMA. Running a brute-force tree search on all matchings showed that the throughput could be improved, but not to the optimum level of a complete set of LRWC's.

#### 4. Conclusions

In this paper, we studied the performance of a bufferless switch in a WDM network with reduced sets of LRWC's on each output fiber under bursty traffic. The results in this paper confirm that optimal PLP can be obtained for switches with few FRWC's, as well as for switches with complete sets of LRWC's with low conversion range (using the OMA). For reduced sets of LRWC's, the PLP's are sub-optimal due to the added constraint of reduced conversions. Based on the simulation results, a trade-off between conversion range and number of LRWC's must be made to reach a PLP threshold while minimizing a user-defined cost function. The cost function could depend on the number and conversion range of the TOWC's, scaled by complexity, price and technological limitation parameters. In all cases, cost savings can be made while still accounting for the realistic physical limitations of wavelength conversion.

#### References

- [1] C. A. Brackett, IEEE Journal in Comms, vol. 8, pp. 948-964, Aug 1990.
- [2] S. L. Danielsen et al, J. Lightwave Technol., vol. 15, pp. 219-226, Feb 1997.
- [3] S. L. Danielsen et al, IEEE Photonics Technol Letters, vol. 10, pp. 896-898, Jun 1998.
- [4] S. L. Danielsen et al, J. Lightwave Technol., vol. 16, pp. 729-734, May 1998.
- [5] V. Eramo et al, J. Lightwave Technol., vol. 21, pp. 340-355, 2003.
- 6] V. Eramo et al, J. Lightwave Technol., vol. 18, pp. 1818-1833, Dec 2000.
- [7] V. Eramo et al, IEEE Photonics Technol Letters, vol. 16, pp. 644-646, Feb 2004.
- 8] G. Shen et al, *IEEE Comms Letters*, vol. 5, pp. 432-434, Oct 2001.
- [9] P. K. Agarwal and K. R. Varadarajan, presented at SCG, Brooklyn, NY, June 2004.

# 11 Appendix D: Laboratory Pictures of the PCC Setup

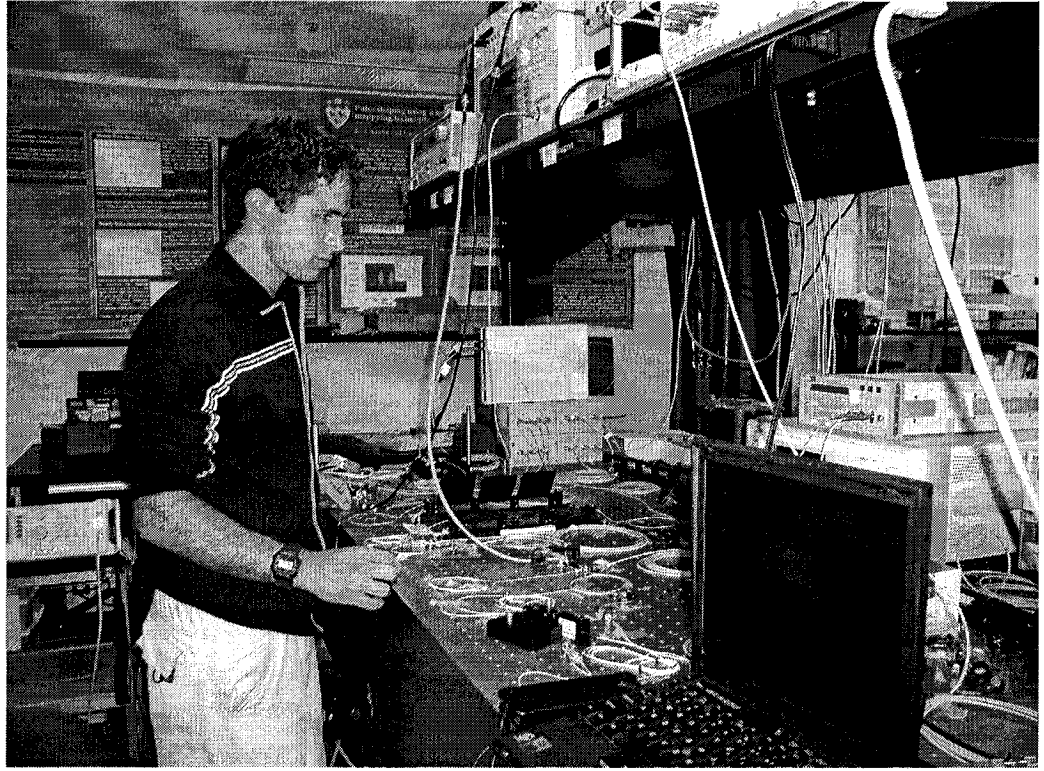


Figure 11.1: Reuven Gordon characterising stages of initial PCC.



Figure 11.2: Final PCC setup to make step response measurements.

Figure 11.3: Panorama view of all-photonic clock recovery setup.